

Advanced Methodology to Simulate Boiling Water
Reactor Transient Using Coupled
Thermal-Hydraulic/Neutron-Kinetic Codes

Zur Erlangung des akademischen Grades

Doktor der Ingenieurwissenschaften

der Fakultät für Maschinenbau

Karlsruher Institut für Technologie (KIT)

genehmigte

Dissertation

von

Dipl.-Ing. Christoph Oliver Hartmann

Tag der mündlichen Prüfung: 13. Juni 2016

Hauptreferent: Prof. Dr. Robert Stieglitz (KIT)

Korreferent: Prof. Dr. Rafael Macian-Juan (TU München)

Acknowledgments

This work was prepared during my work as a PhD student of Westinghouse Electric Germany GmbH (WEG) in cooperation with the Institute for Neutron Physics and Reactor Technology (INR) at the Karlsruhe Institute of Technology (KIT).

My special thanks to Prof. Robert Stieglitz for the support and constructive criticism in the recent years, and Prof. Rafael Macian for the acceptance as second reviewer.

My heartfelt thanks to my academic supervisor Dr. Victor Sanchez without his knowledge and active support this project would not have been possible and I had never met my wonderful wife.

Further I would like to thank Dr. Tietsch and Westinghouse Electric Germany GmbH. Without them I would not have worked on this thesis.

I want also thank my colleagues at INR, Dr. Wadim Jäger, Dr. Armando Gomez, Dr. Manuel Calleja, Dr. Jorge Pérez, Dr. Markus Schlenker and Rodrigo Gómez plus Markus Esch, Mark Thieme and Felix Sassen at WEG for the good working relationship.

Robert Holzer and the company NIS Ingenieurgesellschaft mbH I would like to thank for providing the fuel assembly data.

A big thank you also goes to the secretaries of the INR, Petra Klug, Ingeborg Schwartz and Birgit Zagolla plus Monika Vondung, Nicole Koch and Petra Fiebig at WEG.

Last but not least, I would like to thank my family and my wife Ana Hartmann. Thanks Amor that you have always supported and spurred me to complete the work successfully.

Danksagung

Die vorliegende Arbeit entstand während meiner Tätigkeit als Doktorand der Firma Westinghouse Electric Germany GmbH (WEG) in Kooperation mit dem Institut für Neutronenphysik und Reaktortechnik (INR) am Karlsruher Institut für Technologie (KIT).

Mein herzlicher Dank geht an Prof. Robert Stieglitz für die fortwährende Unterstützung und konstruktive Kritik in den vergangenen Jahren sowie Prof. Rafael Macian für die Übernahme des Mitberichts.

Mein besonderer Dank geht an meinen wissenschaftlichen Betreuer Dr. Sanchez ohne dessen Wissen und tatkräftige Unterstützung dieses Vorhaben nicht durchführbar gewesen wäre und ich nie meine wundervolle Frau getroffen hätte.

Weiter möchte ich mich bei Herrn Doktor Tietsch und der Firma Westinghouse Electric Germany GmbH bedanken, die mir erst die Arbeit an dieser Dissertation ermöglicht haben.

Für die gute Zusammenarbeit mit meinen Kollegen am INR, Dr. Wadim Jäger, Dr. Armando Gomez, Dr. Manuel Calleja, Dr. Jorge Pérez, Dr. Markus Schlenker und Rodrigo Gómez sowie Markus Esch, Mark Thieme und Felix Sassen bei WEG möchte ich mich ebenfalls bedanken.

Auch Robert Holzer und der Firma NIS Ingenieursgesellschaft mbH möchte ich meinen Dank für das Bereitstellen der Brennelementdaten aussprechen.

Ein großes Dankeschön geht auch an das Sekretariat des INR, Petra Klug, Ingeborg Schwartz und Birgit Zagolla sowie an Monika Vondung, Nicole Koch und Petra Fiebig bei WEG.

Als letztes möchte ich mich ganz herzlichst bei meiner Familie und meiner Frau Ana Hartmann bedanken. Danke Amor, dass du mich immer unterstützt und angespornt hast die Arbeit erfolgreich abzuschließen.

Abstract

Advanced Methodology to Simulate Boiling Water Reactor Transient Using Coupled Thermal-hydraulic – Neutron – Kinetic Codes

Coupled Thermal-hydraulic/Neutron-kinetic (TH/NK) simulations of Boiling Water Reactor transients require well validated and accurate simulation tools. The generation of cross-section (XS) libraries, depending on the individual thermal-hydraulic state parameters, is of paramount importance for coupled simulations. Problem-dependent XS-sets for 3D core simulations are being generated mainly by well validated, fast running commercial and user-friendly lattice codes such as CASMO and HELIOS. In this dissertation a computational route, based on the lattice code SCALE6/TRITON, the cross-section interface GenPMAXS, the best-estimate thermal-hydraulic system code TRACE and the core simulator PARCS, for best-estimate simulations of Boiling Water (BWR) transients has been developed and validated. The computational route has been supplemented by a subsequent uncertainty and sensitivity study based on Monte Carlo sampling and propagation of the uncertainties of input parameters to the output (SUSA code).

The analysis of a single BWR fuel assembly depletion problem with PARCS using SCALE/TRITON cross-sections has been shown a good agreement with the results obtained with CASMO cross-section sets. However, to compensate the deficiencies of the interface program GenPMAXS, PYTHON scripts had to be developed to incorporate missing data, as the yields of Iodine, Xenon and Promethium, into the cross-section-data sets (PMAXS-format) generated by GenPMAXS from the SCALE/TRITON output. The results of the depletion analysis of a full BWR core with PARCS have indicated the importance of considering history effects, adequate modeling of the reflector region and the control rods, as the PARCS simulations for depleted fuel and all control rods inserted (ARI) differs significantly at the fuel assembly top and bottom. Systematic investigations with the coupled codes TRACE/PARCS have been performed to analyse the core behaviour at different thermal conditions using nuclear data (XS-sets) predicted by SCALE6/TRITON and CASMO. Thereby the coupled TRACE/PARCS simulations reproduced the single fuel assembly depletion and stand-alone PARCS results.

A turbine trip event, occurred at a BWR plant of type 72, has been investigated in detail using the cross-section libraries generated with SCALE/TRITON and CASMO. Thereby the evolution of the integral BWR parameters predicted by the coupled codes using cross-sections from SCALE/TRITON is very close to the global trends calculated using CASMO cross-sections. Further, to implement uncertainty quantifications, the PARCS reactor dynamic code was extended (uncertainty module) to facilitate the consideration of the uncertainty of neutron kinetic parameters in coupled TRACE/PARCS simulations. For a postulated pressure perturbation, an uncertainty and sensitivity study was performed using TRACE/PARCS and SUSA. The obtained results illustrated the capability of such methodologies which are still under development. Based on this analysis, the uncertainty band for key-parameters, e.g. reactivity, as well as the importance ranking of reactor kinetics parameters could be predicted and identified for this accident scenario.

Kurzfassung

Erweiterte Methodik zur Simulation von Siedewasserreaktor Transienten mit gekoppelten Thermohydraulik – Neutronenkinetik Codes

Gekoppelte Thermohydraulik/Neutronenkinetik (TH/NK) Simulationen von Siedewasserreaktor Transienten erfordern gut validierte und präzise Simulationswerkzeuge. Die Erzeugung der Wirkungsquerschnitte (XS), abhängig von individuellen thermohydraulischen Zustandsparameter, ist von größter Bedeutung für gekoppelte Simulationen. Problemabhängige XS-Sets für 3D-Kern Simulationen werden hauptsächlich von gut validierten, schnell laufenden kommerziellen und benutzerfreundlich Zellcodes wie CASMO und HELIOS erzeugt. In dieser Arbeit soll eine Berechnungsmethode, basierend auf dem Zellcode SCALE6/TRITON, dem XS Interface GenPMAXS, dem „Best-Estimate“ (BE) Systemcode TRACE und dem Kernsimulator PARCS für die Analyse von Siedewasserreaktor (SWR) Transienten vorgestellt werden. Die Rechenroutine ist durch eine weitere Unsicherheit und Sensitivitätsanalyse, basierend auf Monte Carlo Zufallsvariablen und der Fortpflanzung der Unsicherheiten von Eingabeparametern bis zur Ausgabe (SUSA Code) ergänzt.

Die Untersuchung mit PARCS von Abbrandrechnungen eines einzelnen Brennelementes mit von SCALE/TRITON erzeugten XS zeigt eine gute Übereinstimmung mit den Ergebnissen mit den XS von CASMO. Um jedoch Defizite des Interface Programms GenPMAXS zu kompensieren, wurden Python-Skripte entwickelt, um fehlende Daten zu integrieren, z.B. die Ausbeuten an Jod, Xenon und Promethium in die aus der SCALE/TRITON Ausgabe von GenPMAXS generierten XS Datensätze (PMAXS-Format). Die Ergebnisse der Abbrandrechnungen eines ganzen SWR-Kerns zeigen die Wichtigkeit von Abbrandhistorien, adäquater Modellierung der Reflektorregionen und der Kontrollstäbe, da die PARCS Simulationen für abgebrannten Brennstoff und mit allen eingeführten Kontrollstäben an der Brennelementspitze und dem Brennelementende erheblich abweichen. Systematische Untersuchungen mit den gekoppelten Codes TRACE/PARCS wurden durchgeführt, um das Kern Verhalten bei verschiedenen thermischen Bedingungen mit den von SCALE6/TRITON und CASMO erstellten XS-Sets zu analysieren. Dabei geben die gekoppelten Rechnungen mit TRACE/PARCS die Ergebnisse der einzelnen Brennelementabbrandrechnung und der PARCS Rechnungen wieder. Eine Turbinenschnellabschaltung (TUSA), welche in einem SWR Typ-72 auftrat, wurde unter Verwendung der Wirkungsquerschnittsbibliotheken von SCALE/TRITON und CASMO im Detail untersucht. Dabei ist die Entwicklung der integralen SWR-Parameter, welche durch die gekoppelten Codes mit den XS von SCALE/TRITON bestimmt wurden sehr nah an den globalen Trends berechnet mit den CASMO XS. Weiter wurde der reaktordynamische Code PARCS erweitert (Unsicherheitsmodul), um die Berücksichtigung der Unsicherheiten der neutronenkinetischen Parameter in gekoppelten TRACE/PARCS Simulationen zu erleichtern. Für einen postulierten Druckstoß wurden eine Unsicherheit und Sensitivitätsanalyse mit TRACE/PARCS und SUSA durchgeführt. Die erhaltenen Ergebnisse zeigen die Fähigkeit solcher Methoden, die sich noch in der Entwicklung befinden. Basierend auf diesen Analysen konnte das Unsicherheitsband für Schlüsselparameter, wie z.B. Reaktivität, sowie die Bedeutung der neutronenkinetischen Parameter für diese Unfallszenarien bestimmt und identifiziert werden.

TABLE OF CONTENTS

1	Introduction.....	1
1.1	Motivation	1
1.2	Goal of the thesis	2
1.3	Structure of the thesis	2
2	State of the Art	4
2.1	Best-Estimate Methodologies.....	4
2.1.1	Multi-dimensional trend	4
2.1.2	Pin power reconstruction.....	5
2.1.3	BWR transient analysis	5
2.2	Generation of Nodal Macroscopic Cross-sections for 3D Transient Simulations	6
2.2.1	Generation of multi-group cross-sections	7
2.2.2	Condensation of microscopic cross-sections.....	9
2.2.3	Homogenization of microscopic cross-sections	9
2.2.4	Branch calculations	11
2.2.5	Transformation in appropriate format	12
2.3	Thermal-Hydraulic / Neutronics Coupled Solutions	12
2.3.1	Internal and external coupling	13
2.3.2	Spatial coupling between the neutronic and thermal-hydraulic domains.....	14
2.3.3	Temporal coupling.....	16
2.4	Uncertainty and Sensitivity Methodologies	17
2.4.1	Quantification of uncertainties	17
2.4.2	Quantification of the sensitivity	21
3	Computational Route for 3D Analysis of BWR Transients.....	22
3.1	Short description of the computational route	22
3.2	Lattice Physics Codes.....	23
3.3	Reactor Dynamics.....	28
3.4	The Thermal-Hydraulic System Code TRACE.....	31
3.5	Uncertainty and Sensitivity Quantification Method for Coupled Codes	33
4	Generation of nodal Cross-sections for a Reference BWR Core.....	36
4.1	Main BWR-72 Plant Characteristics	36
4.2	BWR-72 Core Description	39
4.3	Neutron Physical Modelling of the BWR Core	40
4.4	Generation of the PMAXS Nuclear Data Libraries for 3D Transient Analysis	43
5	Validation of generated Cross-section Libraries.....	45
5.1	Single Fuel Assembly Depletion.....	46
5.1.1	Impact of Xenon and Samarium on depletion calculations	46
5.1.2	Effects of different evaluated nuclear data libraries on the FA depletion calculation	50
5.1.3	Influence of the history effect on the FA depletion calculation	51
5.1.4	Validation of the XS Generation Approach by Code-to-Code Comparison	53
5.1.5	Void and Fuel Temperature Reactivity Coefficients	54
5.2	Depletion Analysis of a full BWR Core with PARCS	56

5.2.1	The PARCS Core Model	56
5.2.2	Validation of Cross-section Generation Approach by Code-to-Code Comparison	57
5.3	Analysis of the BWR Core with TRACE/PARCS	62
5.3.1	The thermal-hydraulic TRACE Core Model	62
5.3.2	Neutronic/Thermal-hydraulic Mapping	63
5.3.3	Comparison of the TRACE/PARCS Simulations using different nodal Cross-section Sets based on SCALE and CASMO-4	64
6	Validation of a Turbine Trip Event with TRACE/PARCS using BWR Plant Data	69
6.1	Description of the Turbine Trip Event	69
6.2	TRACE integral plant model	72
6.3	Neutron-kinetic PARCS 3D Model	73
6.4	Analysis of the Turbine Trip Event with TRACE/PARCS	74
6.5	Comparison of the TRACE/PARCS Predictions with the plant data	75
7	Uncertainty and Sensitivity Analysis	81
7.1	Uncertainties in neutronic data	81
7.2	Uncertainty Quantification for the Pressure Perturbation Case	82
7.2.1	Quantification of uncertainties	82
7.2.2	Sensitivity analysis for the pressure perturbation case	85
7.2.3	Time dependent sensitivity analysis	91
7.3	Conclusions	94
8	Summary	96
9	Outlook	98
10	Literature	99
Annex A	PMAXS format	108
Annex B	Branch structure	109

LIST OF ABBREVIATIONS

ADF	Assembly Discontinuity Factor
ADS	Automatic Depressurization System
AHTLM	Adaptive Table Look-up Method
ANM	Analytical Nodal Method
ARI	All Rods In
ARO	All Rods Out
ATWS	Anticipated Transient Without SCRAM
BE	Best Estimate
BEPU	Best Estimate Plus Uncertainty
BOL	Begin Of Life
BR	Branch
BU	Burn Up
BWR	Boiling Water reactor
CIAU	Code with Capability of internal Assessment of Uncertainty
CMFD	Coarse Mesh Finite Difference
CPR	Critical Power Ratio
CR	Control Rod
CRDA	Control Rod Drop Accident
CSAU	Code Scaling, Applicability and Uncertainty
DC	Density of Coolant
ENDF	Evaluated Nuclear Data File
EOL	End Of Life
ESC	Extended Step Characteristic
FA	Fuel Assembly
FLD	Full Load Day
FMFD	Fine Mesh Finite Difference
Gd	Gadolinium
GPD	Generalized Perturbation Theory
GRS	Gesellschaft für Reaktorsicherheit
HFP	Hot Full Power
HIST	History effect XS generation
HPIS	High Pressure Injection System
I	Iodine
INR	Institut für Neutronenphysik und Reaktortechnik
IR	Intermediate Resonance

JEFF	Joint Evaluated Fission and Fusion File
JENDL	Japanese Evaluated Nuclear Data Library
KIT	Karlsruher Institut für Technologie
LOCA	Loss Of Coolant Accident
LWR	Light Water Reactor
MOX	Mixed Oxide fuel
MRP	Main Recirculation Pump
NEMMG	Nodal Expansion Method
NK	Neutron Kinetic
OECD	Organisation for Economic Co-operation and Development
PCT	Peak Cladding Temperature
PDF	Probability Density Function
PIRT	Phenomena Identification Ranking Table
Pm	Promethium
PMAXS	Perdue Macroscopic XS
PPR	Pin Power Reconstruction
PSA	Probabilistic Safety Analysis
PSR	Periodic Safety Report
PVM	Parallel Virtual Machine
PWR	Pressurized Water Reactor
RIA	Reactivity Insertion Accident
RPV	Reactor Pressure Vessel
SB	Small Break
Sm	Samarium
SSA	Safety Status Analysis
SUSA	Software for Uncertainty and Sensitivity Analyses
SWR	Siedewasserreaktor
TBV	Turbine Bypass Valve
TC	Temperature of Coolant
TF	Temperature of Fuel
TH	Thermal Hydraulic
TSV	Turbine Stop Valve
TT	Turbine Trip
TUSA	Turbinenschnellabschaltung
U&S	Uncertainty and Sensitivity
UAM	Benchmark for Uncertainty Analysis in Best-estimate Modelling
US NRC	United States Nuclear Regulatory Commission

UOX	Uranium Oxide
Xe	Xenon
XS	Cross-section

LIST OF SYMBOLS

C	Control rod fraction (PMAXS)
c_i	Momentum exchange term (TRACE)
c_w	Wall fraction loss term (TRACE)
E	Energy
H	History Parameter (PMAXS)
H	Enthalpy
$I.R.$	Intermediate Resonance approximation
k_{eff}	Multiplication factor
N	Number density
N	Neighbour fuel element (PMAXS)
N	Number of runs
P	Legendre polynomial
P	Power
q_d	Dissipation (TRACE)
q_i	Interphase energy exchange
q_w	Wall heat flux (TRACE)
R	Pearson's product moment correlation coefficient
$R.I.$	Resonance Integral
R^2	Correlation coefficient of determination (Pearson)
S	State variable (PMAXS)
V	Homogenized Volume
V	Velocity
X	Value (Pearson)
Y	Value (Pearson)
Γ	Effective yield
A	Fractile (Wilk's formula)
A	Control Rod fraction (PARCS)
A	Phase indicator (TRACE)
A	Reactivity coefficient

B	Confidence Level
Γ	Mass transfer (TRACE)
λ	Decay Constant
A	Parameter (Goldstein)
M	Angle
P	Density
σ	Microscopic XS
Σ	Macroscopic XS
Φ	Neutron Flux

1 Introduction

1.1 Motivation

The energy consumption worldwide continues growing driven by the rapid increase of the population and the industrialization of the developing countries. The huge demand for electricity is mainly supplied by coal, gas, oil, nuclear and renewable energy. Since Fukushima globally the electricity generation by nuclear reactors was decreasing, however several further nuclear power reactors are planned or under construction, especially in countries such as India, Russia, China, Korea and Japan. In Germany, nuclear energy will contribute to the electricity generation for the next 8 years according to the decision taken by the German Bundestag to abandon this option of energy generation by the end of 2022. The nuclear reactors remaining in operation are Boiling Water Reactors (BWR) and Pressurized Water Reactors (PWR). The last BWR Gundremmingen C will be taken from the grid in 2021. The safe operation of the nuclear power plants in Germany is assured by the plant operators under surveillance of the regulators according to the German Atomic Energy Act [2]. The continuous evaluation of the safety status of the nuclear power plants is prescribed by the Atomic Energy Act. For example, all nuclear power plants must undergo a Periodic Safety Review (PSR) each ten years. In addition, any modification of safety relevant systems, new core loadings, etc. requires a license from the regulatory authorities. In the frame of PSR and any license for plant modifications, a safety analysis has to be elaborated by the utilities. A central element of this safety analysis report is the accident and transient analysis of the nuclear power plants using complementary deterministic and probabilistic methodologies. In Germany, the safety assessment must be performed according to the state of the art in science and technology. Therefore different guidelines and rules have been established by federal government [3], which have to be taken into account by the license's applicants. Based on the recommendations of the Reactor Safety Commission, a PSR must include a Safety Status Analysis (SSA) and a Probabilistic Safety Analysis (PSA) [4]:

The SSA is a pure deterministic analysis methodology that makes use of numerical simulations codes to evaluate the plant behaviour under postulated transient and accidental conditions. Hence the safety demonstration relies mainly on numerical simulation codes that describe the key safety relevant phenomena occurring in a nuclear power plant and, therefore demands extensive validation and qualification for the specific purpose.

Thermal-hydraulic system codes have been developed since many years to assess the safety of Light Water Reactors (LWR). The improvement and validation of their physical models are a continuous effort of the international community. The advances of the experimental techniques lead to a considerable enhancement of the knowledge and understanding of key safety relevant processes taking place in LWR during normal, abnormal as well as accidental conditions, which was reflected in the continuous improvement of the prediction capability of the safety analysis codes. Moreover the rapid increase of computer power facilitated the transition from one dimensional to multidimensional thermal-hydraulic models and in the implementation of multi-physical and multi-scale coupled solutions also in the area of reactor technology and safety. Meanwhile coupled neutron-kinetics / thermal-

hydraulic codes are being developed and validated worldwide that permit a more realistic evaluation of the safety status of operating LWRs or new reactor concepts.

The use of the so called "Best-Estimate" (BE) coupled Thermal-Hydraulics (TH) and Neutron Kinetics (NK) code systems such as ATHLET-DYN3D, TRACE/PARCS in the frame of licensing processes is under intensive discussion and their final success will depend on the degree of validation and on the maturity of the methods for the quantification of the code's uncertainties. These numerical simulation codes can be applied not only to assess the safety features of LWR but also to optimize the core, plant and safety system design assuring a flexible and safe plant operation and at a high availability. Thus the safety margins obtained in the BE analysis will more closely reflect the real margins in the plant and enables a more efficient plant operation at the same safety level [5].

The use of BE thermal-hydraulic system codes with 3D neutron kinetic models requires the availability of a full set of cross-sections describing the actual core material composition and burnup state, which depend on state parameters such as fuel temperature, moderator density, control rod position, etc..

Modern core loading of both PWR and BWR are becoming more heterogeneous, which is reflected by fuel assemblies of different geometry and also by their material composition (enrichment, UO_2 - and MOX fuel, water rods, part length rods, etc.). These new core loadings are challenging to neutron physical, reactor dynamical and thermal-hydraulic code systems.

At present, no computational route for BWR based on non-commercial simulation codes is available that encompasses the whole chain of steps for transient 3D simulations based on coupled codes, which scope cross-section generation, flux solvers, depletion solver and thermal-hydraulic solvers and uncertainty quantification methodologies.

1.2 Goal of the thesis

The goal of this thesis is to prepare and to validate a Best-Estimate (BE) computational route for BWR transient analysis using coupled neutron-kinetics / thermal-hydraulic codes including three dimensional models for the description of the main phenomena inside the Reactor Pressure Vessel (RPV) and the core, which may play a role during BWR transients. This computational route should include an advanced and automated methodology for the generation of nodal cross-section for BWR core loadings taking into account any depletion state of the core. By these means a transient analysis of BWR with best-estimate coupled codes including the quantification of the embedded uncertainty and sensitivity of numerical codes can be performed.

1.3 Structure of the thesis

The thesis is divided into 10 sections. Section two is devoted to the state of the art on safety analysis methodologies for the simulation of BWR transients, methods for the generation of homogenized cross-sections for 3D nodal transient simulations, neutron-kinetics / thermal-hydraulic coupling codes, methodologies for the quantification of the uncertainties and

sensitivities. In Section 3, the description of the developed computational route for 3D transient analysis and of the involved numerical codes and methods will be given. The main peculiarities and data of the BWR plant selected as “reference” here are presented in Section 4. Section 5 contains the validation of the first steps of the computational route by the calculation of a fuel assembly depletion problem. Further the proof-of-principle application of the complete computational route to investigate a whole BWR core at Hot Full Power conditions (HFP) for different cases (all rods in, all rods out, critical rod position) is subject in Section 5. In section 6 the analysis of a turbine trip event in the reference plant using the developed and validated computational route is analysed by comparison of selected plant parameters predicted by the codes with these of the plant data. Finally an uncertainty quantification of the codes is conducted in Section 7 based on the transient case of pressure wave propagation into the core. A summary as well as an outlook is given at the end of the dissertation.

2 State of the Art

2.1 Best-Estimate Methodologies

2.1.1 Multi-dimensional trend

The analysis of BWR transients with numerical simulation tools has changed in the last decades due to the rapid increase of computer power and to the improvements of both mathematical-numerical algorithms. Initially, one dimensional system codes with point kinetics models and coarse BWR plant representations were used. Later on, best-estimate thermal-hydraulic system codes with one dimensional thermal-hydraulic models were developed and extensively validated against experimental data. In such codes, the core is represented by one dimensional parallel channels with a common lower and upper plenum. Prominent examples are TRAC-BF1 [7], RELAP5 [8], ATHLET [9], RAMONA [10], etc... . The majority of these codes solve transient two phase flow problems in one dimensional geometry for non-homogeneous, non-equilibrium flow conditions including heat transfer mechanisms between solid heated structures like the fuel rods, piping and RPV wall structures, as well as internal support structure components and the fluid. The two-fluid, two-phase flow models are derived from the spatial and time-averaged conservation equations for mass, momentum and energy of the two phases (liquid, vapour) with allowances for soluble components in the liquid phase and non-condensable components in the vapour phase [5].

Due to the advances of the computer power and the improved understanding of the physical phenomena taking place in nuclear power plants during the normal operation and in case of accidental conditions, the BE system codes are being improved continuously. One goal is the transition from an empirical to a more mechanistically description of the key heat transfer mechanisms within the reactor. The developments are concentrated on advanced multidimensional thermal-hydraulic models for a more realistic description of the physical processes within the RPV. These developments are reflected in the extensions of BE codes by implementing coarse mesh 3D thermal-hydraulic models in codes such as TRACE [11], RELAP 3D [12], ATHLET/ FLUBOX [13]. Additionally, the BE 1D/3D system codes have been coupled with nodal 3D neutron-kinetic models such as PARCS [14], DYN3D [15], QUABOX/CUBBOX [16] or SIMULATE-3K (S3K) [17] for a most realistic description of the core behaviour during non-symmetrical transients where the neutronic and the thermal-hydraulics strongly interacts with each other. Such conditions are encountered e.g. in Reactivity Insertion Accidents (RIA), Anticipated Transients Without Scram (ATWS), main recirculation pump failure, etc. For these events, coupled, fast running and computationally efficient code systems e.g. RELAP-3D/S3K [18], ATHLET/DYN3D [19], ATHLET-QUABOX/CUBBOX [20], TRACE/PARCS [21], POLCA-T [22], etc. have been elaborated to assess the safety analysis of BWR plants.

The reactor dynamics codes usually use the nodal two group diffusion approximation to calculate the 3D nodal neutron flux distribution. This has been found adequate for steady-state and transient applications for which core loading ate mainly homogenous [23]. In the meantime, modern core loadings are heterogeneous consisting of both Uranium (UOX) and

Mixed Oxide (MOX) fuel assemblies close to each other. Moreover, the fuel assembly (FA) design itself has changed dramatically in the last years aiming to improve the economics at simultaneously maintaining sufficient safety margins. Consequently current FA may consist of fuel pins with different enrichments radially distributed and with different size and shape of water rods and last not least Gadolinium rods and part length rods. Such configuration are characterized by larger neutron flux gradients and therefore the diffusion approximation is no longer valid. Hence, new multi-group time-dependent approaches such as the simplified SP3 method to solve the neutron transport equation instead of the diffusion approximation are required and implemented in core simulators such as PARCS, DYN3D and CRONOS [24].

Coupled TH/NK code systems based on nodal diffusion approximations are able to predict the fuel assembly power and thereby the hottest fuel assembly within the core in an accurate manner. But the safety relevant parameters such as Critical Power Ratio (CPR), maximum cladding and fuel temperature, etc. are local parameters. Traditionally, these important safety parameters are derived by a combination of the nodal predicted parameters with the conservative hot channel factors approach, which introduces conservatism in the methodology.

2.1.2 Pin power reconstruction

One alternative way to predict the fuel rod based parameters represents the so called “Pin Power Reconstruction (PPR)” method that combines the average power predicted by the nodal solutions with a form function calculated a priori by a 2D transport simulation of the hottest fuel assembly or by applying analytical approximations. The PPR method is implemented in most core simulators and its main disadvantage is that the PPR does not consider the feedbacks between the neutronics and thermal-hydraulics at a pin or sub-channel level as occurring in reality. A direct prediction of the pin power and other local safety parameters necessitates a coupling of the SP3-transport method with at least a sub-channel code as shown in [25].

2.1.3 BWR transient analysis

In recent years, BWR transients such as Small-Break Loss of Coolant Accident (SB-LOCA) [26], RIA [27], inlet sub-cooling transient [28], Turbine Trip (TT) [22][29][33], stability events [17][21][32][34], ATWS [30][31] etc. were investigated by different approaches and code systems.

A key issue of TH/NK coupled simulations is the quality of the cross-section data sets in addition to the neutronic / thermal-hydraulic mapping. By means of the cross-section models of each core simulator, the interaction of the neutronics and the thermal-hydraulics is taken into account. Hence, a precise characterization of the real material composition of the core at the time window of interest for the investigated transient is essential. Most nodal cross-sections for 3D transient simulations are generated by commercial codes such as HELIOS [35], CASMO [36]. Considerable effort is put worldwide to improve the capability of lattice codes such as SCALE6/TRITON [37], APOLLO2 [38], DRAGON [39] to generate complete core data sets depending not only on thermal-hydraulic state variables but also history effects and burnup states.

Besides the improvement of the prediction capability of coupled TH/NK BE codes, the validation and qualification is a task of paramount importance together with the quantification of the embedded code's uncertainties. Only an extensively validated and qualified code system will be accepted during a licensing process. Many international initiatives are focused on the validation and qualification of coupled TH/NK codes. The availability of experimental data of single effect, bundle, integral tests as well as plant data are critical to enable a code validation. Regarding BWRs, the following international benchmarks are of vital importance:

- OECD Ringhals 1 Stability Benchmark [32]
- OECD BWR Turbine Trip (TT) Benchmark [33]
- OECD Oskarsham-2 Benchmark [34]

2.2 Generation of Nodal Macroscopic Cross-sections for 3D Transient Simulations

The solution of the 3D neutron diffusion equation for a real LWR core requires information on geometry, material composition, thermal-hydraulic conditions and boundary conditions of the computational domain. Therefore the whole core is discretized in computational nodes, which contains the information on macroscopic cross-sections of the different reaction types, e.g. absorption, capture and scattering cross-section. Typically these nodal cross-sections for a whole core are generated in advance in a multi-step approach employing several approximations and assumptions [40][41][42]. The microscopic continuous energy cross-sections are collected in so called evaluated nuclear data files such as ENDF/B [43], JEFF [44] or JENDL [45]. The data have been derived from experiments and complemented by nuclear physics simulations.

The complex process of generation of nodal 3D macroscopic cross-sections comprises the following steps:

1. Generation of microscopic point-wise or multi-group cross-sections
→ knowledge of neutron spectrum (flux (E)) is needed for weighting
2. Condensation of microscopic cross-sections in two or multi-group (energy averaging) → knowledge of neutron spectrum (flux (E)) is needed for weighting
3. Homogenization of microscopic cross-sections from e.g. fuel rods, water rods to fuel assembly level (volume averaging) → knowledge of flux (E, space) is needed for weighting
4. Branch calculations for the generation of macroscopic cross-sections as function of the thermal-hydraulic state parameters, history effects and burnup conditions of the real core
5. Transformation of the few group cross-section data in the appropriate formats of the core simulators

2.2.1 Generation of multi-group cross-sections

In the first step, microscopic point or multi-group data are generated from the evaluated nuclear data libraries. This is necessary since the nuclear data libraries are voluminous and cannot be read directly by transport codes. For the processing of the point data, dedicated codes such as NJOY [47] or AMPX-2000 [48] are used. Figure 2-1 shows the point data based microscopic cross-sections of Uranium-235 taken from the nuclear data library ENDF/B-VII.0. Thermal neutrons are neutrons with an energy up to 1 eV and fast neutrons have an energy between 1.0E+4 eV und 2.0E+7 eV. The region between 1 and 1.0E+4 eV is the so called resonance area. Using point data the resonances are well mapped.

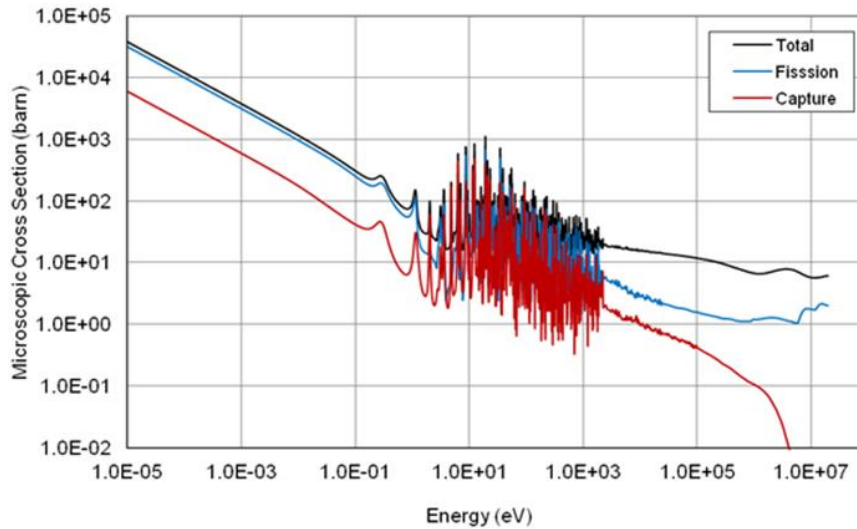


Figure 2-1: Point data of the microscopic cross-sections of Uranium-235 taken from ENDF/B-VII.0 [46].

In Figure 2-2 the microscopic cross-sections for a 238-group nuclear data library are shown. In contrast to the point data the multi-group data are discretized into energy groups and averaged over a prescribed energy range. The calculation of averaged cross-sections for reaction x and the group g according to Stamm'ler [40] is defined by the following equation:

$$\langle \sigma_x \rangle_g = \frac{\int_{E_{g+1}}^{E_g} \sigma_x(E) \Phi(E) dE}{\int_{E_{g+1}}^{E_g} \Phi(E) dE}. \quad (2.1)$$

In this connection $\sigma_x(E)$ is the microscopic cross-section taken from a nuclear data library, and $\Phi(E)$ a typical flux spectrum of group g . The finer the group structure is, the smaller the uncertainties in σ_{xg} are. Through the use of point data, the resonance region is better reflected than by using the multi-group data.

According to Trkov [41] the differential energy and angle scattering cross-sections (the elastic and the inelastic cross-section in the fast and the thermal range) can be grouped into

the scattering matrix. The angular dependence can be taken into account through Legendre polynomial expansion. The elements of the l^{th} Legendre moment of the scattering matrix are defined by the following equation:

$$\left\langle \sigma_{s,l}^{g \rightarrow h} \right\rangle_g = \frac{\int_{-1}^1 d\mu \int_{E_{g+1}}^{E_g} dE \Phi(E) \int_{E_{h+1}}^{E_h} dE' \sigma_s(E \rightarrow E', \mu) P_l(\mu)}{\int_{E_{g+1}}^{E_g} \Phi(E) dE}, \quad (2.2)$$

where μ is the cosine of the scattering angle φ in laboratory system, $P_l(\mu)$ the Legendre polynomial of degree l and $\sigma_s(E \rightarrow E')$ the cross-section for scattering from energy E into energy E' at an angle μ .

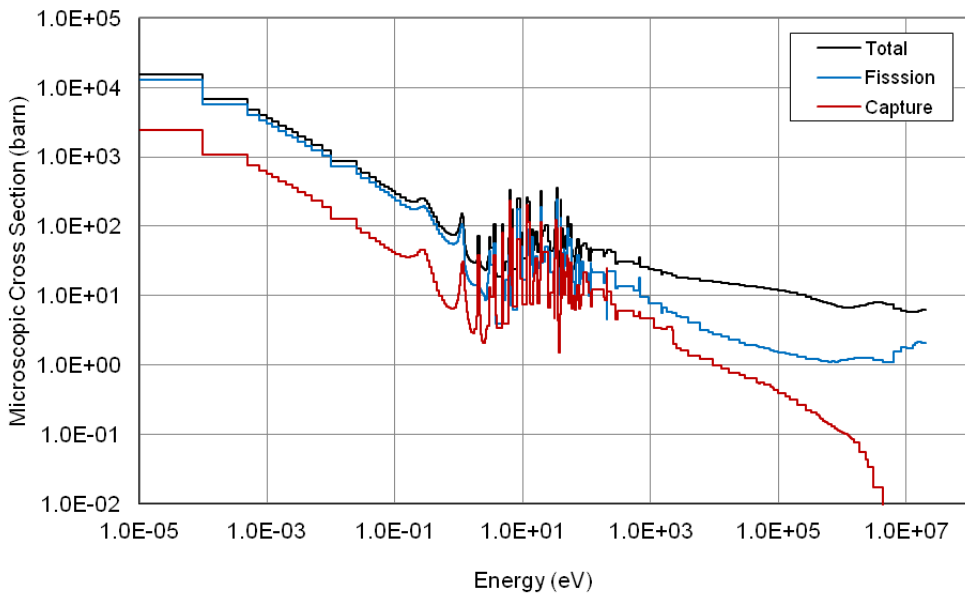


Figure 2-2: Microscopic multi-group cross-sections of Uranium-235 taken from ENDF/B-VII.0-238g SCALE library.

Average cross-sections of strong absorbers can be rigorously calculated by solving the slowing down equation for mixtures of the absorber with an idealized hydrogenous moderator of constant scattering cross-section and different concentrations. In this way the self-shielded absorber cross-sections can be parameterized as a function of the Bondarenko background cross-section σ_0 , which is the macroscopic “moderator” cross-section per absorber atom. A rigorous solution of the neutron slowing down equation is rather tedious. Several approximations have been developed to calculate the average cross-sections of strong absorbers. Similar to equation (2.1) Trkov describes a resonance integral (*R.I.*) [41]:

$$R.I. = \int_{E_{g+1}}^{E_g} \sigma(E) \Phi^*(E) dE, \quad (2.3)$$

where Φ^* is the usual smooth neutron weighting spectrum. Based on the Intermediate Resonance approximation (IR), introduced by Goldstein and Cohen [49] a parameter λ is defined so that the cross-section weighting neutron spectrum is:

$$\Phi^*(E) = \frac{\sigma_0 + \lambda\sigma_p(E)}{\sigma_0 + \lambda\sigma_a(E) + \sigma_s(E)} \Phi(E), \quad (2.4)$$

in which σ_0 denotes the Bondarenko background cross-section, σ_a the absorption cross-section, σ_s the scattering cross-section, σ_p the potential scattering cross-section and λ the Goldstein-Cohen parameter. The Goldstein-Cohen parameter is a “measure” of the resonance width.

2.2.2 Condensation of microscopic cross-sections

In a second step, the energy condensation (energy averaging) from multi-group or point data to few energy group data is performed. Assuming that the data are given on a fine grid, a neutron spectrum averaged over the same energy grid is required. The neutron spectrum is needed for the weighting process. A number of fine groups can be collapsed into coarse group by a procedure similar to (2.1), except that the integral sign is replaced by a summation over the fine groups g which constitute the coarse group h [41]:

$$\langle \sigma_x \rangle_h = \frac{\sum_g \langle \sigma_x \rangle_g \langle \Phi \rangle_g}{\sum_g \langle \Phi \rangle_g}. \quad (2.5)$$

2.2.3 Homogenization of microscopic cross-sections

In the third step, the spatial homogenization (volume averaging) of the cross-sections is carried out. This process transfers a micro region or structure to a macro structure (node). Here again the precise knowledge of the neutron flux for weighting purposes is needed, as it is given by:

$$\langle \sigma_x \rangle = \frac{\int_V \sigma_x(r) \Phi(r) dV}{\int_V \Phi(r) dV}. \quad (2.6)$$

Herein, V is the homogenization volume, where r is the position vector inside V . For clarity the index of the energy group g is omitted. Similar procedure is applied to the scattering matrices and the resonance integrals.

The few group data are created as a function of various parameters (such as the local burnup and the thermal-hydraulic feedback effect parameters) for each fuel assembly type present in the core. Typical methods for solving a 2D transport problem are the collision probability (HELIOS), method of characteristics (CASMO, APOLLO2, DRAGON) or the discrete ordinates method (SCALE6/NEWT/TRITON). Regardless of the method used, the reactor core or fuel assembly is divided into cells. A cell can represent an entire fuel

assembly or one fuel rod only. An example of single fuel rod or pin cell is illustrated in Figure 2-3, whereas Figure 2-4 shows an exemplary BWR fuel assembly with a central water rod, gadolinium rods and fuel rods with different enrichments. Over this cell or parts of it, the materials (fuel, moderator, coolant and absorber or structure material) are spatially homogenized and macroscopic so called condensed cross-sections are calculated and dumped through the cell code.

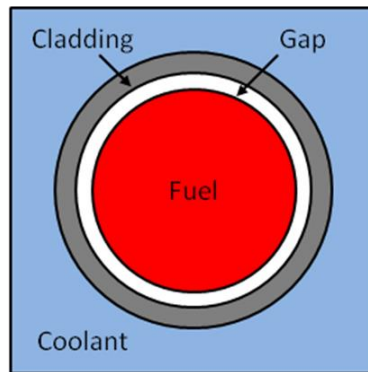


Figure 2-3: Example of a single fuel rod (pin cell)

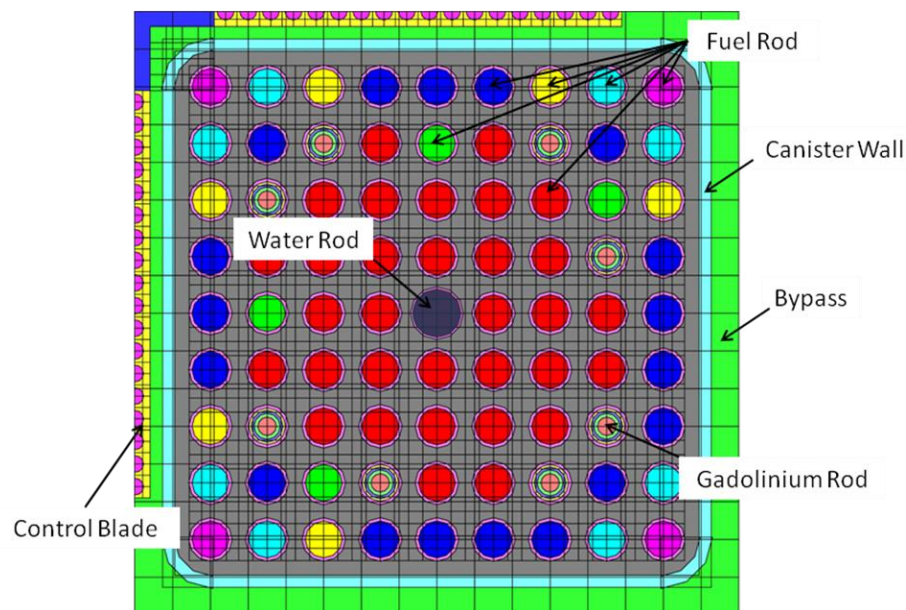


Figure 2-4: Fuel assembly of a BWR with a central water rod and Gadolinium rods. The different colors of the fuel rods dedicate different fuel enrichments.

Figure 2-5 shows the macroscopic 2-group cross-sections of a BWR fuel assembly, as illustrated in Figure 2-4, for fresh fuel conditions and a void fraction of 40 %. The void fraction indicates the amount of voids inside the coolant. The cross-sections are grouped into a fast ($2E+7$ eV to 3 eV) and into a thermal energy group (3 eV to $1E-5$ eV). The cross-sections are assumed to be constant throughout both energy ranges.

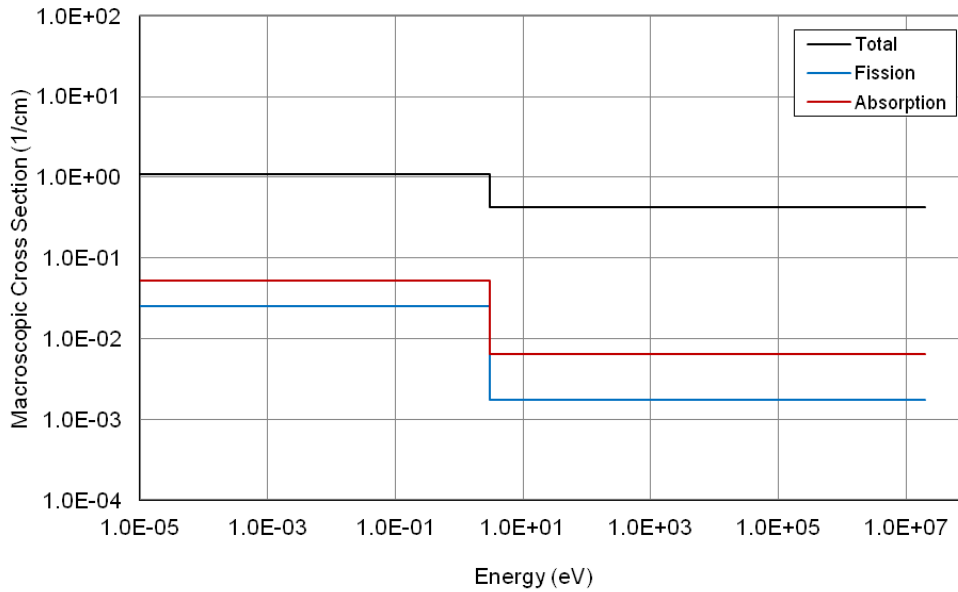


Figure 2-5: Macroscopic 2-Group cross-sections of a fresh BWR fuel assembly with 40 % void of the fuel assembly illustrated in Figure 2-4.

The spatial homogenization of cells/fuel assemblies and the assumption of reflective boundary conditions, which implies neglecting any impact from neighbouring fuel assembly, introduce approximations that may not reflect the real conditions existing in the core. This holds mainly in domains revealing large flux gradients as in the vicinity of control rods and reflector regions or locations in which different fuel types of Uranium and MOX appear. By introducing so-called “Assembly Discontinuity Factors (ADF)” and other important parameters, as the inverse neutron velocity, form functions, yields of neutron poisons like Xenon and Samarium, an improved description of the real core conditions can be achieved.

2.2.4 Branch calculations

In the fourth step data sets of homogenized condensed cross-sections are calculated in dependence on the instantaneous and history parameters for each material composition of all fuel assembly types of a specific core loading. The generation of such cross-section sets is achieved by performing numerous so-called branch calculations using a SCALE/NEWT/TRITON depletion sequence. Thereby for a reference state, the isotopic composition of the fuel is calculated. Subsequently the feedback parameters are varied to determine the cross-section for these conditions allowing the consideration of cross-correlation effects (when two or more parameters change simultaneously).

Since the neutron spectrum changes for different feedback parameter conditions, fuel depleted at different conditions will have different isotope content that affects significantly the core calculation. This effect is called history effect. The history dependence is a burnup dependence whereas the history parameters scope the irradiation, control rod history and the spectral history. For BWR, where the axial moderator density varies considerably, the spectral history effect of the moderator density is relevant as reported in [50] and must be carefully taken into account in the computational route.

2.2.5 Transformation in appropriate format

In the fifth step the generated few group cross-section data sets are transformed the formats which can be read in by the 3D core simulators. In principle many formats for the cross-section data sets such as the high-order Adaptive Table Look-up Method (AHTLM) [50] or the Purdue Macroscopic XS (PMAXS) format [51] developed for PARCS parameterization are available.

Interface programs have been developed for the transformation of the cross-sections generated by a lattice code (Step 2 to 4) into these specific libraries. The GenPMAXS code [51] is being developed at the University of Michigan for the generation of cross-section data sets in the PARCS PMAXS-format. The GenPMAXS is applicable to different lattice codes e.g. HELIOS, CASMO and SCALE6/TRITON. Another interface program with similar capabilities is mentioned in [52]. At the Karlsruhe Institute of Technology (KIT) Institute for Neutron Physics and Reactor Technology (INR), several interfaces based on PYTHON [90] have been developed to transform cross-sections generated by APOLLO2 and SCALE6/TRITON in look-up tables that can be used by core simulator codes such as DYN3D and PARCS.

However this cross-section generation approach features some limitations. Since the cross-section calculations are confined to a single rod or fuel assembly. Mutual interactions of neighbouring elements are not considered. This leads to errors because the calculated neutron spectra, which is used as weighting function, is not the same as that encompassing the entire core. Also the multi-dimensional tables cannot represent all core state conditions precisely because of the finite number of state points. The more heterogeneous the core, the more single fuel assembly calculations have to be performed. This leads to more computational effort.

A new trend in the generation of cross-sections for LWR transient analysis is the integrated cross-section and ADF generation by an embedded lattice transport methodology, as presented by [53][54]. Finally, the use of Monte-Carlo Methods for the generation of few group cross-sections for deterministic core simulators seems to be very promising [55], [56], [57].

2.3 Thermal-Hydraulic / Neutronics Coupled Solutions

Coupled thermal-hydraulic/neutron-kinetic (TH/NK) code systems based on nodal diffusion approximation have been developed since many years. In the last decade, the validation, qualification and application of 3D coupled codes have expanded considerably thanks to the increased computer power. For their use as best-estimate numerical tools in the frame of a licensing process, further improvements, extensive validation and the quantification of the code's uncertainty are necessary.

The key elements of paramount importance for coupled thermal-hydraulic/neutron-kinetic solutions are [6], [58], [61]

- internal and external coupling,

- spatial coupling and
- temporal coupling.

The challenge is to provide a fast running, numerically stable and physically consistent code system which can be applied for the analysis of a wide range of transients.

2.3.1 Internal and external coupling

The coupling between a TH and NK code is usually done in two ways, internal and external.

In case of the internal coupling as denoted in Figure 2-6, the 3D nodal NK code is integrated into the TH system code. The information exchange of heat (q), fuel temperature (T_f), moderator temperature (T_m), moderator density (D_m) and soluble boron concentration (C_B) is realized directly via the memory (common blocks or include files). The main disadvantage of this method is that significant changes for both codes are required. This effort has been executed e.g. within the coupled system TRACE/ PARCS.

The computational scheme of an external coupling is illustrated in Figure 2-7. Here the core is completely described by the NK code while the rest of the plant is represented by the system code. This requires that the NK code has a thermal-hydraulic module. In this case the exchange of parameters between the NK and TH code is minimal, namely the boundary conditions at the core inlet and outlet, such as pressure (p), mass flow (G) and enthalpy (H) or coolant temperature. One of the advantages of this coupling type is that it does only require marginal changes within the NK and TH codes. An example is the coupled DYN3D-ATHLET code system [19].

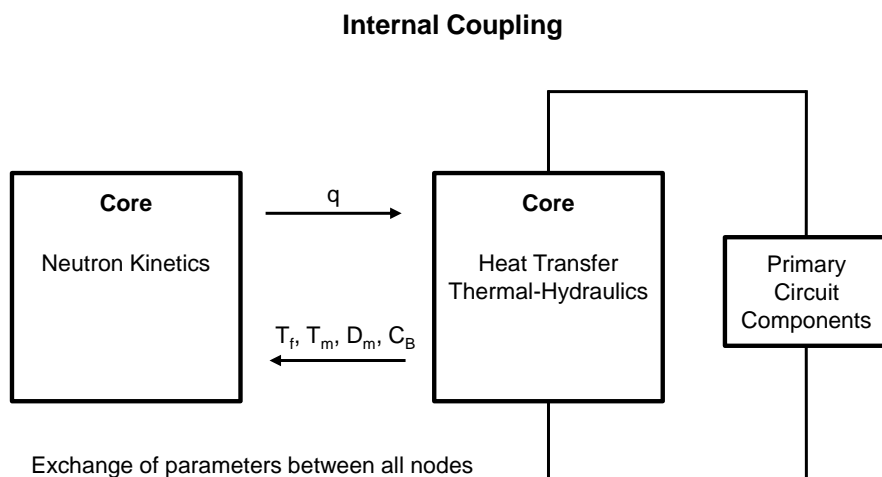


Figure 2-6: Sketch of computational scheme of an internal coupling between TH and NK from [58].

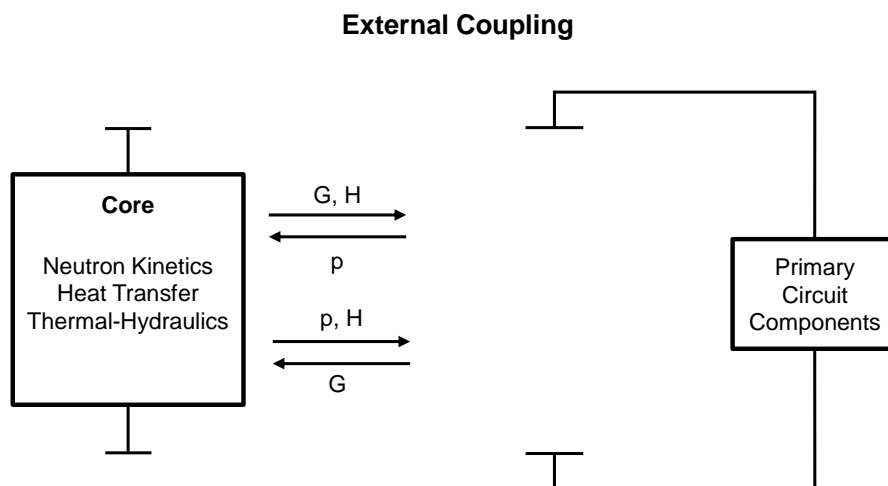


Figure 2-7: Sketch of computational scheme of an external coupling between TH and NK from [58].

2.3.2 Spatial coupling between the neutronic and thermal-hydraulic domains

The information exchange between the two domains is very important to assure that the physical phenomena are described correctly. This is performed based on the spatial mapping of the neutronic and thermal-hydraulic computational domain, in both radial and axial direction. In the majority of nodal coupled TH/NK codes, specific matrices and vectors have been programmed to ensure the storage and retrieval of the feedback parameters at a nodal level between the two domains. Provisions must be also foreseen to guarantee the consistency of data exchange in cases where the neutronic radial discretization of the core (mostly 1 FA per node) differs from the thermal-hydraulic one (core is mostly represented by much fewer number of parallel channels than the number of neutronic nodes).

In the European NURISP project [59] a novel approach has been developed for a flexible coupling of multiphysical codes based on the automatic superposition of the spatial meshes of the participating domains (NK and TH). It utilizes in-built interpolation function scheme in case of mismatch between the axial or radial core discretization of the involved domains.

Figure 2-8 shows an example of the radial mapping of a BWR used for the Peach Bottom reactor transient [33]. The 764 fuel assemblies of the reactor are represented by 33 thermal-hydraulic channels (see also numbers 1-33 in Figure 2-8). Thereby, the radial reflector (number 0) is not modelled as channel by the TH code.

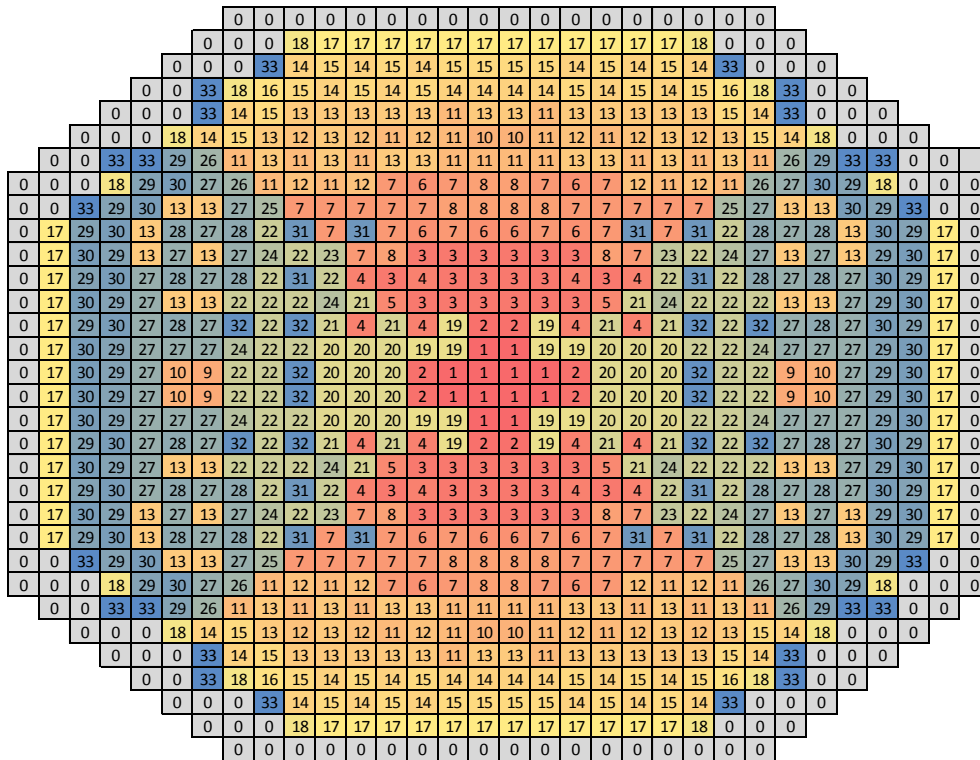


Figure 2-8: Typical radial reactor core mapping of the Peach Bottom reactor from [33] later used for reactor transient calculations.

Often the axial discretization of the TH domain differs from the one of the neutronic domain, as illustrated in Figure 2-9. In such situations, the coupling schemes must serve appropriate interpolation / extrapolation models to allow a consistent exchange of the feedback parameters between the domains; improper mappings may lead to inaccurate prediction of safety parameters [60].

In case that the number of thermal-hydraulic channels is lower than the number of fuel assemblies, care must be taken if fuel assemblies are merged to representative thermal-hydraulic channels. This grouping can be performed taking into account e.g. fuel assembly power, burnup, type of fuel assemblies (MOX, UO₂), FA foot, etc.. The criteria for the FA grouping are problem dependent.

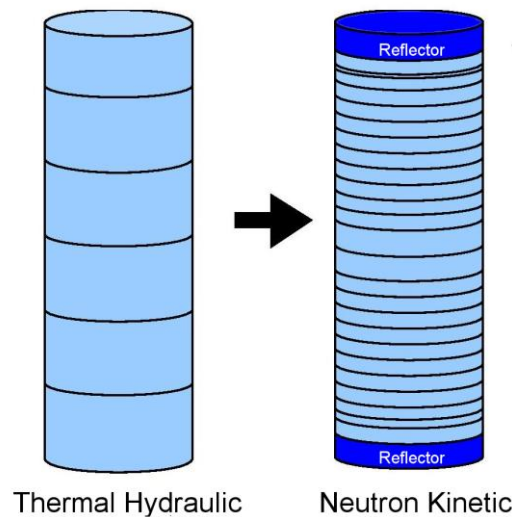


Figure 2-9: Schematic example of a different axial mapping of TH and NK domains.

2.3.3 Temporal coupling

The temporal coupling and the time step selection plays an important role in the coupling of TH and NK codes. One code must act as the Master and the other as Slave. In case of the TRACE/PARCS package, the TH module TRACE is the master and thus time step advancement controller. During one time step, the TH parameters (pressure, coolant/fuel temperature, void fraction etc.) are calculated by the TH code and then passed to the NK code. The NK code uses these parameters to update the cross-sections, based on the spatial mapping, and to calculate the local fluxes. Then these data such as the local power are returned as feedback to the TH model.

In addition to the time step size, the timing of the data exchange between the neutron-kinetics and the thermal-hydraulics code is important. This can be classified into three different categories of coupling:

- explicit,
- implicit or,
- semi-implicit.

Using the explicit coupling, first the master code converges and sends its parameters to the slave. After the slave code is converged, the data are transferred back to the master and a new time step size is determined by the master code and the process is repeated for each new time step. Such a scheme is depicted in Figure 2-10. The coupling between the TH code TRACE and the NK code PARCS is an example of explicit operators splitting coupling method.

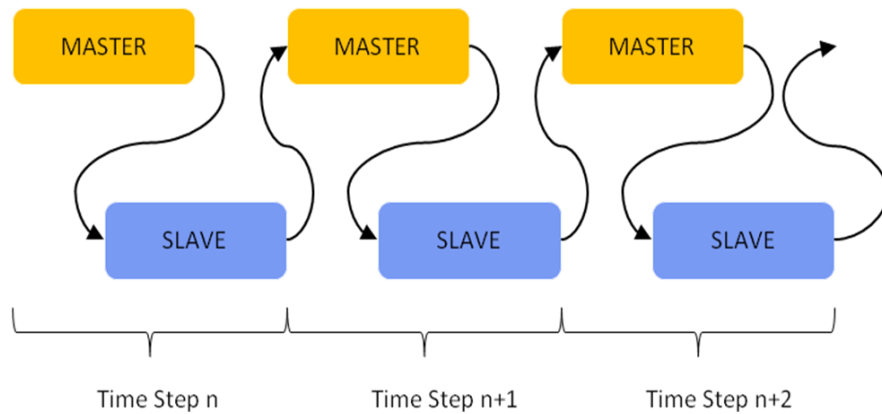


Figure 2-10: Explicit process flow for coupled Master/Slave code system.

The semi-implicit method uses feedback parameters from a mix of a previous time step and from the actual time step. Such a coupling scheme is realized e.g. in the TH/NK code system TRAC-PF1/NEM. The disadvantage of the explicit and semi-implicit methods is, that small time steps are required to maintain the accuracy of exchanged parameters. Instabilities can emerge during the transient caused by non-convergence of these parameters due to the mixing. Therefore, the current trends are directed towards an implicit time integration scheme. In this type of coupling not only the individual codes are converged but the feedback parameters are also converged. In [61] Watson describes an implicit time-integration method for the TH/NK system TRACE/PARCS.

2.4 Uncertainty and Sensitivity Methodologies

2.4.1 Quantification of uncertainties

The application of best-estimate (BE) thermal-hydraulic system codes and of TH/NK coupled codes for the safety evaluation of nuclear power plants requires the quantification of the embedded code's uncertainties [62], [63], [64]. Code predictions are uncertain due to several sources such as:

- code or model uncertainties,
- representation uncertainties,
- scaling uncertainty,
- plant uncertainty and
- user effect.

These uncertainties, for example, originate from scatter of measured values, approximations of modeling, variation or imprecise knowledge of initial and boundary conditions. Further most of the available experiments are performed on small scales compared to the plant size. Computer code models developed based on these experiments can simulate the complex

behavior of a reactor plant under accident conditions only in a simplified way. More details about the different uncertainties may be found in [62].

Uncertainty due to imprecise knowledge of parameter values in calculations is quantified by ranges and probability distributions. These distributions have to be considered for the input parameters instead of taking one discrete value only [65].

The propagation of all these uncertainties through the BE code permits the quantification of the uncertainty range of the calculations. Thereby the main objective of the safety analysis is to demonstrate in a robust way that all safety requirements are met. This applies if sufficiently large safety margin exists between the acceptance criterion, for example the Peak Cladding Temperature (PCT) and the upper limit of the calculated cladding temperature distribution, as schematically illustrated in Figure 2-11. Using this "Best Estimate Plus Uncertainty" (BEPU) method, more precise specification of safety margins is possible and thus greater operational flexibility can be achieved as using conservative calculation methodologies.

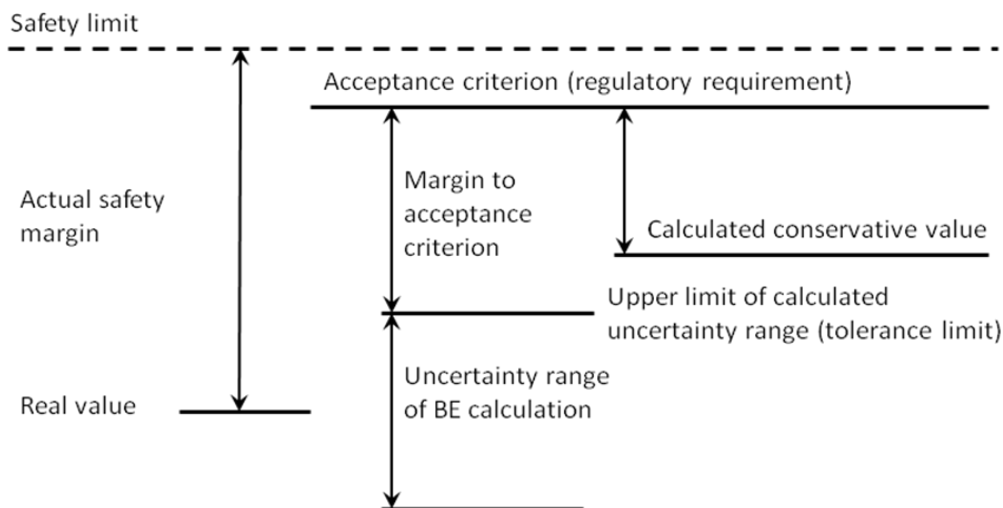


Figure 2-11: Schematic concept of safety margins

Several methods has been proposed for the quantification of the uncertainty of best-estimate TH computer codes, among others are

- a) the GRS method based on SUSA [65],
- b) the CIAU method of the Pisa university [66],
- c) the Code Scaling, Applicability and Uncertainty" method (CSAU) [67] and
- d) the Cacuci method based on the adjoint sensitivity [68].

One of the most applied methods is the GRS-method which is based on the Monte Carlo sampling approach. In this method the uncertainties of the input and model parameters are propagated to the output parameters.

Uncertainty methodologies are being developed not only by private companies but also by regulators and research institutions [62][66][72]. A large number of applications were performed for thermal-hydraulic system codes [73]. There are only a few investigations devoted to TH/NK coupled simulations [74][76].

The methods are mainly based on the two approaches:

- propagation of code input errors
- propagation of code output errors

A third and independent approach is that proposed by Cacuci, in which experimental and calculated data are combined mathematically to predict uncertainties [66]. The first two approaches, illustrated in Figure 2-12 and Figure 2-13, will be considered in more detail.

Performing TH/NK coupled simulations, the quality of the overall predictions are also determined by the neutron physical data (XS) and the way how they were generated by the lattice codes. Currently in the frame of the OECD UAM-Benchmark [69] different methods for the uncertainty quantification and propagation in coupled simulations are being developed. Two of these approaches are:

- the XSUSA statistical approach based on SUSA code [70]
- the “Two-Step” method that combines generalized perturbation theory (GPT) and the stochastic sampling [71]

Both methods are based on the SCALE code and several runs are required to generate a complete set of XS-files for each assembly type. Also SCALE is limited by the current GPT capabilities. Here in this work an alternative way based on PARCS/SUSA to assess and propagate the uncertainty of macroscopic XS and kinetics parameters will be presented in section 3.5.

2.4.1.1 Propagation of Code Input Errors

This approach uses a statistical variation of uncertainty afflicted input parameters, in order to calculate the propagation of errors through the code. Typically the model of a system code has approx. 10^5 input parameters. As uncertainty calculations for all input variables lead to unacceptably high computational costs, usually only a few set of parameters ($<10^2$) are selected. This can be done by identifying the most relevant phenomena by experts for a selected plant scenario and list them in a Phenomena Identification and Ranking Table (PIRT) [76]. For each considered parameter in the analysis, then a Probability Density Function (PDF) and the range of variation has to be assigned. The number of required calculations can be determined using the Wilk's formula (see also section 3.5).

Methods using this approach are the GRS method and CSAU propagated by the U.S. NRC. The drawback of these methods is the need for a technical evaluation, the identification of the uncertainty parameters and the determination of the PDFs. Nevertheless, this approach is, the currently most adopted procedure, endorsed by industry and regulators.

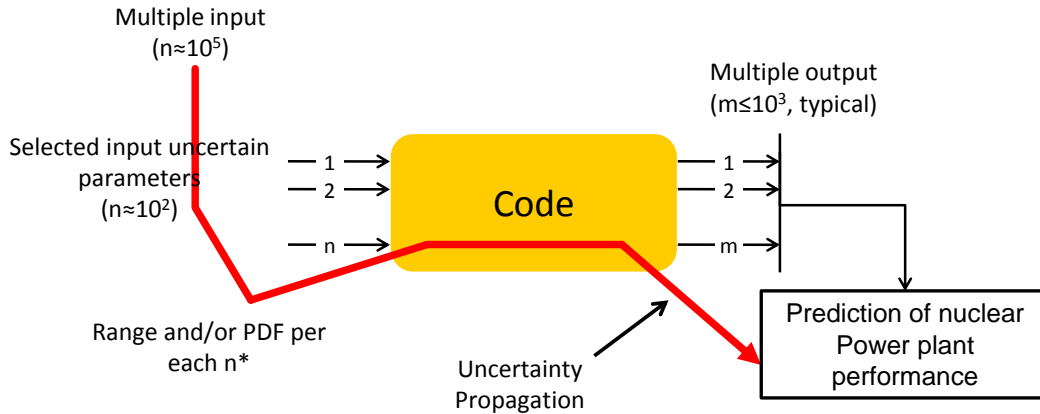


Figure 2-12: Propagation of input uncertainties through the computational scheme.

2.4.1.2 Propagation of Code Output Errors

This approach is based on the assumption that the difference between the results of simulations and experimental data is the result of errors. The experimental data originate mostly either from test facilities or real plants. The errors are processed and extrapolated to obtain the uncertainty of the code. The advantage of this approach compared to the previous one is that no input parameters have to be identified. However, it requires a huge amount of experimental data covering all conceivable accidental scenarios. This requires the establishing of an adequate error database, which takes many resources. Another drawback of this method is that the combination of errors, which originate from different sources, is not physical and needs a detailed validation [66]. Representative for this approach is the UMAE-CIAU (Uncertainty Method based upon Accuracy Extrapolation „embedded“ into the Code with Capability of Internal Assessment of Uncertainty) method and is used only in a few cases by industry.

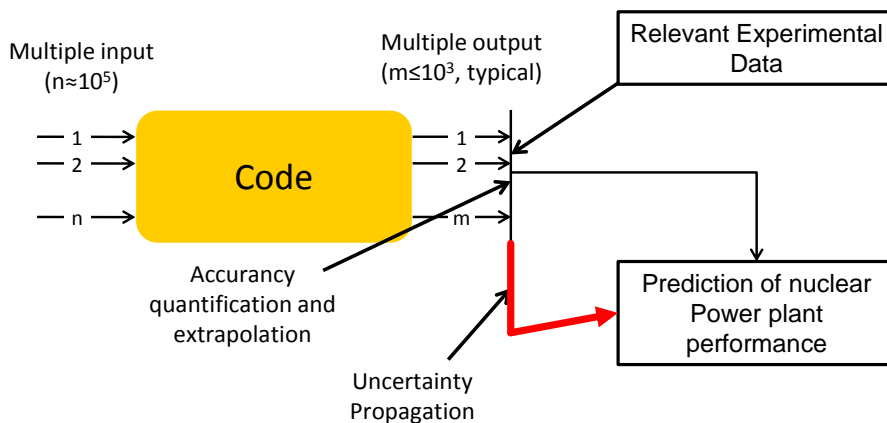


Figure 2-13: Propagation of output uncertainties through the computational scheme.

2.4.2 Quantification of the sensitivity

The uncertainty analysis should also be complemented by a sensitivity study, which identifies the major parameters influencing a target safety parameter. In this context, sensitivity analysis means evaluation of the effect of variation in the input or modelling parameters on code results, whereas uncertainty analysis means the deviation of quantitative statements on the uncertainty of computer code results from the uncertainties of the input parameters propagated through the model [62].

The aim of sensitivity analysis is to assess the rate of change in the output of a model with respect to changes of the model inputs. Sensitivity is measured by using regression or correlation techniques from sets of input parameters and from the corresponding output values allowing the ranking of the uncertain input parameters in relation to their contribution to the output uncertainty [66]. A large array of randomly selected input parameters values and calculated output values permits the determination of the parameter's sensitivity by using correlations such as:

- the ordinary Pearson product-moment correlation coefficient and
- the Spearman's rank correlation.

Details and more techniques for parameter sensitivity analysis are described by Hamby in [78].

3 Computational Route for 3D Analysis of BWR Transients

After a critical review of the numerical simulation codes available for the multidimensional analysis of BWR transients, a set of codes has been selected to cover the whole computational chain from the cross-section generation to the coupled TH/NK plant simulations. During the selection process, the availability of the codes including the source, their prediction capability regarding the goals of the thesis and the developer team were considered. The selected computational route consists of the following codes:

- a) Lattice physics: SCALE
- b) Reactor dynamics: PARCS
- c) Thermal-hydraulic system code: TRACE
- d) U&S quantification: SUSANA

In the next subchapters, a description of this computational route and of the involved codes is given.

3.1 Short description of the computational route

A schematic representation of the computational route is given in Figure 3-1, where the sequence and the interrelation of the involved codes to perform a 3D transient reactor dynamic simulation are depicted. At present, mostly commercial tools such as CASMO are used for the generation of complete cross-section libraries of PWR and BWR real core loadings. No references were found for the generation of nodal cross-section libraries of BWR cores using SCALE6/NEWT/TRITON for a transient analysis with coupled N/TH codes.

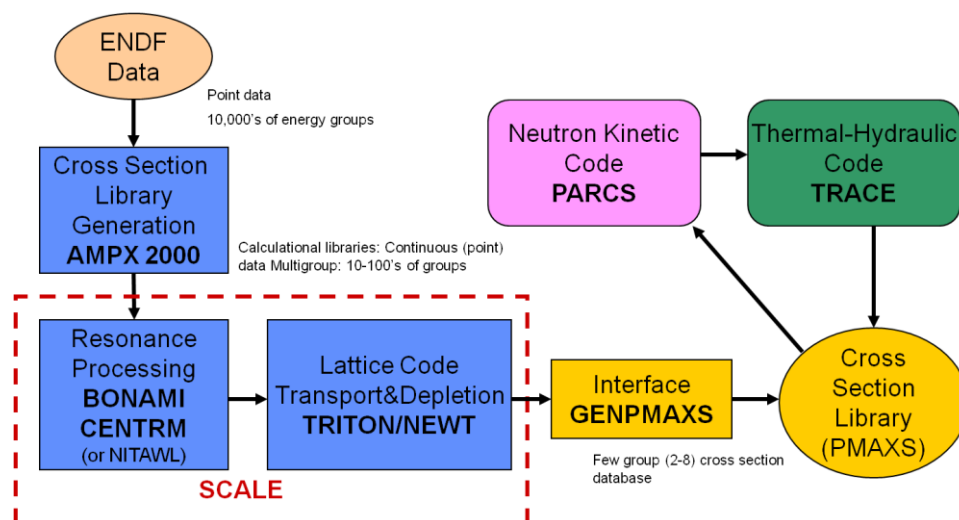


Figure 3-1: Computational route with selected code systems applied.

The calculation of problem dependent cross-sections is performed by the lattice physics capability of the SCALE code system. The generated cross-section files are converted with the GenPMAXS (Generation of the Purdue MAcroscopic XS set) code into the Purdue MAcroscopic XS format PMAXS for the use in the reactor dynamic code PARCS during a coupled TRACE/PARCS calculations. The quantification of the uncertainty of TRACE and PARCS is performed with the SUSA code.

3.2 Lattice Physics Codes

The basic microscopic cross-section data needed by the lattice physics codes is available in international Evaluated Nuclear Data Files (ENDF), JENDL or JEFF. In SCALE6 [37] the AMPX 2000 master file contains continuous data of 10-100's energy groups built based on the ENDF library. For problem dependent calculations of cross-sections, the lattice module NEWT make use of the AMPX 2000 master file via the TRITON module. NEWT solves the neutron transport equation in a 2D arbitrary geometry based on the Extended Step Characteristic (ESC) approach. In addition, the modules BONAMI (BONDarenko AMPX Interpolator) and CENTRM (Continuous ENergy TRAnsport Module) are used for the prediction of the resolved and unresolved resonances of important nuclides such as U-238, etc.

With SCALE6/TRITON/NEWT problem dependent macroscopic cross-sections can be generated for different fuel assembly types of a core loading taking into account relevant parameter ranges of thermal-hydraulic parameters and burnup steps.

Hereafter, the main tasks of selected SCALE modules will be shortly described.

TRITON/NEWT Lattice Physics Depletion

TRITON is a SCALE control module that automates 2D and 3D lattice physics depletion calculations [79]. It provides the possibility to solve the transport equation in a 2D arbitrary geometry using the flexible mesh discrete ordinates NEW Transport Algorithm (NEWT) [81] or in a 3D Monte-Carlo based approach using KENO [80]. In this work the TRITON/NEWT depletion sequence (T-DEPL) is used to generate homogenized cross-section data for a BWR core (Figure 3-2).

The required input file contains all geometrical and material (mixtures) data, as well as the information about the lattice cell structure for each fuel assembly or material zone of a given core. The SCALE driver reads the input file and calls TRITON, which prepares the input file for the resonance treatment.

Resonance self-shielding is predicted by the BONAMI module [83] in the unresolved resonance range based on the Bondarenko method and by CENTRM [84] and PMC [85] in the resolved resonance range. The module CENTRM computes the continuous-energy spectra in 0-D or 2-D geometry by solving the Boltzmann transport equation using a combination of pointwise and multigroup nuclear data. By this way, problem specific fluxes on a fine energy mesh (>10 000 points) are calculated for later use to generate self-shielded multigroup cross-sections for subsequent transport calculations. The multigroup data

processing is performed by the PMC module, which reads the CENTRM continuous-energy flux spectra and cross-section data. The results are problem dependent, group averaged cross-sections as required by NEWT for the multigroup calculations [82].

t-depl depletion sequence

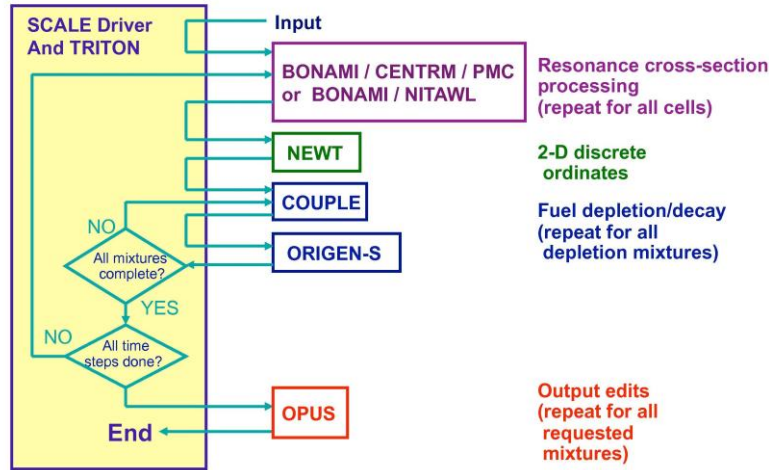


Figure 3-2: Flowchart for TRITON/NEWT depletion sequence [82].

The NEWT ESC approach [86] allows a spatial discretization of a fuel assembly on an arbitrary mesh structure. This approach uses arbitrary polygons for the accurate representation of non-orthogonal geometries such as a fuel-assembly lattice.

Once the NEWT transport calculation is finished, the neutron flux and cross-section data are passed to the COUPLE module [87]. It processes these data to provide an updated cross-section library for the ORIGEN-S module [88]. It calculates the time-dependent concentrations, the decay heat and radiation source terms of a large number of isotopes produced by transmutation, fission or radioactive decay. After each time step, these data are passed back to the modules BONAMI/CENTRM/PMC for the calculation of the resonance self-shielding. In ORIGEN-S, the change of the concentration of a particular nuclide, N_i , in time is predicted as follows:

$$\frac{dN_i}{dt} = \sum_j \gamma_{ji} \sigma_{f,j} N_j \Phi + \sigma_{c,i-1} N_{i-1} \Phi + \lambda'_i N'_i - \sigma_{f,i} N_i \Phi - \sigma_{c,i} N_i \Phi - \lambda_i N_i . \quad (3.1)$$

$\sum_j \gamma_{ji} \sigma_{f,j} N_j \Phi$: yield rate of N_i due to the fission of all nuclides N_j

$\sigma_{c,i-1} N_{i-1} \Phi$: rate of transmutation into N_i due to radioactive neutron capture by nuclide N_{i-1}

$\lambda'_i N'_i$: rate of formation of N_i due to the radioactive decay of nuclides N_i

$\sigma_{f,i} N_i \Phi$: destruction rate of N_i due to fission

$\sigma_{c,i} N_i \Phi$: destruction rate of N_i due to all forms of neutron absorption other than fission (n- γ , n- α , n-p, n-2n, n-3n)

$\lambda_i N_i$: radioactive decay rate of N_i

The equation (3.1) is solved in ORIGEN-S either by an exponential matrix approximation or by the direct solution of the Bateman equations for nuclides with short half-lives. This procedure is repeated until all depletion steps are done.

The data generated by ORIGEN-S such as burnup, activation, build-up of fission products, photon and neutron source spectrum are reformatted by the OPUS [89] module and written in specific formats that can be read by graphic programs.

Furthermore, the cross-sections and other neutronic data such as Assembly Discontinuity Factors (ADFs), inverse neutron velocities, etc. are stored in a binary (*xfile016*) and an ASCII (*txtfile16*) cross-section output files for the subsequent use.

The version SCALE6.0 doesn't write the yields of Xenon, Iodine and Promethium into the cross-section output files *xfile016* and *txtfile16*. Therefore an own program based on PYTHON [90] to automatically extract these information from the mentioned files and write it in the PMAXS files has been developed.

For the consistent prediction of the nodal cross-sections considering the fuel depletion in a real core, the TRITON depletion sequence uses a multi-step approach based on a predictor-corrector scheme. The T-DEPL calculation consists of two parts during the iteration process:

- Transport calculations (T) are performed to predict the fluxes and create weighted cross-sections and other lattice physics parameters such as Assembly Discontinuity Factors (ADFs) and inverse neutron velocities for a given set of nuclide concentrations.
- Depletion calculations (D) are used to calculate the nuclide concentrations, which are used in the following transport calculation.

The calculations are performed stepwise by:

- Step 1: The TRITON transport/depletion calculation process started with a transport calculation (T_0) for fresh fuel concentrations.
- Step 2: Depletion calculation (D_0) for initial fuel concentrations i.e. time 0 till the mid-point of cycle 1. ORIGEN-S uses few group cross-sections weighted with the flux predicted by T_0 .
- Step 3: Transport calculation (T_1) at the middle of the cycle 1 using the nuclide concentrations predicted by ORIGEN-S at the midpoint of cycle 1 (end of D_0 calculation).

- Step 4:
 - Depletion calculation (D_{1a}) is performed over whole cycle 1 including the down time using the few group cross-sections weighted with the fluxes predicted at the midpoint of cycle 1 by T_1 .
 - Depletion calculation (D_{1b}) from D_{1a} to the midpoint of Cycle 2 using few group cross-sections weighted with the fluxes predicted at the midpoint of cycle 1 by T_1 .
- Step 5: Transport calculation (T_2) at midpoint of Cycle 2 using the nuclide concentrations predicted by D_{1b} at the midpoint of Cycle 2.

From step 6 onwards it is a repetition of step 3 and 4 until the depletion is calculated for all cycles. In Figure 3-3 this predictor-corrector procedure for a hypothetical three cycle depletion case is illustrated.

During this TRITON transport/depletion calculation process, TRITON stores the cross-section data in the cross-section output files. Thereby the user has the option to refine the solution either by defining intermediate steps for one cycle or by dividing the cycle into several subintervals. The latter approach is more accurate for cases, where cross-sections change rapidly, e.g. for fuel assembly with poison rods [82]. In this work the subintervals approach is used.

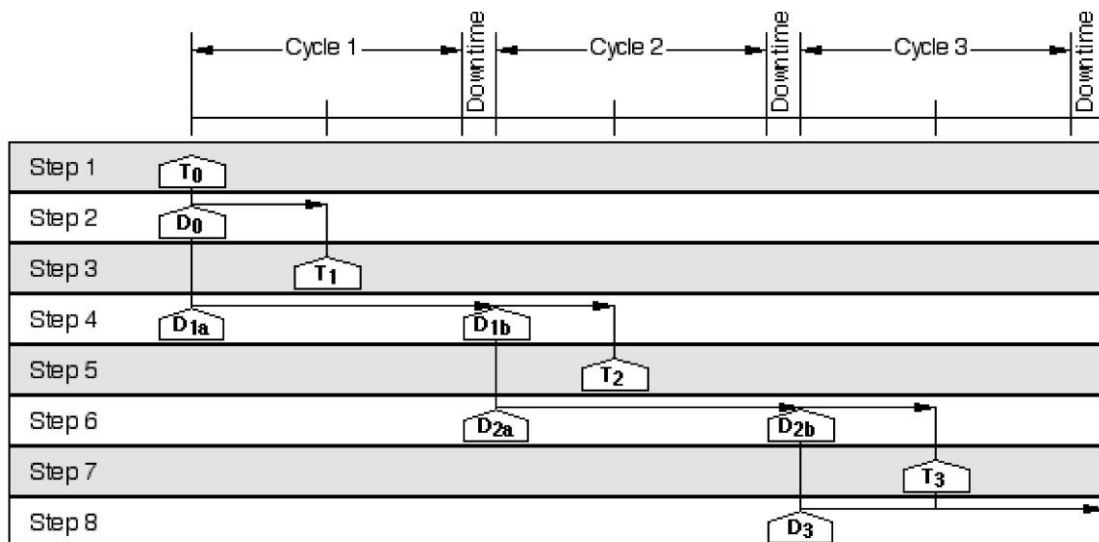


Figure 3-3: Sketch of TRITON transport/depletion calculation process [79].

3D transient reactor dynamic simulation of real cores requires the availability of nodal cross-sections for actual core thermal-hydraulic conditions during a transient scenario. These cross-sections can be calculated by the TRITON T-DEPL sequence performing so called branch calculations. TRITON supports the variation of fuel temperature, moderator temperature, moderator density, soluble boron concentration and control rod insertion. In Figure 3-4 the TRITON module sequence for branch calculations is shown. At the begin of

each depletion step, ORIGEN-S calculates the nuclide concentration of a reference state (Branch0). Then transport calculations are performed for the nuclide concentrations of Branch 0. Thereby the perturbation parameters can be combined in any order. The result of these calculations is a cross-section library, which includes macroscopic homogenized cross-sections, ADFs, pin power peaking factors and other problem dependent lattice physics data.

The automatic approach followed for the generation of 3D nodal cross-sections libraries for whole core static and dynamic simulations will be explained hereafter.

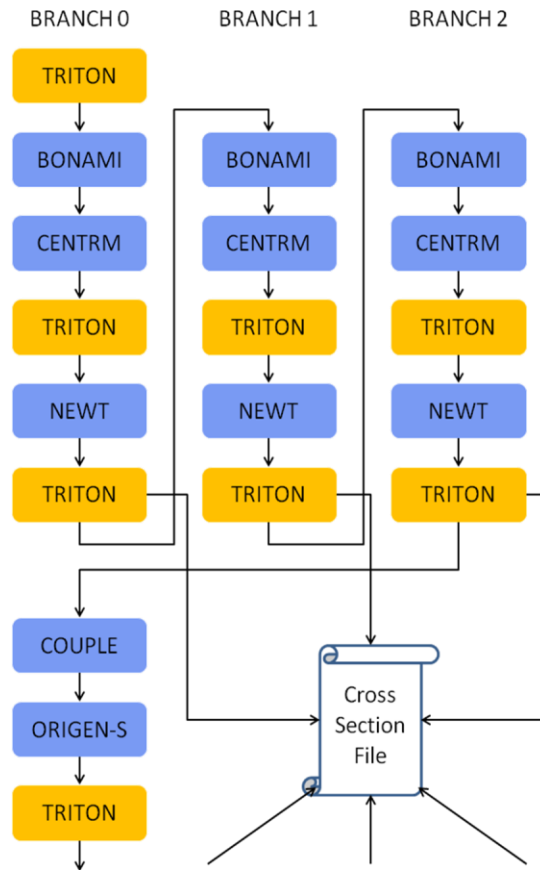


Figure 3-4: TRITON code flow for branch calculations.

Automatic Cross-section Library Generation for 3D Nodal Core Analysis

In this context, an automatic approach for the generation of nodal cross-sections in the PMAXS format based on SCALE6.0 has been developed, which complements the computational route under development by the US NRC. In Figure 3-5 the flow chart of the automatic cross-section library generation using TRITON, GenPMAXs and the developed PYTHON script is presented. The PYTHON [90] script executes the following steps:

- It calls GenPMAXS to generate PMAXS library files without yields. By this the library *noYields.PMAXS* is generated.
- It reads the yields from the standard TRITON output *TRITON.out* and inserts them into the *noYields.PMAXS* file. The new library file is called *Yields.PMAXS*.

The *Yields.PMAXS* library contains all necessary information e.g. yield of Xenon (Xe), Iodine (I), Promethium (Pm) required by PARCS to calculate the number densities of Xenon on Samarium using the equations described in section 3.3. However, this approach is only able to generate PMAXS files without consideration of different history cases.

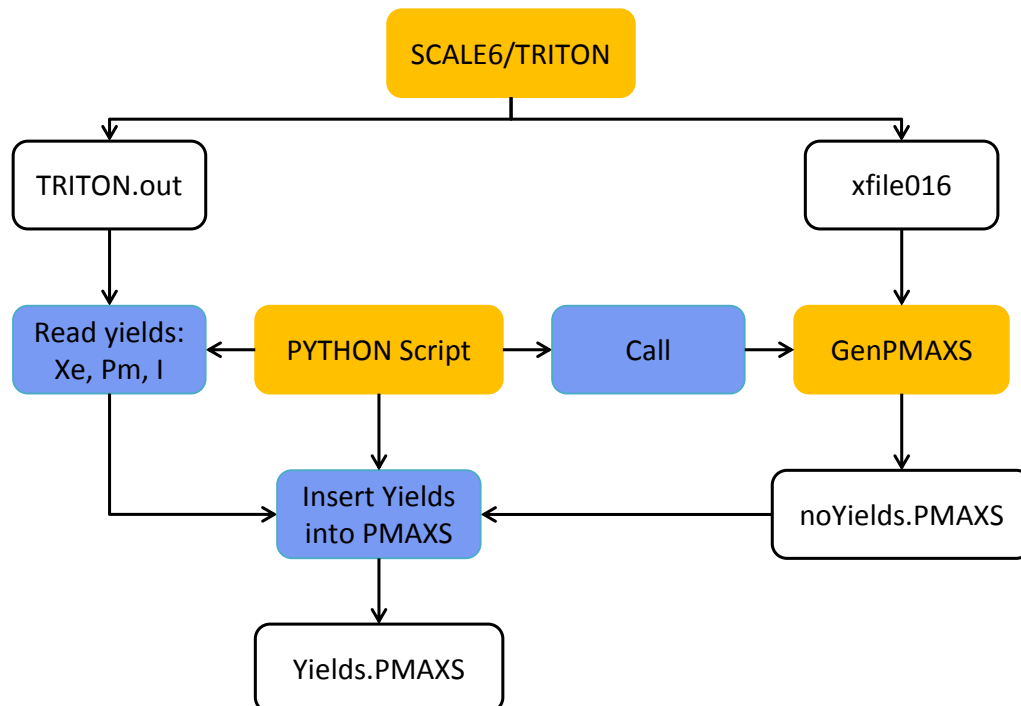


Figure 3-5: Flow chart of improved PMAXS for a single history

In order to generate nuclear data considering history effects, first different histories of a fuel assembly are computed by single SCALE6/TRITON calculations. Then the PYTHON script mentioned above is used to generate the *Yields.PMAXS* of the different cases. Afterwards a library *History.PMAXS* containing all history cases, but without considering the yields, is generated by GenPMAXS. In a last step, the yields of the single *Yields.PMAXS* files is copied to the *History.PMAXS*.

Due to an error in SCALE6.0 *xfile016*, the ADFs are not written in a correct manner in the PMAXS-files by GenPMAXS. Hence a modified version of GenPMAXS from the University of Michigan has been used. This version allows the user to order the ADFs as needed.

3.3 Reactor Dynamics

The PARCS core simulator solves the steady-state and time-dependent multi-group diffusion and low-order (SP3) transport equations in 3D Cartesian, hexagonal and cylindrical coordinates to predict the eigenvalue and the neutron flux distribution within the core. Coupled with a thermal-hydraulic system code, PARCS is able to describe the core dynamic response to reactivity perturbations caused by changes of the thermal-hydraulic conditions or control rod movements. Dedicated models are implemented in PARCS to describe e.g. the decay power, Xenon and Samarium transients, fuel depletion, the interaction between the neutronics and the thermal-hydraulics (cross-section feedback models), pin power reconstruction, adjoint flux solution, etc. There are many solvers implemented in PARCS for

the spatial discretization of the computational domain at nodal or on cell level. For example for square geometries, the "Analytical Nodal Method" (ANM), the multigroup "Nodal Expansion Method" (NEMMG), the Coarse Mesh Finite Difference (CMFD) and the Fine Mesh Finite Difference (FMFD) can be mentioned. The PARCS pin power reconstruction method e.g. requires cross-sections, shape functions and other parameters (fission yields of I, Xe and Pm, heavy metal density, etc.) which are given in the PMAXS files. PARCS is coupled to RELAP5 via the PVM Interface and is fully integrated into TRACE [14], [91].

PARCS Cross-section Model

The feedback mechanisms between the core neutronics and the thermal-hydraulics are taken into account by the cross-section model. It requires the determination of burnup dependent cross-sections (Σ) as a function of boron concentration (S_b), fuel temperature (T_f), coolant temperature (T_c), coolant density (D_c) and the control rod (Cr) fraction (α). In addition, these cross-sections must be calculated as a function of history parameters, such as control rod position and coolant density (void).

One of the first cross-section models implemented into PARCS doesn't consider the dependence of the cross-sections from burnup and history parameters [91]. The nodal cross-section (Σ) is only dependent of thermal-hydraulic parameters as shown in equation (3.2).

$$\Sigma(\alpha, T_f, T_m, D_m, S_b) = \Sigma^r + \alpha \Delta \Sigma^{Cr} + \frac{\partial \Sigma}{\partial \sqrt{T_f}} \Delta \sqrt{T_f} + \frac{\partial \Sigma}{\partial T_m} \Delta T_m + \frac{\partial \Sigma}{\partial D_c} \Delta D_c + \frac{\partial \Sigma}{\partial S_b} \Delta S_b + \frac{\partial^2 \Sigma}{\partial D_c^2} (\Delta D_c)^2 \quad (3.2)$$

In this model, the partial derivatives of a given variable are independent of the other variables. This model is therefore only applicable to certain cases in which the flow conditions are nearby the reference state. However LWR transients may cover a wide range of thermal-hydraulic states and may occur at different burnup steps. Hence, a new cross-section model has been implemented in PARCS to facilitate the calculation of cross-sections in a more accurate way than the previous methodologies. It is based on the PMAXS format that not only considers the cross-section dependence on the thermal-hydraulic state variables but also on the burnup and history parameters.

The PMAXS library contains the macroscopic cross-sections, the microscopic cross-sections of Xenon and Samarium as well as some additional parameters such as ADF, group-wise form functions, heavy metal densities, yields and information on the delayed neutrons for various branches and histories. The macroscopic cross-section Σ of node l can be described dependent on the control rod fraction C , the selected state variables S , the neighbouring fuel elements N and the history parameter H for a particular state by the following equation [51]:

$$\Sigma^l(C, S, N, H) = \Sigma^{E,l}(C, S, N, H) + N_{Xe}^l \sigma_{Xe}^l(C, S, N, H) + N_{Sm}^l \sigma_{Sm}^l(C, S, N, H) \quad (3.3)$$

As can be seen in Eq. 3.3, Xenon and Samarium are treated differently than the other nuclides, namely by the product microscopic cross-sections (σ_{Xe} & σ_{Sm}) and number densities (N_{Xe} & N_{Sm}). PARCS is able to calculate the Xenon and Samarium equilibrium and

transient conditions. The time-dependent depletion of the fission products Iodine, Xenon, Promethium, and Samarium used for updating the number densities and thus the absorption cross-sections, is described in PARCS by the following differential equations [51]:

$$\frac{d}{dt} N_I = \gamma_I \sum_{g=1}^G \Sigma_{fg}(t) \Phi_g(t) - \lambda_I N_I(t) \quad , \quad (3.4)$$

$$\frac{d}{dt} N_{Xe}(t) = \lambda_I N_I(t) + \gamma_{Xe} \sum_{g=1}^G \Sigma_{fg}(t) \Phi_g(t) - \lambda_{Xe} N_{Xe}(t) - \sum_{g=1}^G \sigma_{Xe,ag}(t) \Phi_g(t) N_{Xe}(t) \quad , \quad (3.5)$$

$$\frac{d}{dt} N_{Pm} = \gamma_{Pm} \sum_{g=1}^G \Sigma_{fg}(t) \Phi_g(t) - \lambda_{Pm} N_{Pm}(t) \quad , \quad (3.6)$$

$$\frac{d}{dt} N_{Sm}(t) = \lambda_{Pm} N_{Pm}(t) - \sum_{g=1}^G \sigma_{Sm,ag}(t) \Phi_g(t) N_{Sm}(t) \quad , \quad (3.7)$$

where the following variables are used:

- N_i : number densities of isotope I ,
- Σ_{fg} : groupwise macroscopic fission cross-section,
- Φ_g : groupwise flux,
- $\sigma_{i,ag}(t)$: groupwise absorption cross-section of isotope i ,
- γ_i : effective yield (atoms/fission) of isotope i ,
- λ_i : decay constant of isotope i .

The macroscopic cross-section Σ^E can be described by the following approximations:

$$\Sigma^E(C, S, N, H) = \sum_{i=0}^{Nc} c_i \Sigma_i(S, N, H) \quad , \quad (3.8)$$

$$\Sigma_i(S, N, H) = \Sigma^r(H) + \Delta \Sigma_i^{CR}(H) + \sum_{j=2}^{Ns} \Delta S_j \frac{\partial \Sigma_i}{\partial S_j} (S_j^m, N^r, H) + \sum_{j=1}^4 \left(\sum_{k=1}^{Nn} n_{j,k} \frac{\partial \Sigma_i}{\partial n_k} (S, N_{j,k}^m, H) \right) \quad (3.9)$$

in which the parameters denote:

- C : fraction of control rod type, $C = [c_1, \dots, c_{Nc}]$
 N_c = number of types,
- S : state variables of the current node, $S = [s_2, \dots, s_{Ns}] = [DC, PC, \dots]$
 N_s = number of state variables,
- N : difference of state variable between 4 neighbouring assemblies and the current node
 $N = [(n_{1,1}, \dots, n_{1,Nn}), (n_{2,1}, \dots, n_{2,Nn}), (n_{3,1}, \dots, n_{3,Nn}), (n_{4,1}, \dots, n_{4,Nn})]$,
 N_n = number of state variables for the neighbour information,
- H : history state.

3.4 The Thermal-Hydraulic System Code TRACE

The best-estimate code TRACE solves the fluid dynamic equations for one - and two-phase flows in one or three dimensions based on the two fluid approach. To close the system of equations representing the mass, momentum and energy conservation for the vapour and liquid phase, additional constitutive relations are needed. They describe the heat transfer on vertical and horizontal flow patterns as well as the pressure drop, etc. Furthermore TRACE contains specific models e.g. for heat conduction in structures, transport of Boron in the liquid phase and non-condensable gases in the vapour phase, reflooding, temperature stratification, critical flow, level tracking, reactor kinetics, etc.

The code TRACE is written in a modular way and it consists of several components allowing to represent all important systems and subsystems of a nuclear power plant or experimental facility. Dedicated components are present for BWR and PWR such as the CHAN component (BWR fuel assembly representation), SEPARATOR component (BWR steam separator and dryer representation) PRESSURIZER (PWR pressurizer representation). The VESSEL component permits the representation of 3D flow conditions within the reactor pressure vessel of both PWR and BWR. It can be used as a 1D, 2D or 3D component.

TRACE simulation capabilities covers the analysis of both steady state and transient behaviour of LWR in a wide range of operational transients and postulated design basis accidents. Transients with strong interactions between the core neutronic and thermal-hydraulics can be described with either the in-built point-kinetic model or coupled by the 3D core simulator PARCS.

Mass Conservation Equations:

The mixture and the vapour mass conservation equations in TRACE with α as phase indicator are described in eq. (3.10) and eq. (3.11), where the indices "g" and "l" refer in each case to the vapour or liquid phase. Γ represents the interphase mass transfer rate from the liquid into the gas phase. ρ is the coolant density and v the coolant velocity.

$$\frac{\partial[\alpha\rho_g + (1-\alpha)\rho_l]}{\partial t} + \text{div}[\alpha\rho_g\bar{v}_g + (1-\alpha)\rho_l\bar{v}_l] = 0, \quad (3.10)$$

$$\frac{\partial(\alpha\rho_g)}{\partial t} + \text{div}(\alpha\rho_g\bar{v}_g) = \Gamma. \quad (3.11)$$

Momentum Conservation Equations:

The momentum conservation equations, eq. (3.12) and eq. (3.13) are formulated as the balance of the momentum flux density (or equivalent surface forces) and body forces on the fluid, where c_i describes the momentum exchange term due to interphase friction, c_{wl} and c_{wg}

the wall friction and form loss terms. Γ describes the interphase mass transfer term and g is the acceleration term due to the gravitation.

$$\begin{aligned} \frac{\partial \bar{v}_l}{\partial t} + (\bar{v}_l \text{ grad}) \bar{v}_l = & -\frac{1}{\rho_l} \text{grad } P + \frac{c_i}{(1-\alpha)\rho_l} |\bar{v}_g - \bar{v}_l| (\bar{v}_g - \bar{v}_l) + \\ & -\frac{\Gamma^-}{(1-\alpha)\rho_l} (\bar{v}_g - \bar{v}_l) - \frac{c_{wl}}{(1-\alpha)\rho_l} |\bar{v}_l| \bar{v}_l + \bar{g} \end{aligned} \quad (3.12)$$

$$\begin{aligned} \frac{\partial \bar{v}_g}{\partial t} + (\bar{v}_g \text{ grad}) \bar{v}_g = & -\frac{1}{\rho_g} \text{grad } P - \frac{c_i}{\alpha\rho_g} |\bar{v}_g - \bar{v}_l| (\bar{v}_g - \bar{v}_l) + \\ & -\frac{\Gamma^+}{\alpha\rho_g} (\bar{v}_g - \bar{v}_l) - \frac{c_{wg}}{\alpha\rho_g} |\bar{v}_g| \bar{v}_g + \bar{g} \end{aligned} \quad (3.13)$$

Energy Conservation Equations:

The energy balance equations are expressed as a mixture balance equation (3.14) and the vapor balance equation (3.15). They describe the temporal change of internal energy in the control volume (term 1), the in- and out-going thermal energy flows (term 2), the reversible volume change energies $P \cdot \text{div}(\alpha \cdot v_g)$ and $P \cdot \text{div}[\alpha \cdot v_g + (1-\alpha) \cdot v_l]$, the wall heat fluxes q_{wl} and q_{wg} , the dissipation q_{dlv} and q_{dg} as well as the interphase energy exchange q_{ig} as result of heat flows of the temporal change of the vapor content $P \cdot \partial\alpha/\partial t$ and the mass exchange Γ .

$$\begin{aligned} \frac{\partial [\alpha\rho_g e_g + (1-\alpha)\rho_l e_l]}{\partial t} + \text{div}[\alpha\rho_g e_g \bar{v}_g + (1-\alpha)\rho_l e_l \bar{v}_l] = \\ -P \text{div}[\alpha \bar{v}_g + (1-\alpha) \bar{v}_l] + q_{wg} + q_{wl} + q_{dlv} \end{aligned} \quad (3.14)$$

$$\frac{\partial \alpha\rho_g e_g}{\partial t} + \text{div}(\alpha\rho_g e_g \bar{v}_g) = -P \frac{\partial \alpha}{\partial t} - P \text{div}(\alpha \bar{v}_g) + q_{wg} + q_{dg} + q_{ig} + \Gamma h'_v \quad (3.15)$$

3.5 Uncertainty and Sensitivity Quantification Method for Coupled Codes

For the quantification of the uncertainty and sensitivity of the thermal-hydraulic system code TRACE and the reactor dynamic code PARCS, the SUSA software package has been selected. SUSA is a statistical tool based on Monte Carlo sampling for the uncertainty propagation of the input to the output parameters [74] .

To quantify the range and the state of knowledge about all uncertain parameters for a specific scenario Probability Density Functions (PDFs) are used. The selected uncertain parameters are simultaneously varied by random sampling according to given PDFs.

For the quantification of the code's uncertainty, the SUSA tool needs to be coupled with e.g. TRACE, PARCS, etc. Then several runs of the thermal-hydraulic and/or neutron physical code are necessary to get the information about the uncertainty and sensitivity. The number of runs depends on the requested probability content and confidence level of the statistical tolerance limits chosen in SUSA for the uncertainty statements of the results. The required minimum number n of runs is given by Wilks' formula in eq. (3.16) for one-side and in eq. (3.17) for two-sided tolerance limits as follows:

One-sided tolerance limits is expressed by:

$$1 - \alpha^n \geq \beta \quad , \quad (3.16)$$

while for two-sided tolerance limit the following relation is valid:

$$1 - \alpha^n - n(1 - \alpha)\alpha^{n-1} \geq \beta \quad . \quad (3.17)$$

Here β is the upper confidence level for the chosen α fractile. The fractile indicates the probability content of the probability distributions of the code results (e.i. $\alpha = 95\%$ means that the fuel temperature is below the tolerance limit with at least $\alpha = 95\%$ probability).

For the case of a two sided tolerance limit, with a 95 % fractile and a confidence level of 95 %, the minimum number of runs is 93. Consequently, the number n of code runs is independent of the number of selected uncertain input parameters. They depend only on the percentage of the fractile and on the desired confidence level percentage.

In SUSA different methods such as Pearson and Spearman (see also section 2.4.2) are implemented to evaluate the parameter sensitivity which is based on regressions or correlation techniques that are applied to the sets of input parameters and to the corresponding output values. Thereby the ranking of the uncertain input parameter in relation to their contribution to output uncertainty can be calculated. In SUSA both scalar and index dependent (e.g. time) uncertainty and sensitivity analysis can be performed.

Here the uncertainty module developed for PARCS [92] is adapted, modified and extended to for the use for U&S investigation of BWR transients. The modules ModUnclInfo and

ModUncVarM are integrated in the PARCS source code. ModUncVarM contains the module definitions, whereas ModUncInfo reads the random uncertainty values, and stores them in the Neutronic_Unc.dat. Finally, it calculates new cross-section data for the uncertainty quantification. According to this approach, there are four ways for the modification of the cross-section data:

- Type 1: value assignment Param = Value
- Type 2: fractional variation Param = Param*(1.0 + Value)
- Type 3: addition Param = Param + Value
- Type 4: product Param = Param * Value

Currently, it is possible to vary 22 reactor kinetic parameters contained in the PMAXS libraries. These are the fast and thermal $\Sigma_{transport}$, $\Sigma_{absorbtion}$, $\Sigma_{fission}$, $\nu\Sigma_{fission}$, $\Sigma_{scattering}$, $\kappa\Sigma_{fission}$, σ_{Xe} , σ_{Sm} , ADF, inverse velocity the fission yields and the delayed neutrons constants λ and β . Figure 3-6 shows the flow chart of the modified PARCS calculation. The reactor kinetic parameters are modified by PARCS immediately after they are read from the PMAXS files. No other changes has to be done to PARCS.

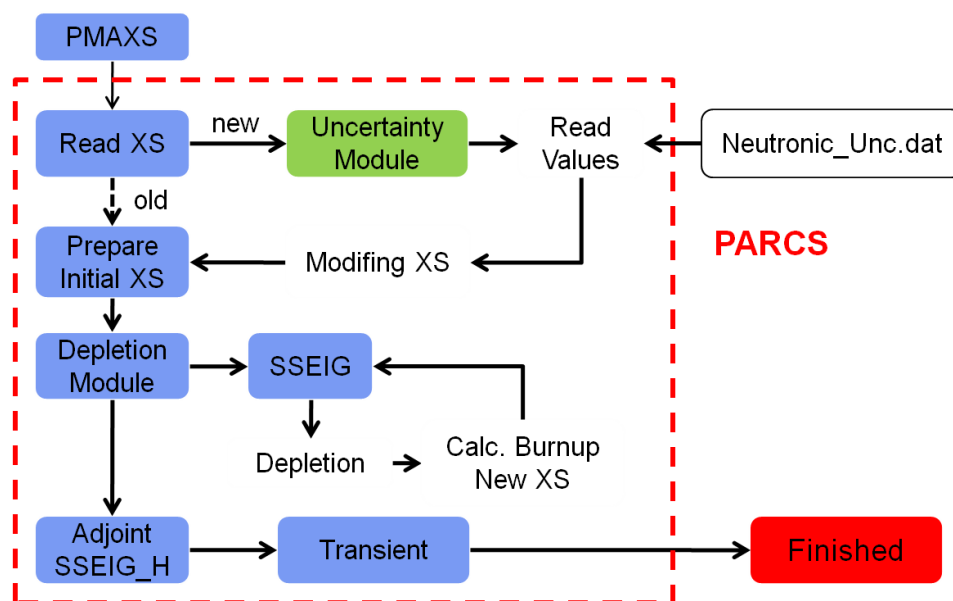


Figure 3-6: Schematic flow chart of the modified PARCS calculation incorporating an uncertainty module.

In Figure 3-7 the sequence of the uncertainty quantification of the reactor kinetic parameters of TRACE/PARCS is shown.

First of all the analyst has to select the number of uncertain parameters and for each of them to define the reference value, the range of variation (reference, maximum and minimum value) and the type of probability distribution (normal, uniform, etc.) including the probability density function (PDF) in SUSA. Depending of the probability content and confidence level fixed by the analyst, SUSA will randomly combine the selected uncertain parameters and

finally generate N sets of parameters. Afterwards a PYTHON script reads the N parameter values, prepare the “*Neutronic_Unc.dat*” file, generate N input decks for TRACE/PARCS and finally it will start successively the N TRACE/PARCS runs. In advance a TRACE stand-alone calculation is performed for all subsequent runs. For each TRACE/PARCS run first the steady-state case is calculated, before running the transient. Once all calculations are finished, another PYTHON script reads the parameters of interest such as core power and Fuel Temperature (TF) from the PARCS summary files and transform them into the SUSA conform format. Finally SUSA reads in the data generated with the PYTHON script from the TRACE/PARCS run to perform the uncertainty and sensitivity quantification.

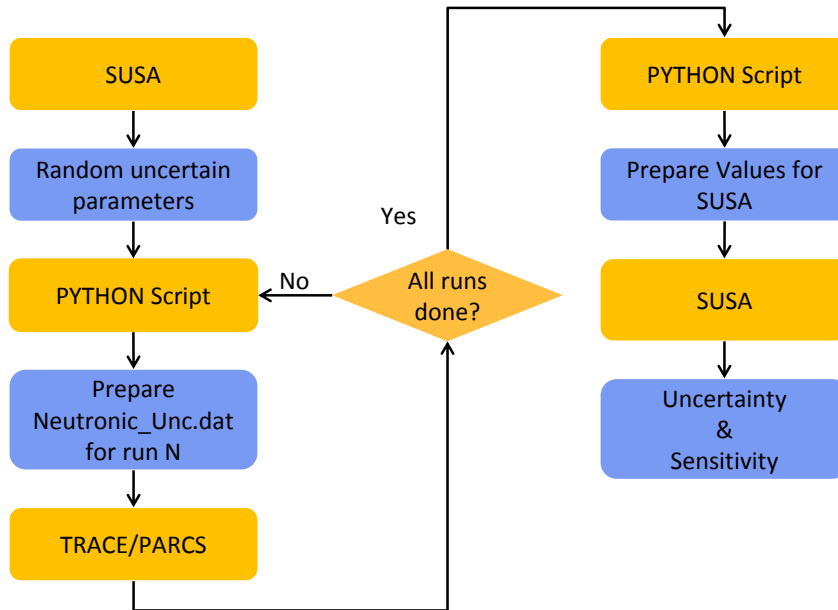


Figure 3-7: Flow chart of SUSA uncertainty quantification of TRACE/PARCS.

4 Generation of nodal Cross-sections for a Reference BWR Core

For the generation of nodal cross-sections for a 3D transient simulation with TRACE/PARCS detailed data of each fuel assembly (FA) type are mandatory. This necessitates the exact geometry of the fuel assemblies including canister, water rods, fuel rods, burnable poisons and absorber elements as well as of the fuel assembly feet and head including the geometry of the radial reflector. The material composition of all fuel assemblies e.g. nuclide inventories, burnup, enrichment, density, etc. are also required for the branch calculations.

The reference plant considered is a German BWR of type-72 (BWR-72). As a turbine trip occurred during the 13th cycle, a set of cross-sections are generated for the core loading of this cycle. The required data are obtained from [93].

4.1 Main BWR-72 Plant Characteristics

The reference BWR-72 plant has internal pumps and the core loading consists of different fuel assembly types. Since the information about the reactor building, containment, does not affect the modelling of the turbine trip event, they are not discussed here. The main thermal-hydraulic parameters of the reference plant are summarized in Table 4-1.

Table 4-1: Main thermal-hydraulic parameters of the BWR-72 reference plant.

Parameters	Values	Units
Thermal reactor power	3840	MW
Pressure RPV outlet	70.6	bar
Saturated steam temperature RPV outlet	286	°C
Core mass flow	14300	kg/s
Steam mass flow RPV outlet	2076	kg/s
Steam moisture RPV outlet	0.02	mass-%
Feed water temperature	175	°C
Steam pressure turbine inlet	67	bar
Steam temperature turbine inlet	283	°C
Number and redundancy of feed water pumps	3 x 50	%
Number and redundancy of condenser pumps	3 x 50	%
Number of condensation system filters	4	-
Number of recirculation pumps	8	-
Rated flow	8731	m ³ /h
Rated head	31.1	m
Rated speed	30.63	s ⁻¹
Number of pre.heater lines HP / LP	2 / 2	-
Number and redundancy of main coolant water pumps	3 x 33.3	%

The reactor pressure vessel (RPV) with the internals is illustrated in Figure 4-1. The control rod drives and guide tubes enter the RPV from the bottom. The eight Main Recirculation

Pumps (MRP) are equal positioned in the downcomer. Their main task is to maintain a forced recirculation flow inside the RPV. Around 13000 kg/s of coolant pass through the core at nominal operation conditions.

The core consists of 784 FA positions for the different fuel rod types. Above the core, steam separators and steam dryers are located in groups. They are arranged in such a manner to assure that the steam leaving the RPV is dry enough. Also the feed water sparger, the control rod guide tubes, the core flow measurement housing tubes, the core shroud, the lower and upper grid plates are located inside the RPV. The fuel assemblies are fixed in the core by the shroud and the lower and upper grid plates.

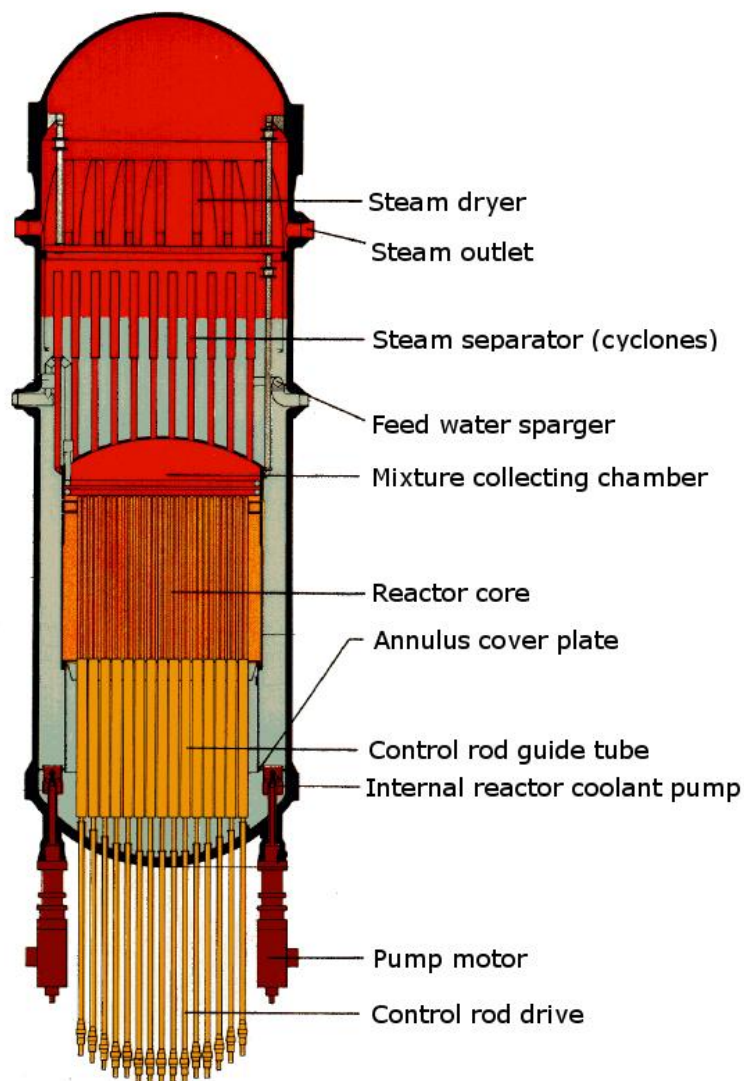


Figure 4-1: Cut through the reactor pressure vessel with the main internals of a BWR-72 reactor.

The main technical data of in the RPV are summarized in Table 4-5.

Table 4-2: Main geometrical data of the reactor pressure vessel of the BWR-72 from [98].

Parameters	Values	Units
Inner diameter	6620	mm
Total height	22350	mm
Design pressure	86.3	bar
Design temperature	300	°C
Cylinder wall thickness + cladding	163+8	mm
Cap wall thickness + cladding	90+8	mm
Bottom wall thickness + cladding	228+8	mm
Material	22NiMoCr37	

The main parameters of the reactor core, the fuel assemblies and the control elements are listed in Table 4-3.

Table 4-3: Main parameters of the reactor core of the BWR-72.

Parameters	Values	Units
Reactor Core		
Number of fuel assemblies	784	
Number of control cross elements	193	
Active core length	3710	mm
Average power density	56.8	kW/l
Average heat flux	46.9	W/cm ²
Fuel	UO ₂ and MOX	
Fuel assemblies		
Total length of fuel assemblies	4474	mm
Cross-section without box	131 x 131	mm
Control elements		
Absorption length	3660	mm
Absorption material	Boron and Hafnium	
Nominal inserting velocity	30	mm/s
Nominal inserting time	122	s
SCRAM velocity	~1200	mm/s
Inserting time for SCRAM	3.2	s

4.2 BWR-72 Core Description

The core loading of the 13th cycle includes six different fuel types, which are radially distributed within the core as shown in Figure 4-2. The positions with named 0 represent reflector element positions. In Table 4-4, the fuel rod arrangements and axial material composition of each fuel assembly type are listed.

The majority of the fuel assemblies are Uranium oxide FA with different enrichment and numbers of Gadolinium rods. The sixteen fuel assemblies of type 4 are MOX fuel assemblies. The fuel assemblies of type 1 to 4 have an axially homogeneous composition, named material A, B, C and D. The fuel assemblies of types 5 and 6 are made axially of different material, named E, F, G, H, I. Hence in total there are nine different material compositions in the whole core. In addition, there are three material compositions representing the lower, upper and radial reflector.

For each material composition a lattice code model is required to describe the geometry, material composition and thermal-hydraulic parameters.

Table 4-4: Fuel assembly types of 13th cycle with axial material composition and fuel rod arrangement.

Type 1 9x9	Type 2 9x9	Type 3 10x10	Type 4 9x9	Type 5 10x10	Type 6 10x10
Top Reflector					
A	B	C	D	E	H
A	B	C	D	F	H
A	B	C	D	E	H
A	B	C	D	F	H
A	B	C	D	F	I
A	B	C	D	G	G
Bottom Refector					

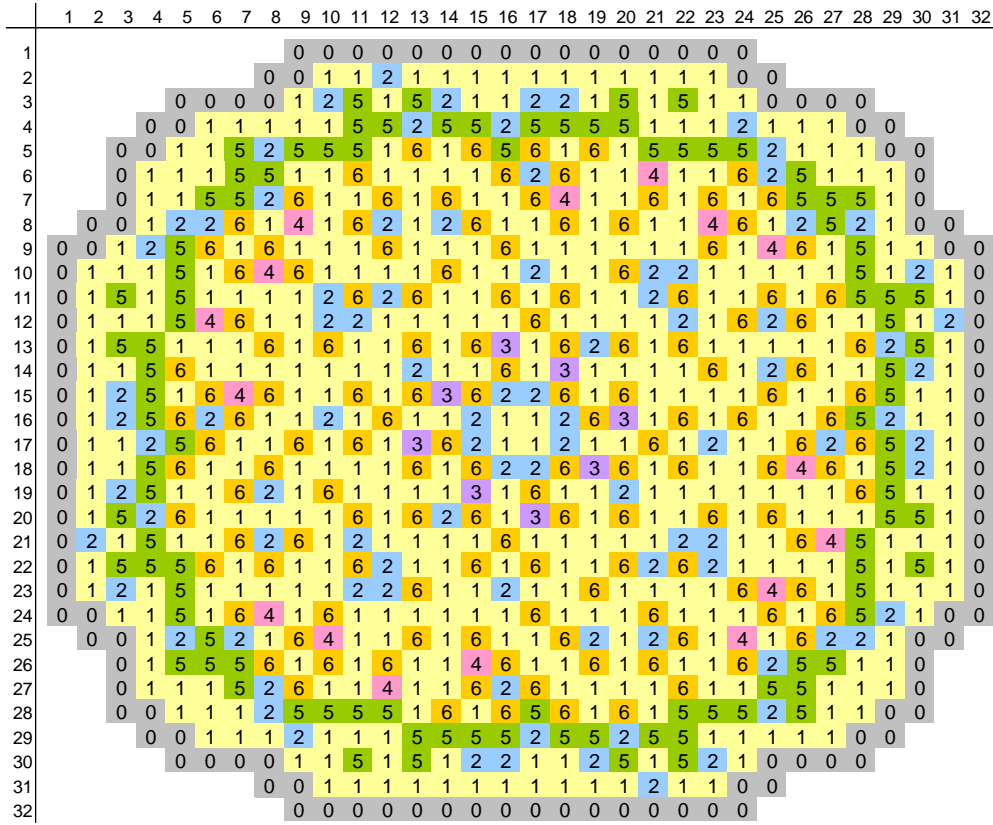


Figure 4-2: Core configuration of the 13th cycle of the BWR-72 plant with FA type indication as in Table 4-4.

4.3 Neutron Physical Modelling of the BWR Core

As mentioned before, the core consists of six FA types and three reflector types. According to the axial material composition of each FA type there are nine different material compositions and three reflector compositions for which nodal cross-sections have to be calculated using SCALE/TRITON/NEWT. For the generation of an input deck for each material composition the following steps are executed:

- Geometrical description of each FA type followed by the spatial discretization of the fuel rods, Gadolinium rods, absorber blades, water rods and canister wall.

Figure 4-3 shows a 2D model of a 9x9 FA with different enrichments, central water rod and Gadolinium rods is shown. The gadolinium pellets consists of four concentric circles of the same area and are surrounded by the cladding. This detailed spatial discretization is required to describe the dependence of gadolinium consumption from the neutron flux (self-shielding effect) adequately. In contrast to conventional fuel rods, the gadolinium rods are depleted by the neutron flux and not by power. For the pin power calculations it should be take care that the pin cells have the same area, because the pin power is normalized by the total area of the pin cells. Using different pin cell areas cause an error.

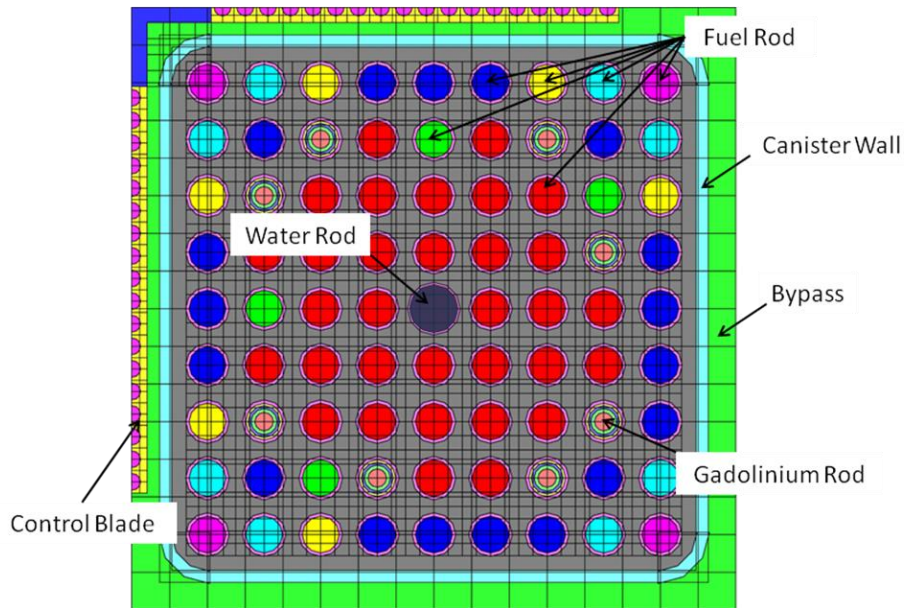


Figure 4-3: Schematic horizontal of a BWR fuel assembly with central water rod and Gadolinium rods as modelled by in TRITON.

- Geometrical modelling of the Reflector Elements: In this case a fuel assembly segment is considered adjacent to the reflector segment. As the reflector segment representing the radial reflector is modelled considering bypass coolant only, the lower and upper reflector segments include the real material composition of the solids below and above the core. For simplification, the structural materials above and below the core are considered together with the coolant as a homogenized material composition in the modelling. The example of a spatial discretization of the lower reflector with different homogenized material compositions is shown Figure 4-4.

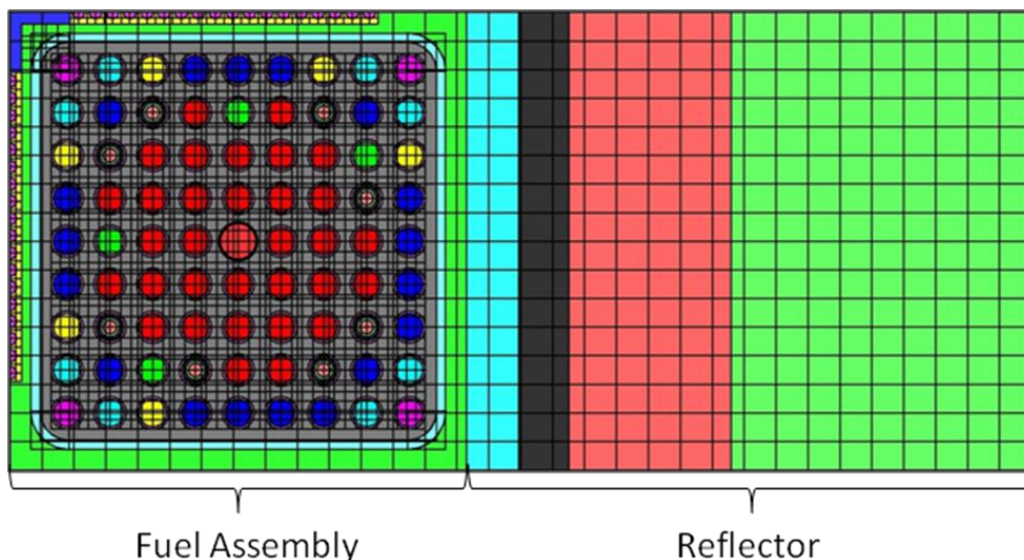


Figure 4-4: TRITON model of the lower reflector.

- Energy group collapsing:

The 2D transport solution in NEWT is based on the ENDF/B-VII library with either 238 or 49 energy groups. TRITON performs a group condensation in two energy group with

following energy bounds: 1.0E-05 eV to 3.0 eV for the thermal and 3.0 eV to 2.0E+7 eV for the fast spectrum (see also section 2.2).

- Spatial homogenisation:

The fuel assembly cross-sections resulting of the TRITON/NEWT calculations are spatially homogenised over the whole fuel assembly area, including canister wall, control blade and bypass. In the case of the reflectors cross-sections, only the modelled reflector segments are spatially homogenized (see also section 2.2).

- Modelling of resolved resonances:

The module CENTRM uses two types of unit cell data to calculate the Dancoff factors and resonance self-shielding. The multi-region unit cell and the lattice unit cell. The cylindrical multi-region, shown in Figure 4-5, is used for the definition of Gd-rods because of the onion skin burnup of Gadolinium. All fuel rings have the same area. The same area of the moderator ring has to be chosen like in the square pitch case, Figure 4-6. For UO₂ and MOX fuel rods the square lattice cell is used. More details about the lattice cell types can be found in the NEWT manual [81]. The unresolved resonances are predicted using BONAMI after the Bondarenko method.

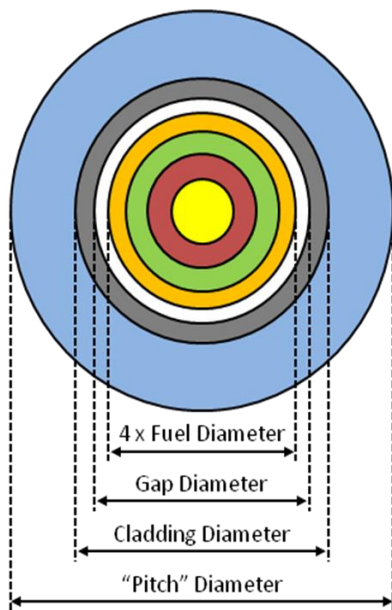


Figure 4-5: Multiregion unit cell model in TRITON/NEWT for Gd-pins.

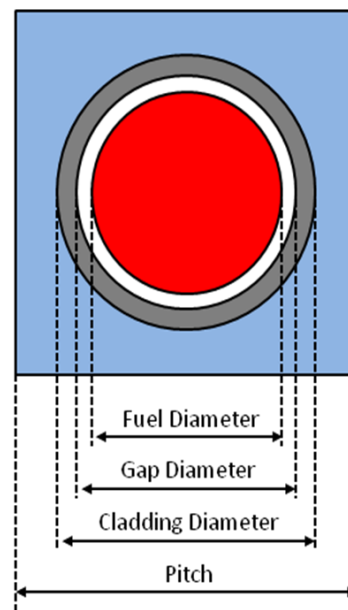


Figure 4-6: Lattice cell model in TRITON/NEWT for UOX/MOX rods.

- Boundary conditions for the lattice calculations:

Reflective boundary conditions are chosen to solve the neutron transport inside the modelled fuel assembly.

4.4 Generation of the PMAXS Nuclear Data Libraries for 3D Transient Analysis

The cross-section data libraries must include the cross-section dependence not only of the geometrical and material specifications but also of the thermal-hydraulic instantaneous and history effects. To generate such kind of cross-section library e.g. in PMAXS format, the expected range of variation of these parameters needs to be considered in the branch calculations. Therefore the branch calculations contain one value for the control rod (CR), five values for the fuel temperatures (TF), one value for the coolant temperature (TC) and five values for the coolant densities (DC). As an example, different values of three parameters, as they are needed for branch calculations are chosen:

TF: 559 K, Reference, 1200 K, 1600 K, 2000 K

TC: 559 K

DC: 0.73989 g/cm³, 0.59921 g/cm³, 0.45854 g/cm³ (Reference), 0.31787 g/cm³ and 0.17720 g/cm³

The reference fuel temperature may vary from fuel type to fuel type. The selected coolant density values correspond to an axial void fraction distribution along the BWR core of 0 %, 20 %, 40 %, 60 % and 80 % for a nominal system pressure of 70 bar.

The exact description of all branches can be found in the Annex A. Since the branch calculations with SCALE6.0 are not yet parallelized and the resonance treatment within SCALE6.0 is time consuming (several days for one FA), the instantaneous and history parameters cannot be subdivided into many ranges. Therefore the investigations have been limited to the number of 30 branches.

The history effects are considered by additional branch calculations for the coolant densities of 0.17720 g/cm³ (void = 80), 0.45854 g/cm³ (void = 40) and 0.73989 g/cm³ (void = 0) at nominal pressure. These cases are used as reference states. SCALE6.0 does not allow the direct consideration of control rod histories. One could do it by exchanging the absorber material composition with the one of the bypass water and vice versa. In addition, GenPMAXS is not able to extract the corresponding data from the SCALE6.0 output and write it in the PMAXS libraries. Hence, no control rod histories are considered in this study.

For the branch calculations, the burnup steps (point) must be defined for each fuel assembly type (material composition). Here 31 fixed burnup points (Table 4-5) are defined for all material zones except for the material composition C (FA-type 3). For the FA-type 3, two additional burnup steps are used since the fuel assemblies of this type reach the highest burnup and to reduce the calculation costs for the other types.

As listed in Table 4-5, the burnup step size chosen is small (0.5 MWd/kg) at the begin of the depletion because all fuel assemblies contain Gadolinium (Gd) and the depletion of Gadolinium shows strong variations (gradients) in time. After one year irradiation, almost all Gd is consumed. But also then the number of burnup steps needs to be carefully selected and limited to a reasonable number, since the branch calculations with SCALE6.0 are time consuming.

Table 4-5: Burnup (BU) step sizes selected for the branch calculations of FA type 3 (*only Type3)

Step	BU (MWd/kg)						
1	0.0	10	4.0	19	8.5	28	35.0
2	0.1	11	4.5	20	9.0	29	40.0
3	0.5	12	5.0	21	9.5	31	45.0
4	1.0	13	5.5	22	10.0	32	50.0
5	1.5	14	6.0	23	12.5	33*	55.0
6	2.0	15	6.5	24	15.0	34*	60.0
7	2.5	16	7.0	25	20.0		
8	3.0	17	7.5	26	25.0		
9	3.5	18	8.0	27	30.0		

The generated homogenized nodal cross-section data for the two energy groups of the material composition of each six fuel assembly type are written in the PMAXS format for the subsequent reactor dynamic code PARCS run. The structure of the PMAXS format is may be found in Annex A.

As the *xfile016* doesn't contain the reflector cross-sections, but homogenized cross-sections including both segments (FA and reflector, see section 4.3), the reflector data are taken from the *TRITON.out* and put in the reflector cross-section PMAXS file.

5 Validation of generated Cross-section Libraries

The validation of the generated neutron physical data of the core is an important step to demonstrate that the selected tools and computational route work correctly. The quality of the cross-sections data files (PMAXS) will determine the quality of the envisaged 3D coupled transient simulations with TRACE/PARCS. Furthermore, the appropriateness of the interface routine GenPMAXS requires an evaluation to ensure that the predicted parameters by the lattice codes are correctly transferred to the PMAXS-libraries.

Therefore, the following validation steps are conducted:

- Analysis of fuel assembly depletion behaviour using the reactor dynamics code PARCS only. Thereby the following aspects are analysed:
 - Effects of using different evaluated nuclear data libraries.
 - Impact of considering different histories in the branch calculations on the FA depletion.
 - Comparison of the FA depletion results predicted using xs generated with two lattice codes (SCALE6.0 and CASMO-4).
 - Single fuel assembly depletion without Xenon and Samarium.
 - Single fuel assembly depletion with Xenon and Samarium.
- Analysis of the depletion behaviour of a full BWR core using PARCS. Here, the following cases were investigated:
 - Core depletion behaviour using different evaluated nuclear data libraries.
 - Core depletion behaviour using different histories.
- Core analysis regarding important safety-related parameters such as axial and radial power distribution for the following cases:
 - ARI (all rods in) for HFP conditions using uniform TH parameters.
 - ARO (all rods out) for HFP conditions using uniform TH parameters.
 - Analysis of a critical core with TRACE/PARCS.

5.1 Single Fuel Assembly Depletion

A fuel assembly model is developed for depletion calculations with both SCALE/TRITON and PARCS. By comparing the predictions, the correctness of the interface module based on GenPMAXS as well as the depletion modules of both codes are to be validated.

The PARCS fuel assembly model for the depletion calculation is shown in Figure 5-1. The fuel assembly is split in 24 equidistant axial nodes of 15.4583 cm height. The node cross-sections are the ones generated in PMAXS format with SCALE6.0/TRITON/NEWT. For the PARCS depletion simulations, reflective boundary conditions at the radial and axial borders are selected.

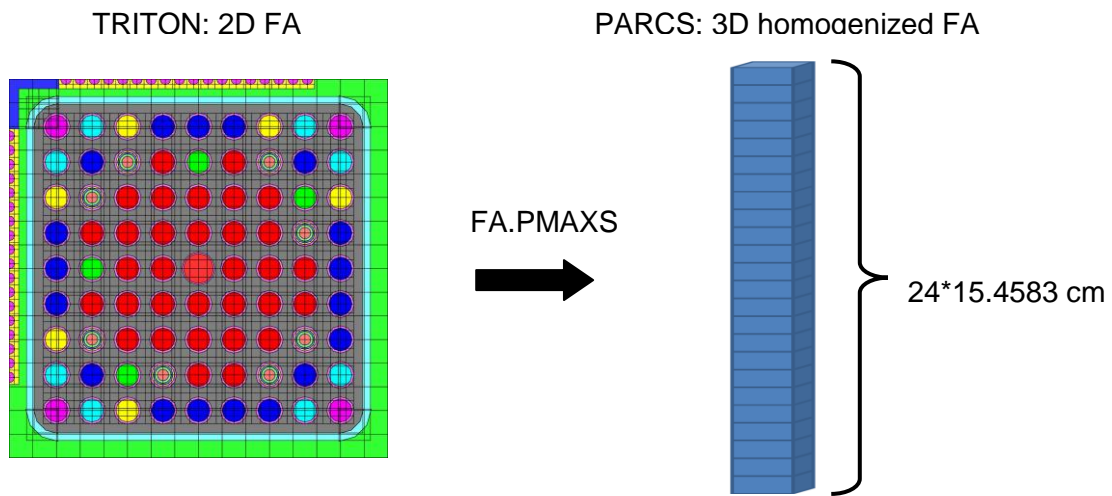


Figure 5-1: SCALE6/TRITON (left) and PARCS (right) fuel assembly nodalization for depletion calculations.

5.1.1 Impact of Xenon and Samarium on depletion calculations

While the SCALE/TRITON depletion calculations always consider Xe and Sm, the PARCS depletion calculations can be done with or without these nuclides. To quantify the impact of these nuclides on the multiplication during the depletion steps, two PARCS simulations are performed with and without Xe and Sm. The predicted multiplication factor k_{∞} is then compared against the SCALE/TRITON predictions. Since the predicted k_{∞} includes the Xenon effect, another k_{eff} factor was derived for a consistent comparison with the PARCS simulation without Xe and Sm as indicated in the following relation:

$$k_{eff} = \frac{\nu \Sigma_{f2} \Sigma_{s12} + \nu \Sigma_{f1} \Sigma_{a2}}{\Sigma_{a1} \Sigma_{a2} + \Sigma_{a2} \Sigma_{s12}}, \quad (5.1)$$

where $\nu \Sigma_f$ is the number of neutrons per fission (ν) \times fission cross-section (Σ_f) of group i , Σ_{s12} the scattering cross-section from group 1 to 2 and Σ_a the absorption cross-section of group i .

The cross-sections data are taken from SCALE/TRITON output file *txtfile16*. The relative difference Δ of the multiplication factor between the two predictions is estimated by:

$$\Delta = \frac{C - R}{R} \quad , \quad (5.2)$$

where C represents the calculated PARCS value und R the SCALE/TRITON reference value.

The multiplication factors of SCALE/TRITON and PARCS for a representative fuel assembly for a set of reference thermal-hydraulic parameters (void = 40 %, TF = 760.4 K, TC = 559 K) are presented in Figure 5-2. No significant difference between both predictions can be observed. Therefore the cross-sections are correctly converted into the PMAXS format and both codes exhibit similar depletion capabilities.

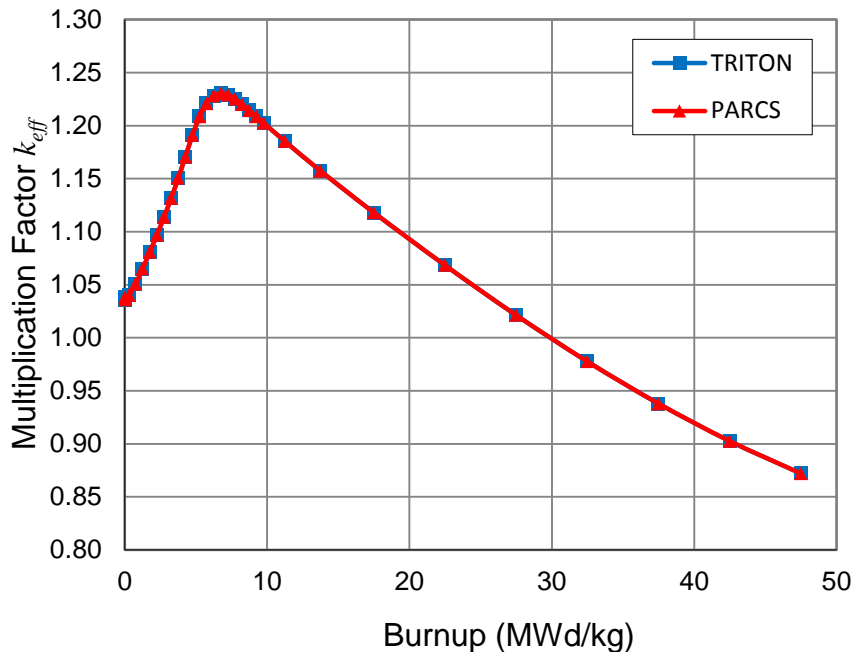


Figure 5-2: Comparison of the multiplication factor k_{eff} without Xe and Sm effect of TRITON and PARCS at defined reference conditions.

The effects of Xe and Sm during the depletion are calculated by PARCS according to the equations (3.4)-(3.7). They are depleted in PARCS using microscopic cross-sections and considering their yields.

A comparison of the multiplication factor predicted by SCALE/TRITON and PARCS considering the effects of Xe and Sm is presented in Figure 5-3. The maximal relative deviation of the PARCS prediction from the TRITON one is about to 0.7 %.

In order to evaluate the reason for this deviation, the number densities of Xe and Sm in both calculations are compared to each other, which are shown for both elements in Figure 5-4 and Figure 5-5. Figure 5-5 illustrates that the number densities of Samarium used in PARCS is far below the one used in SCALE/TRITON. The reason therefore is the fact that both

codes use different methods for the calculation of the number density. In SCALE/TRITON the differential equation (3.1) is solved for several isotopes while in PARCS the number densities are predicted based on an approximation.

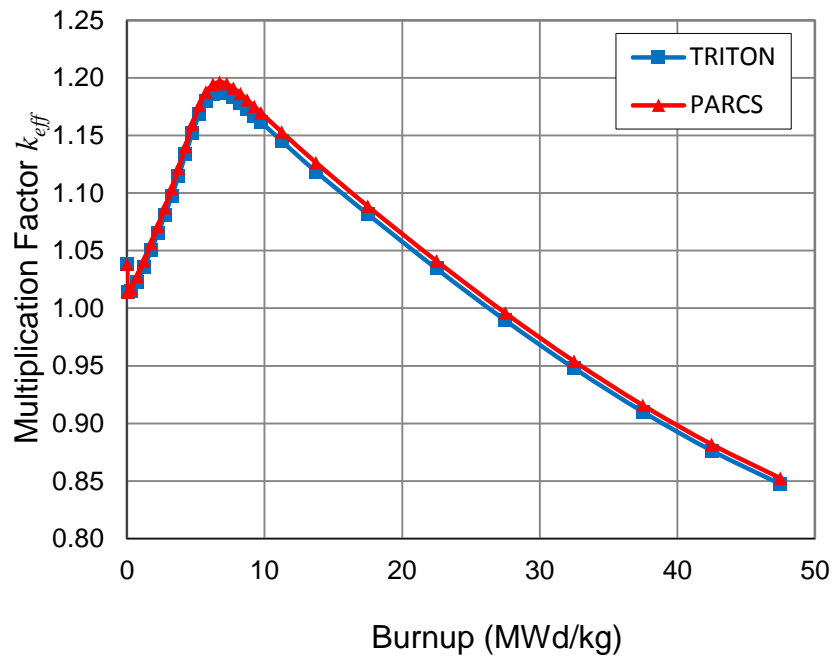


Figure 5-3: Comparison of the multiplication factor k_{eff} of TRITON and PARCS considering the Xe and Sm effects at defined reference conditions.

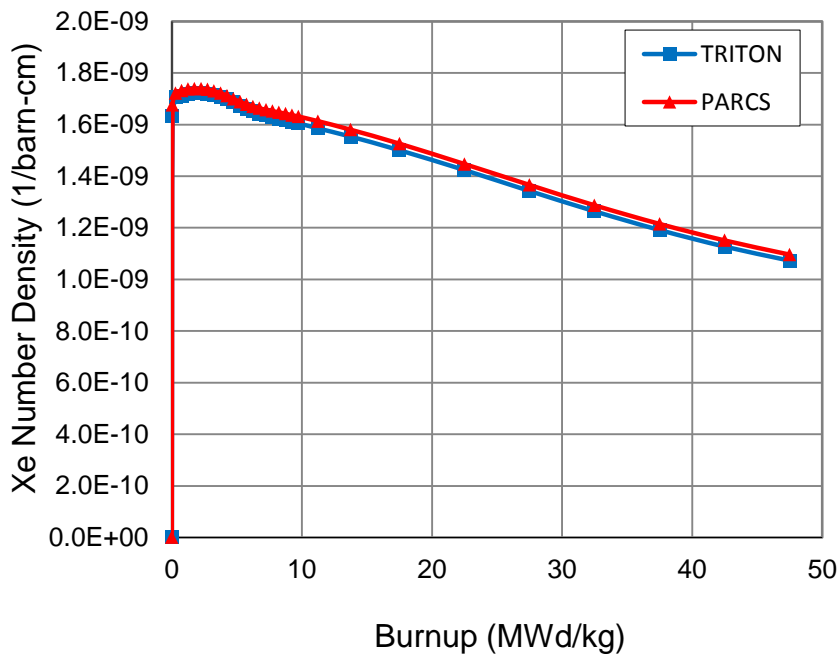


Figure 5-4: Computed number density of Xe at reference conditions by TRITON and PARCS.

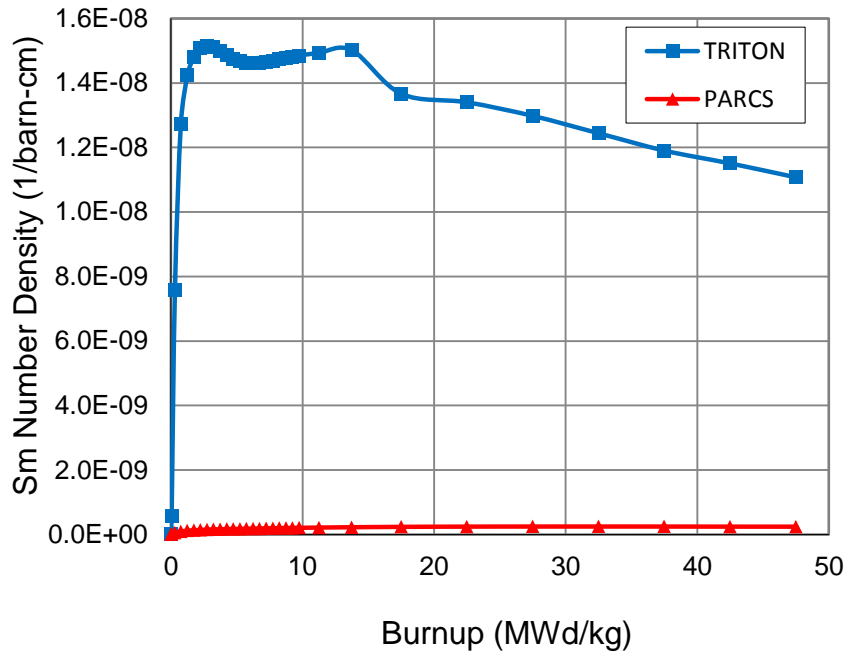


Figure 5-5: Computed number density of Sm at reference conditions by TRITON and PARCS.

However, the deviation of the Sm number densities by several order of magnitude cannot be explained. Hence a close look at the equations (3.4) to (3.7) where important parameters are contained such as microscopic cross-sections σ , the yields γ and the macroscopic fission cross-section Σ_f was necessary. The microscopic cross-sections used by both codes are compared to each other in Figure 5-6. As the graph exhibits no difference between the values used in the codes in a next step the default yields for I, Xe and Pm used in PARCS and the ones in SCALE/TRITON are compared.

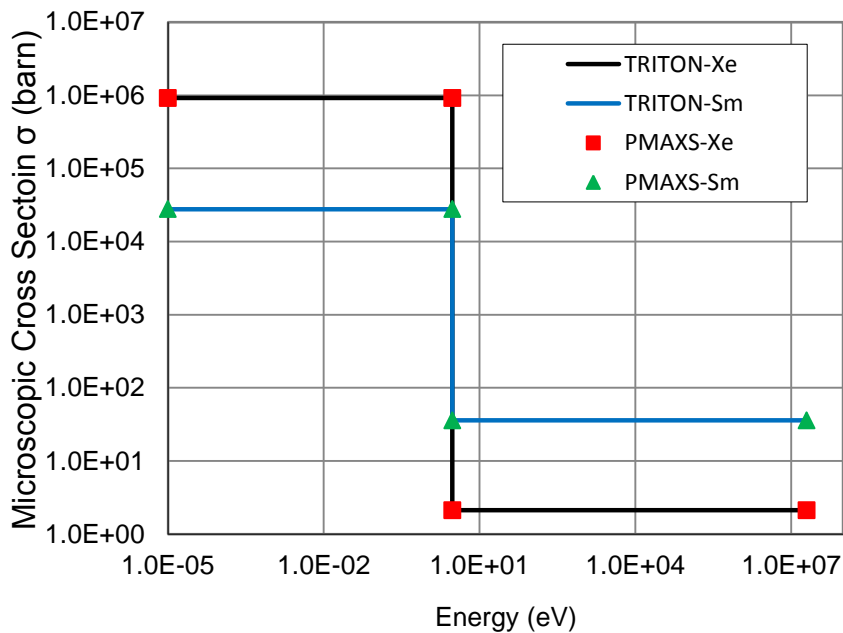


Figure 5-6: Comparison of the microscopic two group cross-sections of Xe and Sm.

Table 5-1 lists the yields for I, Xe and Pm. It can be noted that the yield of I and Sm in both codes are comparable, but the yield of Pm predicted by SCALE/TRITON is far below the one used in PARCS. This underestimation of the Pm yield in TRITON is the major origin of the wrong prediction of capture reaction in the Promethium isotopes Pm-148 and Pm-148m. Consequently, PARCS depletion calculations will be performed using the default values of the Promethium yield.

Table 5-1: Computed effective yields for several nuclides by SCALE/TRITON and PARCS

Yield γ	I	Xe	Pm
TRITON (0 MWd BU)	0.06288	0.00257	0.00006
PARCS	0.06386	0.00228	0.0113

5.1.2 Effects of different evaluated nuclear data libraries on the FA depletion calculation

The accuracy of neutron physics calculation depends strongly on the quality of the nuclear data libraries for the most important isotopes. Hence, a fuel assembly depletion case is analysed using different versions of nuclear data libraries and also different number of energy groups. In Figure 5-7 the multiplication factor k_{eff} for different depletion steps predicted with various ENDF libraries, which are part of the SCALE6 package, are compared for an UOX fuel assembly. Thereby the same set of thermal-hydraulic parameters (void = 40 %, TF = 760.4 K, TC = 559 K) are used. As base for the comparison a reference calculation using the ENDF/B-VII 238-group library is performed.

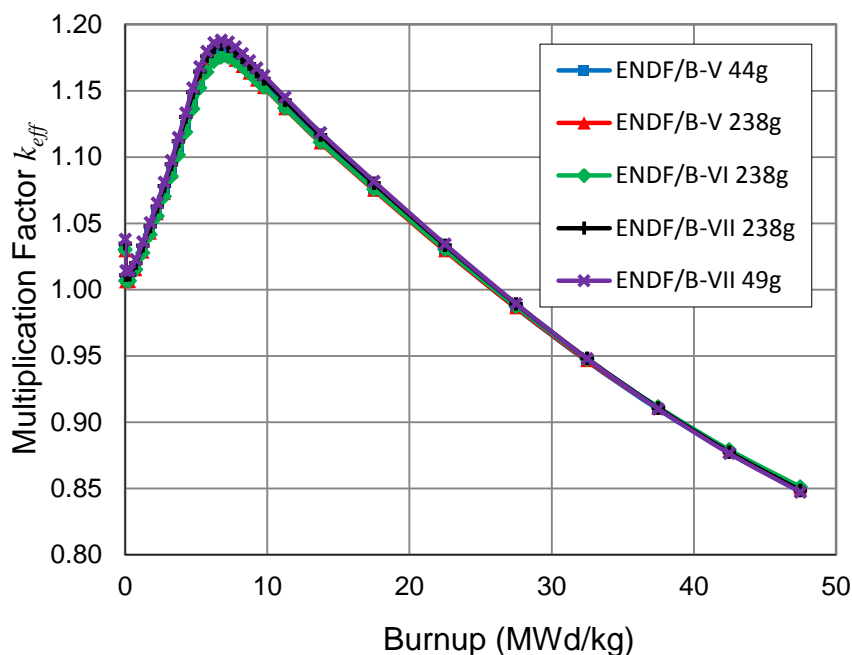


Figure 5-7: Comparison of the multiplication factor k_{eff} of TRITON considering different ENDF multi-group libraries.

The use of the different ENDF libraries leads to a deviation of up to a maximum of about 1.1% for a UOX fuel assembly, as illustrated in Figure 5-8. For the burnup between 0 and 10 MWd/kg, where the depletion of fuel rods contained Gadolinium is important, the deviations are larger than for higher burnups. Since the Gadolinium rods are depleted with the neutron flux and not with power as it is the case for the other rods, the initial burnup steps are more sensitive to changes in the neutron flux distribution than the other ones.

The results of the analysis of the multiplication factor obtained for different nuclear libraries shows the need to consider uncertainties in an appropriate manner. In the investigations of Jatuf et. al [94], the similar conclusions were drawn confirming these investigations regarding the influence of different cross-sections libraries.

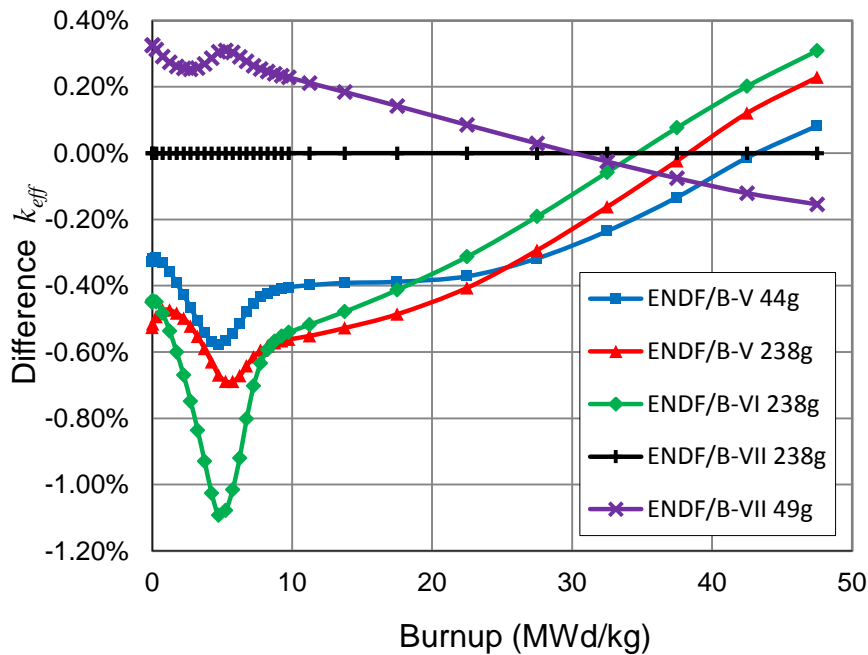


Figure 5-8: Computed deviation of the multiplication factor k_{eff} of TRITON for different nuclear data libraries compared to the ENDF/B-VII library.

5.1.3 Influence of the history effect on the FA depletion calculation

For the generation of nodal cross-sections for real LWR cores both the thermal-hydraulic conditions of the fuel within the core but also the different control rod positions during plant operations have to be considered. Lattice codes offer the possibility to take into account not only instantaneous but also history effects during the generation process of nodal cross-sections for whole core transient simulations. In the case of SCALE/TRITON, several TRITON calculations can be performed for different reference states history effects e.g. void fraction and control rods.

The SCALE6.0 version permits only by means of tricks to consider the control rod history. Also GenPMAXS has serious difficulties to pass the right history effects to the PMAXS files. According to these aspects the present work does not scope the control rod history.

In Figure 5-9 the evolution of the multiplication factor for burnup steps up to 45 MWd/kg is plotted for different cases calculated without and with void history effects. There, results of SCALE/TRITON simulations are presented for different voids ($v = 0\%$, $v = 40\%$ and $v = 80\%$) history effects (HIST), where the other important feedback parameters are kept constant (TF=760.4 K and TC=559 K).

In addition, the multiplication factor of branch calculations without history effect BR is given. In case BR zero void, the multiplication factor is higher than for the case HIST zero void, where the Gadolinium rods are already depleted (>10 MWd/kg). This is due to the moderation conditions during the ORIGEN-S calculation. Every branch calculation uses the nuclide inventory predicted for the reference case. If for example the reference density is higher, there will be also better moderation and the fuel will depletes faster. Thus, the multiplication factor is less compared to BR zero void with HIST zero void. During the Gadolinium depletion phase the effect is opposite, because the Gadolinium depletes also faster. The opposite behavior can be observed for lower densities.

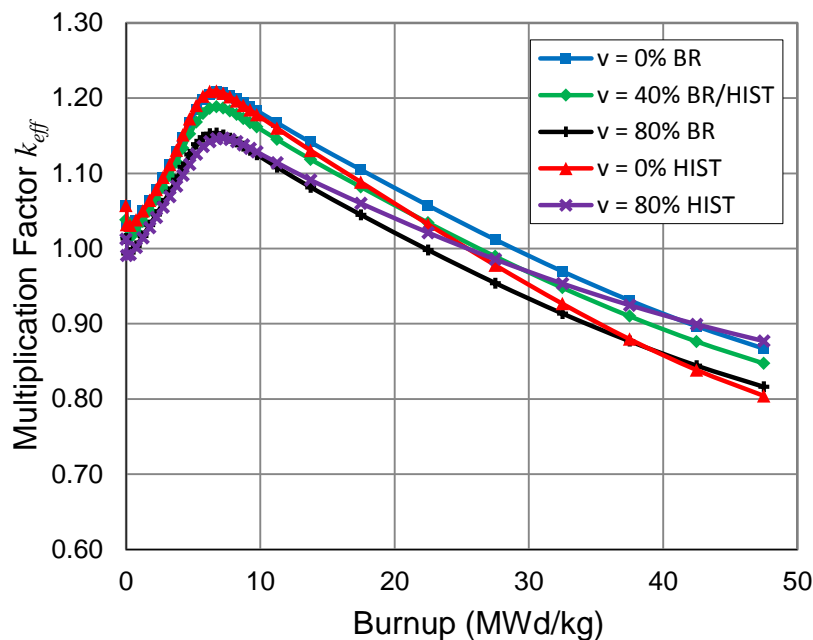


Figure 5-9: Comparison of the multiplication factor k_{eff} of TRITON considering different void histories.

In Figure 5-10 multiplication factor difference between the cases with (HIST) and without (BR) history effects for three void fractions are plotted. For the void fraction of 40 %, which is representative for the averaged void fraction of a BWR core, the BR calculation is identical to the HIST one. Regarding the cases with a void fraction of 0 % and 80 % the difference is increasing with burnup but it remains below $\pm 10\%$.

In consequence 3D reactor dynamics calculations requires appropriate cross section formats considering history effects to predict results in an accurate manner.

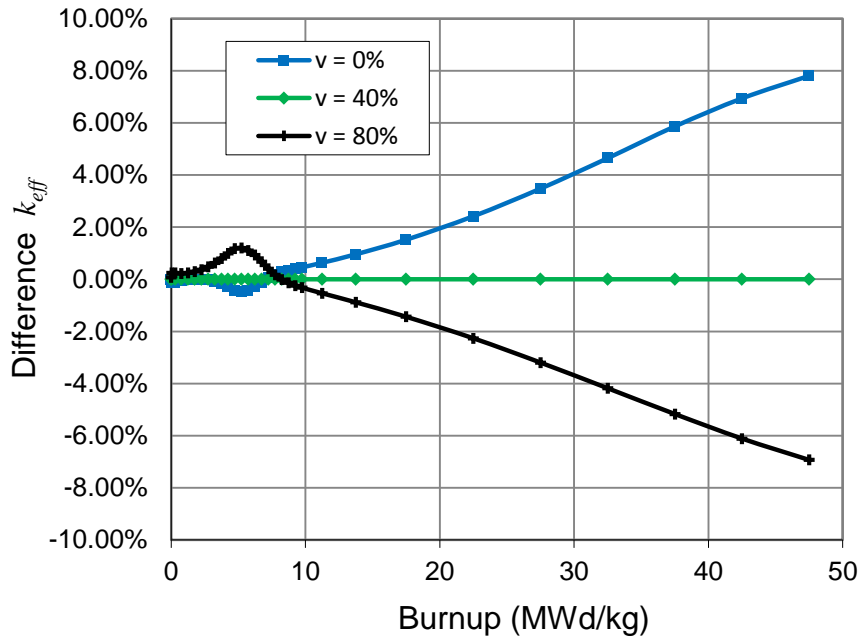


Figure 5-10: Computed deviation of the multiplication factor k_{eff} of TRITON for different nuclear data libraries compared to the ENDF/B-VII library.

5.1.4 Validation of the XS Generation Approach by Code-to-Code Comparison

Since no experimental neutron physical data for the fuel of the reference BWR plant are available, a code-to-code comparison is performed to demonstrate that the results of the SCALE/TRITON simulations correspond to these of the commercial lattice code CASMO-4, which is widely used in the nuclear industry for LWR. For this purposes, similar models of a UOX fuel assembly were developed for SCALE/TRITON and CASMO-4. While the same thermal-hydraulic conditions and the void history (40 % void) are used in both codes, the nuclear data libraries are different. In SCALE/TRITON the ENDF/B-VII.0 library is taken. In CASMO-4 however, the ENDF/B-VI.2 70-group library is used.

In Figure 5-11 the multiplication factor k_{eff} for a burnup close to 50 MWd/kg predicted by the mentioned codes is compared. Both code predictions show the same trend for PWRs (see also [95]). The difference between the predictions is relatively low, around 1 %, for fresh fuel. It decreases to about 0.4 % for a burnup of 5 MWd/kg. Later on, the difference rises rapidly up to a burnup of about 7.5 MWd/kg, reaching a plateau when the multiplication factor obtain its maximal value. Finally the difference increases monotonically to 2.1 % at 47.5 MWd/kg. This can be partly attributed to the different cross-section libraries and also to different methodologies used.

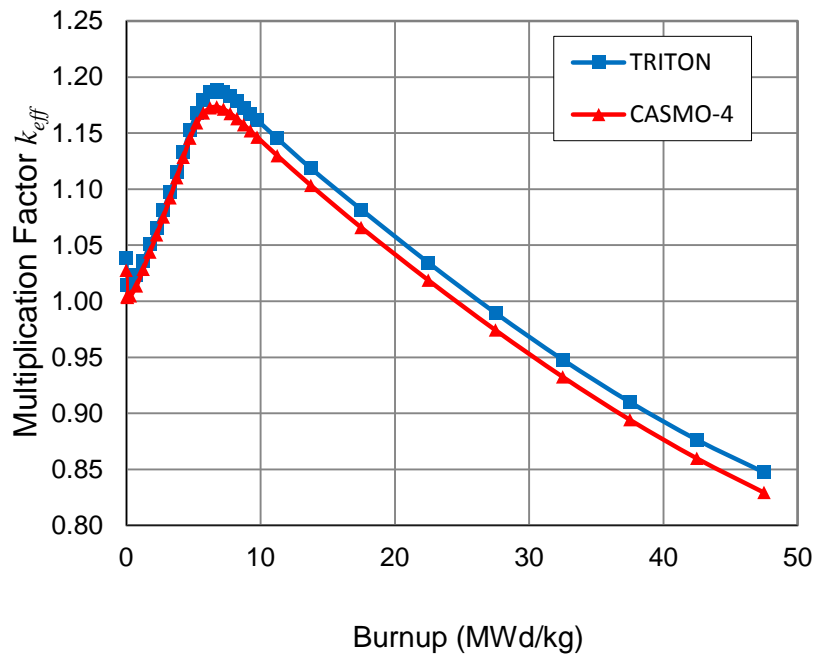


Figure 5-11: Comparison of the multiplication factor k_{eff} for a representative UOX fuel assembly predicted by TRITON and CASMO-4.

5.1.5 Void and Fuel Temperature Reactivity Coefficients

Apart from the neutron physical design of a fuel assembly it is important to assess the inherent safety parameters such as void and fuel temperature reactivity coefficients of a given fuel assembly or reactor core. The void reactivity coefficient α can be expressed as the change of the multiplication factor (in pcm) as consequence of the change of the void fraction (in %) [96]:

$$\alpha = \frac{\Delta k_{eff}}{\Delta void} \quad (5.3)$$

To determine the reactivity coefficients, a certain number of calculations – in this case four - are performed for four different values of void or fuel temperature keeping the other one constant. These calculations are performed for a fresh (zero burnup) and a burnt (47.5 MWd/kg) fuel assembly using cross-sections generated with two codes: SCALE/TRITON and CASMO-4. In Figure 5-12 the evolution of the void reactivity coefficient is plotted in dependence of the void fraction. In general the void reactivity coefficient predicted by CASMO-4 for fresh and burnt fuel conditions is always larger than the ones predicted with SCALE/TRITON. In addition, the void reactivity coefficient at End Of Life (EOL) conditions is larger than the ones predicted by both codes for Begin Of Life (BOL) conditions.

Furthermore, the fuel temperature reactivity coefficient, predicted by both codes for BOL (0 MWd/kg) and EOL (47.5 MWd/kg) conditions, is exhibited in Figure 5-13. The fuel

temperature reactivity coefficient decreases with increasing fuel temperature. For fresh fuel conditions both codes predict a fuel temperature reactivity coefficient which is larger than the one calculated for EOL conditions. But for BOL conditions, the reactivity coefficients predicted by the two codes shows an opposite trend compared to the one calculated for EOL conditions.

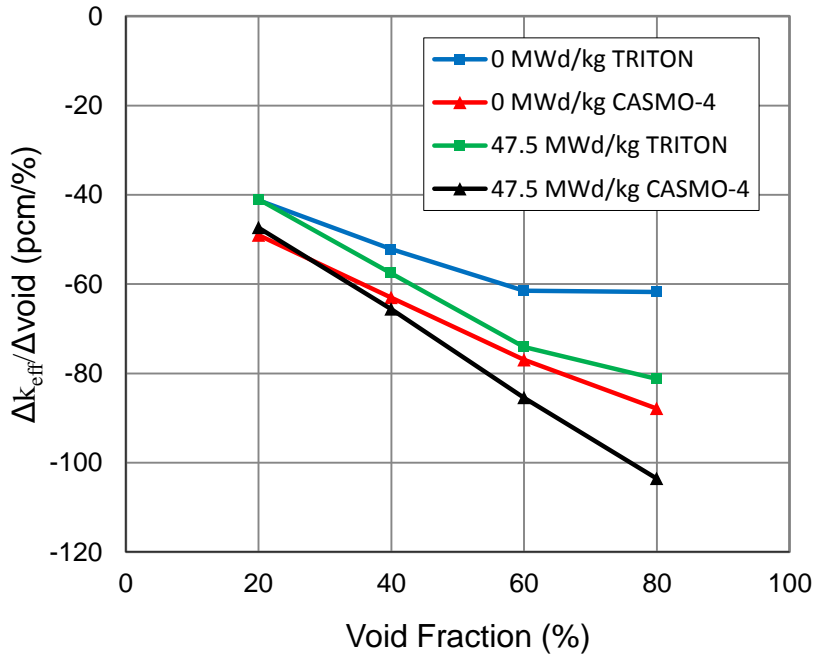


Figure 5-12: Comparison of the void reactivity coefficient in dependence of the void fraction predicted by TRITON and CASMO-4 at different burnups.

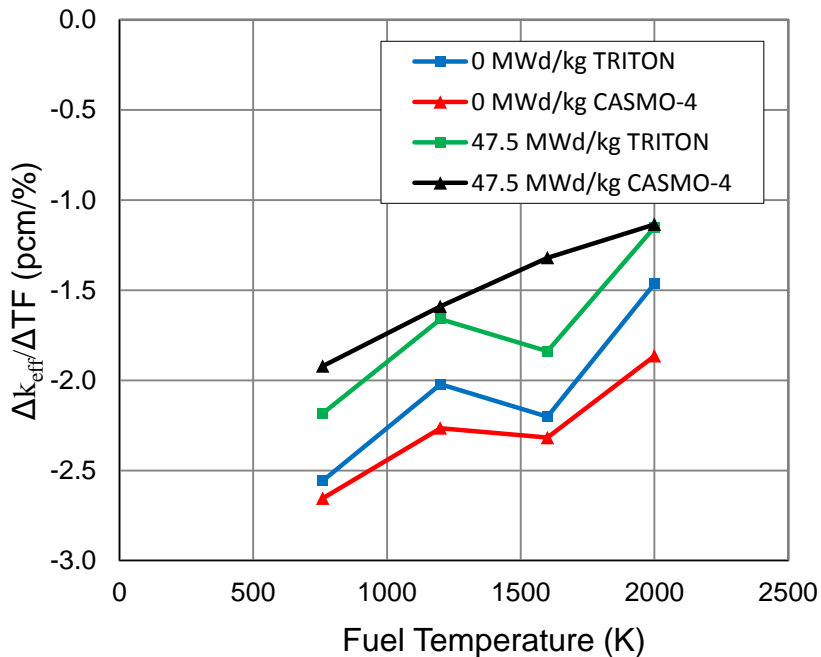


Figure 5-13: Comparison of the fuel temperature reactivity coefficient in dependence of the fuel temperature predicted by TRITON and CASMO at different burnups.

5.2 Depletion Analysis of a full BWR Core with PARCS

The next step is to apply the computational route for the analysis of the core of the reference BWR plant with PARCS using the two cross-section libraries (PMAXS files) generated with SCALE6/TRITON/NEWT and CASMO-4 for all fuel assembly types of core loading (cycle 13). For this analysis, both a thermal-hydraulic core model for TRACE and a neutron physical PARCS model were developed.

First of all, the whole core will be analysed with the stand-alone reactor dynamic code PARCS. Later on, the same BWR core will be simulated with the coupled TRACE/PARCS code.

5.2.1 The PARCS Core Model

The core consists of nine fuel assembly types, a radial reflector, a bottom reflector and a top reflector. The fuel assembly types are radially distributed in the core as shown in Figure 4-2. Thereby, each fuel assembly type consists of a certain material composition as indicated in Table 4-4.

The PARCS model consists of 784 radial nodes and 124 reflector nodes. Each radial node represents a homogenized fuel assembly with a width of 15.25 cm. The active core length of 371 cm is subdivided into 24 equidistant axial nodes with a height of 15.4583 cm.

Further the core is subdivided in 6 axial levels characterized by the different material sets (see Table 5-2). In PARCS the counting starts from the bottom to the top. Level 1 and Level 8 represent the lower and upper reflector, which have the same height as the fuel nodes. The boundary conditions for left and right sides in each direction is zero flux.

The number of axial cells was fixed based on the investigations performed for the Boiling Water Reactor Turbine Trip Benchmark in [33]. The direct energy deposition is specified by three uniform fractions over the whole core for the coolant (0.02), the by-pass (0.017) and the water rod (0.003).

In the Table 5-2 the axial burnup profile for the different fuel assembly types of the 13th cycle after 6.6 full load days is presented. It is a typical BWR profile, with a higher depletion at the bottom due to the better moderation and thus higher power in the lower core part. For the following calculations a complete 3D exposure model for every node will be used.

Table 5-2: Average burnup of the different fuel assembly types in MWd/kg

PARCS Axial Level	Core Height (cm)	FA Type 1	FA Type 2	FA Type 3	FA Type 4	FA Type 5	FA Type 6
Level 8	Top reflector						
Level 7	355.54 - 371.00	0.010	9.758	21.767	10.487	2.126	0.025
Level 6	340.08 - 355.54	15.399	15.623	34.019	17.178	5.353	0.066
Level 5	324.62 - 340.08	19.302	19.588	41.643	21.826	6.899	0.085
Level 5	309.17 - 324.62	21.827	22.151	46.241	24.901	7.847	0.095
Level 4	293.71 - 309.17	23.371	23.781	48.972	26.905	8.366	0.103
Level 4	278.25 - 293.71	24.460	24.840	50.585	28.213	8.694	0.108
Level 4	262.79 - 278.25	25.075	25.536	51.559	29.091	8.889	0.110
Level 4	247.33 - 262.79	25.412	26.019	52.166	29.719	9.008	0.112
Level 4	231.87 - 247.33	25.801	26.405	52.536	30.204	9.089	0.114
Level 3	216.42 - 231.87	26.080	26.731	52.785	30.622	9.191	0.118
Level 3	200.96 - 216.42	26.203	27.018	52.959	31.012	9.227	0.120
Level 3	185.50 - 200.96	26.381	27.305	53.069	31.405	9.246	0.121
Level 3	170.04 - 185.50	26.652	27.605	53.129	31.816	9.255	0.122
Level 3	154.58 - 170.04	26.813	27.907	53.178	32.258	9.261	0.123
Level 3	139.12 - 154.58	26.910	28.215	53.206	32.736	9.270	0.125
Level 3	123.67 - 139.12	27.213	28.542	53.174	33.246	9.288	0.128
Level 3	108.21 - 123.67	27.401	28.858	53.124	33.781	9.318	0.132
Level 3	92.75 - 108.21	27.488	29.158	53.049	34.328	9.366	0.138
Level 3	77.29 - 92.75	27.633	29.424	52.862	34.834	9.435	0.145
Level 3	61.83 - 77.29	27.635	29.565	52.379	35.153	9.515	0.153
Level 2	46.37 - 61.83	27.243	29.321	51.135	34.926	9.500	0.162
Level 2	30.92 - 46.37	26.022	28.152	48.684	33.425	9.286	0.164
Level 2	15.46 - 30.92	23.057	24.999	43.400	29.433	8.340	0.150
Level 2	0.00 - 15.46	16.096	17.528	31.244	20.157	5.717	0.104
Level 1	Bottom reflector						

5.2.2 Validation of Cross-section Generation Approach by Code-to-Code Comparison

The first step to validate the nodal cross-sections generated with SCALE6/TRITON/NEWT is to perform PARCS stand-alone calculations for hot full power (HFP) conditions of the core assuming uniform thermal-hydraulic parameter conditions. The PARCS simulations are carried out using two cross-section libraries (PMAXS) generated with CASMO-4 and SCALE6/TRITON/NEWT for the following core burnup states:

- Begin Of Life (BOL) and
- 6.6 Full Load Days (FLD)

PARCS simulations are conducted for two control rod configurations: all rod in (ARI) and all rod out (ARO) of the core. The thermal-hydraulic parameters are averaged values for a critical core configuration characterized by:

- Coolant density: DC = 0.42421 g/cm³,
- Fuel temperature: TF = 813.18 K,
- Coolant temperature: TC = 558.78 K and
- No Xenon (Xe = 0).

In Table 5-3 a comparison of the multiplication factors (k_{eff}) predicted by PARCS for the above mentioned cases is shown. Thereby SCALE6/TRITON always overestimates the k_{eff} compared to CASMO. These results confirm the trend observed by the previous comparison of the results obtained for the single fuel assembly depletion analysis, as the TRITON and CASMO-4 uses different nuclear libraries.

Table 5-3: PARCS-SA Multiplication Factor k_{eff}

	ARI (BOL)	ARO (BOL)	ARI (6.6 FLD)	ARO (6.6 FLD)
TRITON	0.80993	1.05373	0.80209	1.06286
CASMO	0.79793	1.04245	0.79241	1.05014
Δk_{eff} (pcm)	1503	1082	1222	1212

In Figure 5-14 the corresponding core averaged axial power profiles predicted by PARCS stand alone for the cases listed in Table 5-3 are shown. For the fresh fuel the axial power profile shows a cosine like shape, whereas a shift of the axial power profile to the upper part of the core can be observed for 6.6 FLD. Under real conditions, the fuel is depleted stronger in the lower part due to the higher coolant density. Since uniform thermal-hydraulic conditions are used, the higher enrichment in the upper part compared to the lower part is responsible for the power shift.

In Figure 5-15, the relative deviation of the axial power profile for the listed cases predicted using TRITON cross-sections from the ones predicted using the CASMO-4 cross-sections is illustrated. For the fresh fuel (BOL) and control rod positions (ARI, ARO) the relative deviation is below ± 5 %. This deviation becomes larger at the bottom and upper core nodes indicating that the reflector cross-sections modeled in TRITON and CASMO play an important role.

On the contrary, the deviation of core averaged power profile predicted for the core with 6.6 FLD for the cases ARO and ARI are larger than in case of BOL. The maximal deviation is encountered for the 6.6 FLD and ARI case. It amounts around 14 % over-prediction for the lower core part and -10 % under-prediction for the upper part of the core. One may get the impression that this effect is related to the control rods. However, PARCS simulations for single fuel assembly depletion have shown a similar behavior of the rodded and unrodded core configuration. Additional investigations have shown that modifying the length of the reflector region leads to an error reduction. Hence, the observed deviations are caused by

the superposition of different effects such as control rod modeling, depletion behavior and the reflector modeling.

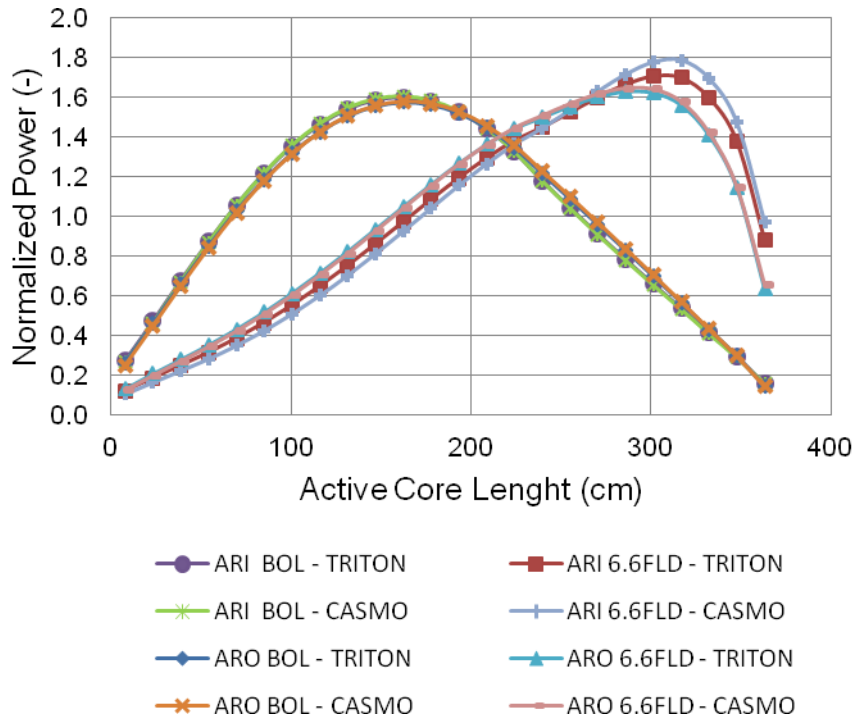


Figure 5-14: Comparison of the axial power distribution predicted by PARCS stand-alone calculations using TRITON and CASMO-4 cross-sections sets at HFP for different burnup and control rod positions.

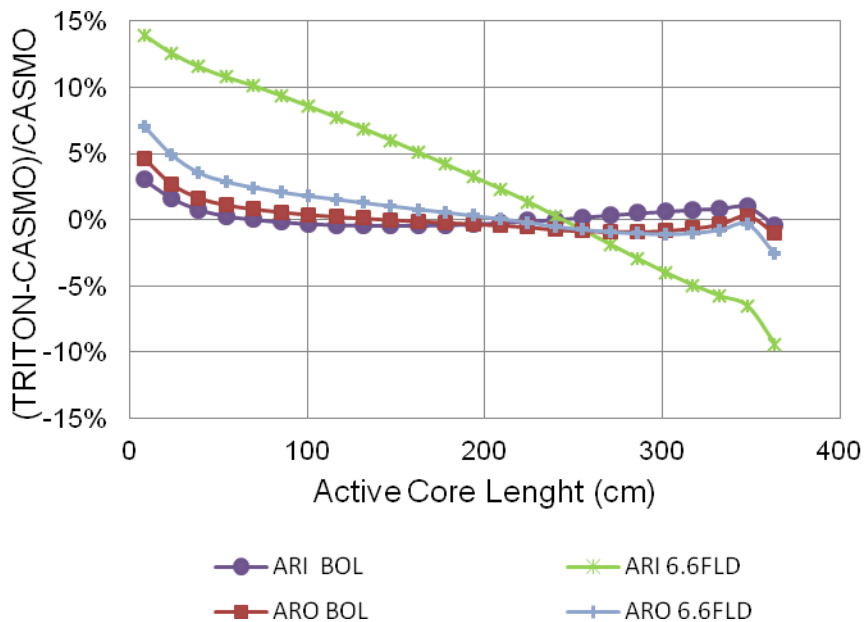


Figure 5-15: Computed difference in axial power between the TRITON and CASMO-4 cases at HFP for different burnup and control rod positions.

In Figure 5-16 to Figure 5-19 the relative deviation (%) of the radial power distribution predicted with PARCS stand-alone using the cross-section libraries (PMAXS files) generated with SCALE/TRITON from the one calculated using the CASMO-4 nuclear data for BOL and 6.6 VLD and for the control rod positions ARI and ARO is presented. In general it can be stated that the larger deviations are encountered in regions where MOX FA and UO₂ FA are close to each other and also close to the reflectors. The largest deviations are predicted for the 6.6 VLD core in both ARO and ARI cases, where PARCS with SCALE/TRITON cross-sections tends to underpredict the power of the fuel assemblies located in the outer regions and to overpredict the FA located in the central part of the core. For the ARI case, the deviation varies from 5.5 % to -8.0 % and the ARO case it varies from 3.6 % to -6.2 %.

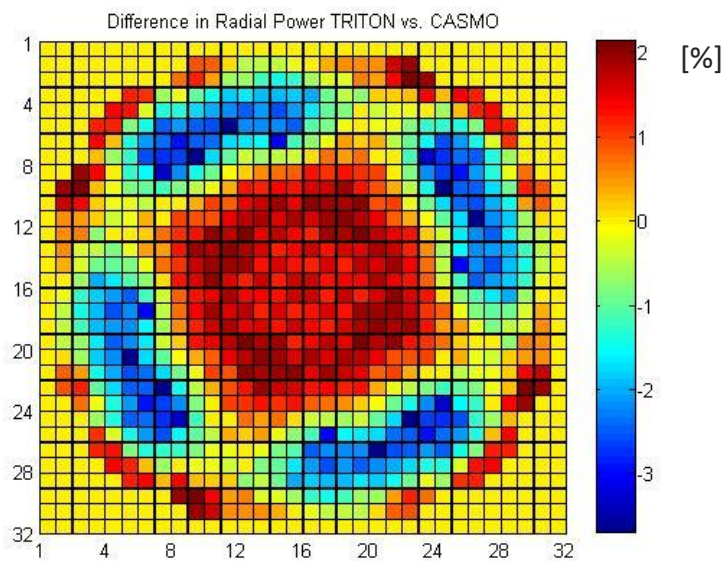


Figure 5-16: Computed difference of the average radial power distribution between TRITON and CASMO-4 at HFP for ARI and BOL.

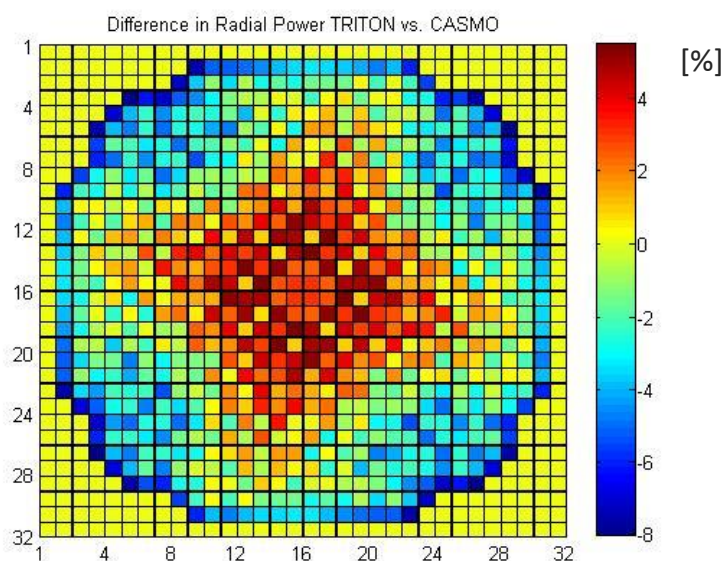


Figure 5-17: Computed difference of the average radial power distribution between TRITON and CASMO-4 at HFP for ARI and 6.6 VLD.

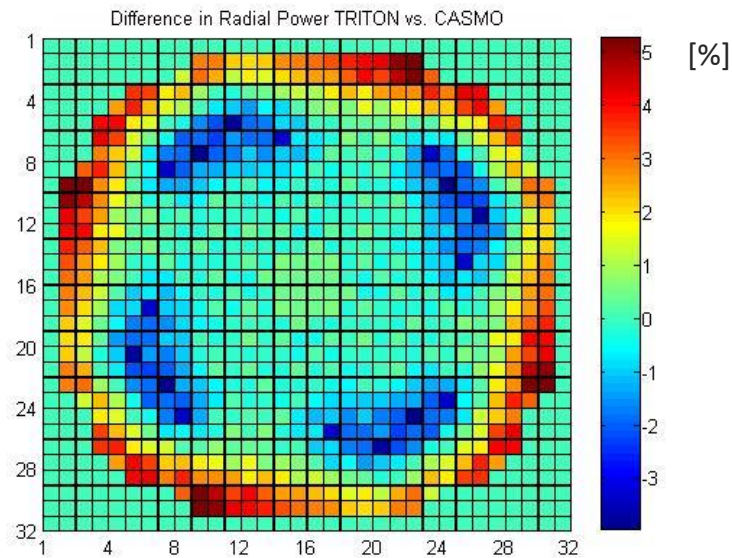


Figure 5-18: Computed difference of the average radial power distribution between TRITON and CASMO-4 at HFP for ARO and BOL.

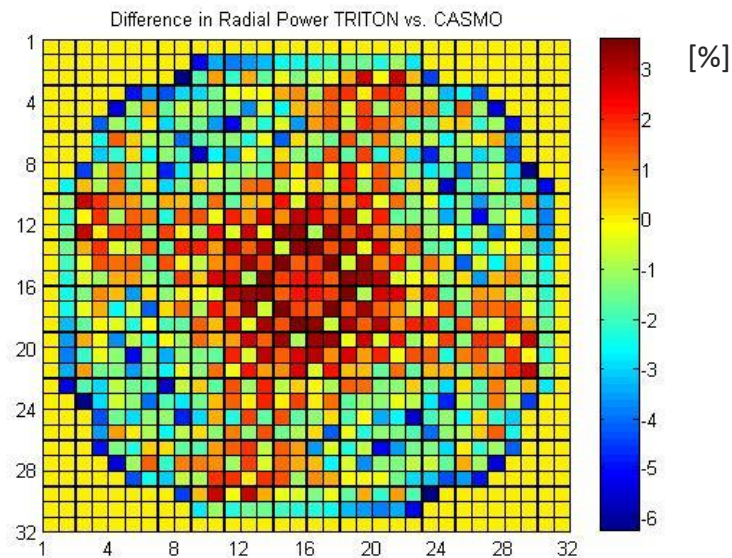


Figure 5-19: Computed difference of the average radial power distribution between TRITON and CASMO-4 at HFP for ARO and 6.6 VLD.

For fresh fuel the deviations are less ranging between 2.1 % and -3.7 % for the ARI case and between 5.2 % and -3.9 % for ARO case. These deviations are still within an acceptable range of ± 10 %.

These results underline the importance of an adequate modelling of the ADF of such heterogeneous core like this BWR core. In core regions with strong flux gradients such as in the interface between MOX and UOX fuel assemblies, in the neighbourhood of control elements and in the interface core/reflector ADFs must be taken into account in the simulations to improve the prediction accuracy of the diffusion approximation [97].

5.3 Analysis of the BWR Core with TRACE/PARCS

In the last subchapter, whole core analysis using PARCS for assumed thermal-hydraulic boundary conditions were performed with the goal of validation of the lattice physics computational route. In this chapter, a more realistic analysis of the BWR core is performed using coupled neutronic/thermal-hydraulic codes such as TRACE/PARCS to determine the thermal-hydraulic core parameters for the conditions important for follow-up transient analysis of the whole plant to be described in the subsequent chapters.

The neutronic core model to be used in PARCS is already described in Subchapter 5.2. Hereafter the thermal-hydraulic core model of the reference plant will be described as well as the mapping scheme between the neutronic and thermal-hydraulic computational domains.

5.3.1 The thermal-hydraulic TRACE Core Model

To verify the calculation schema and the mapping between TRACE and PARCS a simplified thermal-hydraulic model of the core, consisting on the VESSEL and the CHAN components in TRACE is developed. A schematic representation of the TRACE core model is shown in Figure 5-20. The VESSEL component consists of a radial ring and four levels. The first and last level represents the lower and upper plenum. The two middle layers form the bypass via the active core length. In this core model, the 784 fuel assemblies of the core are mapped, based on the fuel type and location in the core, in 20 CHAN components as illustrated in Figure 5-21.

The CHAN component allows a realistic TH description of BWR fuel assemblies, including part length fuel rods, water rods and the canister wall. Axially the CHAN components are divided into 27 nodes. Thereby, the nodalization of 24 axial nodes for the active core length is the same as in the PARCS model. The fuel assembly foot is modeled by two and the fuel assembly head by one node. Also the bypass hole in the fuel assembly foot is considered. The boundary conditions, such as pressure, coolant inlet temperature and mass flow are specified by a BREAK and FILL component.

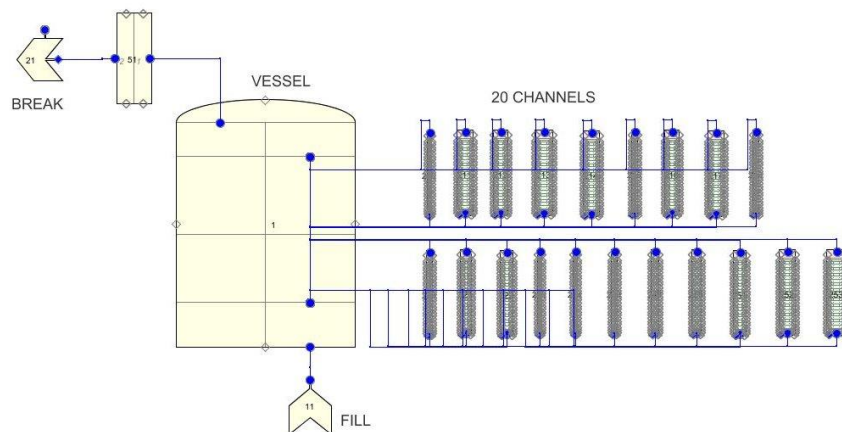


Figure 5-20: Sketch of the simplified thermal-hydraulic TRACE core model.

5.3.2 Neutronic/Thermal-hydraulic Mapping

For a proper data exchange between the neutronic and the thermal-hydraulic domains describing the reactor core, the definition of a mapping scheme as part of the PARCS input is mandatory. The mapping scheme assures that the neutronics nodes are provided with the thermal-hydraulic feedback parameters such as void fraction, fuel temperature, etc. from the corresponding thermal-hydraulic channel (CHAN component in TRACE) and fuel assembly model (HTSTR component in TRACE), which in turn enables the update of the cross-sections during the steady state and transient simulation according to the TH state of the core.

By defining the position of the CHAN components as indicated in Figure 5-21 a correspondence is established between the thermal-hydraulic domain and the neutronic domain, which is defined by the fuel assembly types distributions as given in Figure 4-2. PARCS merely makes a superposition of this neutronic domain with the thermal-hydraulic one to fix the correspondence between the neutronic and thermal-hydraulic mapping.

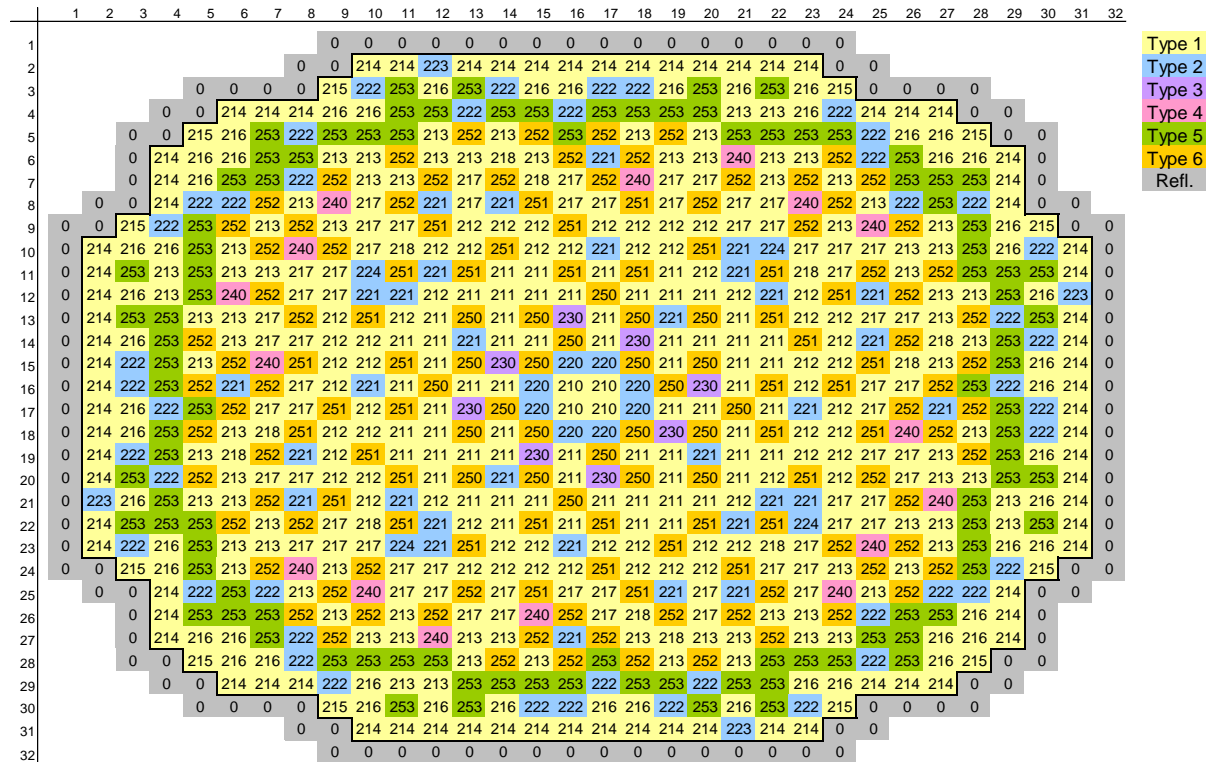


Figure 5-21: TRACE/PARCS mapping of the core with respect to the TH mapping for 20 CHANs (0: Reflector; 210-253: CHAN), color code denotes fuel types and numbering the treatment of TH.

5.3.3 Comparison of the TRACE/PARCS Simulations using different nodal Cross-section Sets based on SCALE and CASMO-4

The TRACE/PARCS simulations are performed for HFP conditions of the BWR core characterized by the 3D exposure of 6.6 FLD and the control rod arrangement for a critical core configuration as illustrated in Figure 5-22. The couple simulations are carried out with two different cross-section libraries; one generated with SCALE6.0/TRITON/NEWT and the other one with CASMO. Both libraries are converted into the PMAXS format using GenPMAXS and additional tools developed for this purpose.

In addition, the influence of the void history effect (HIST) on the core simulations is investigated by comparing the TRACE/PARCS results with the ones predicted without considering the void history effects (no HIST).

In total four TRACE/PARCS steady state simulations have been performed where two of them are using the PMAXS libraries generated with SCALE6.0/TRITON/NEWT and the other two the ones generated with CASMO-4. In the Table 5-4 the effective multiplication factor as calculated for both the no HIST and the HIST cases are summarized. The table shows that the core simulations using PMAXS libraries based on SCALE/TRITON/NEWT (TRITON) tends to overpredict the k_{eff} compared to the predictions using PMAXS libraries based on CASMO-4. On the other hand, the TRACE/PARCS predicts a higher k_{eff} value when the void history effect is taken into account.

The over-prediction by using the TRITON PMAXS libraries compared to the CASMO-4 cross-section sets is described in the sections 5.1.4 and 5.2.2. The higher k_{eff} by considering the history effect originates in the core average void fraction. The average void fraction as function of the core height is illustrated in Figure 5-24. Thereby, the “HIST” cases show higher void fractions as the “no HIST” ones. As mentioned in section 5.1.3 a case with zero void fraction has a higher k_{eff} than the case with a void fraction of 80 %. Thus, k_{eff} of the “HIST” cases is higher.

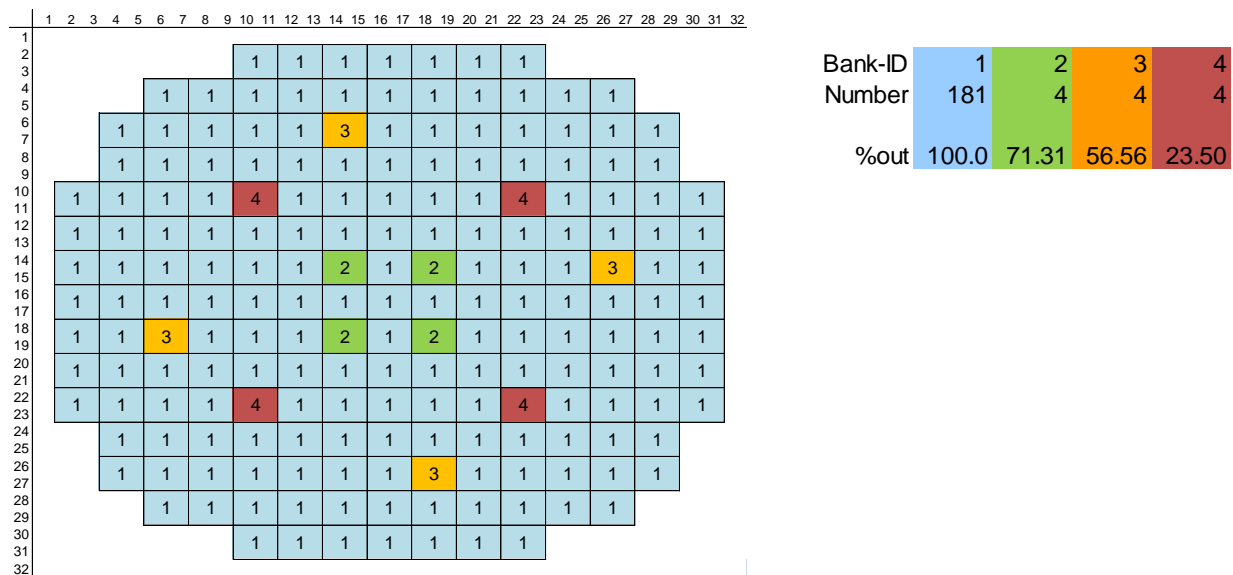


Figure 5-22: Control rod arrangement and corresponding position in [%] for a critical configuration of the BWR Critical core control positions.

Table 5-4: TRACE/PARCS Multiplication factor k_{eff}

	no HIST	HIST
TRITON	1.00672	1.00807
CASMO	0.98886	0.99057
Δk_{eff} (pcm)	1806	1767

The calculated core averaged axial power profile as a function of the core height is shown in Figure 5-23. The axial power profiles predicted without considering the history effect of the cross-sections exhibit a peak shifted to the lower core part while the ones calculated taking into account the history cases reveal a flat profile. As mentioned above and in section 5.1.3 a case with zero void fraction has a higher k_{eff} than the case with a void fraction of 80 % where the burnup is larger. Hence the power level of the “no HIST” cases, using only the branches of the reference history case (here void = 40 %), is higher in the lower and less in the upper core domain than that of the “HIST” case.

The higher power level of the CASMO-4 simulation in the lower core part is resulting from the void reactivity feedback as shown in Section 5.1.5. The CASMO-4 cross-sections are stronger affected by void and leading to a more pronounced shift of power to the bottom core part compared to TRITON. The deviation of the axial power profile predicted by PARCS using the TRITON cross-section set from these predicted by PARCS using the CASMO cross-section set amounts to -7.6 % neglecting the history effect and -10.6 % considering the history effect.

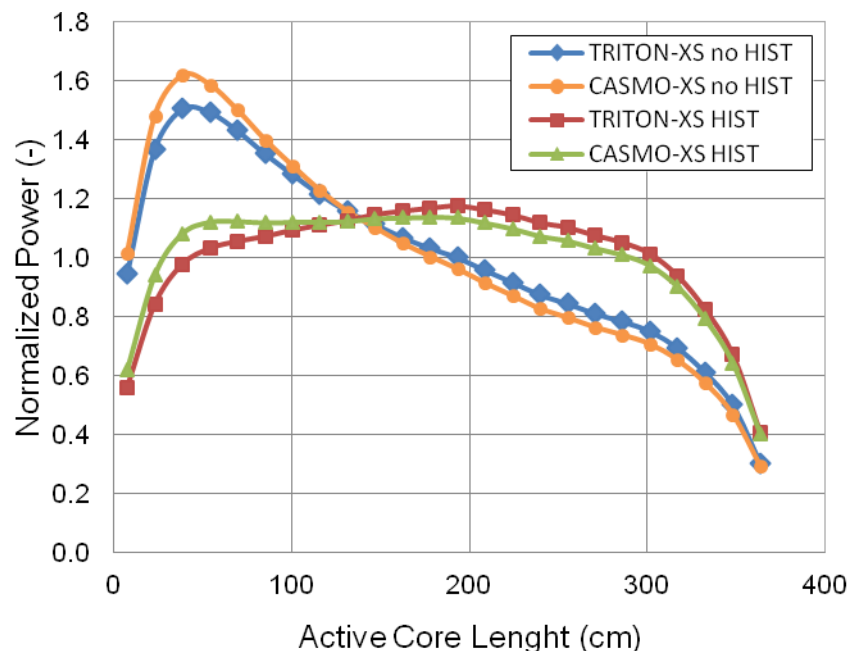


Figure 5-23: Computed normalized power as a function of the core height of a BWR core at 6.6 FLD for TRACE/PARCS simulations based on different cross-section sets with and without incorporating history (HIST) effects.

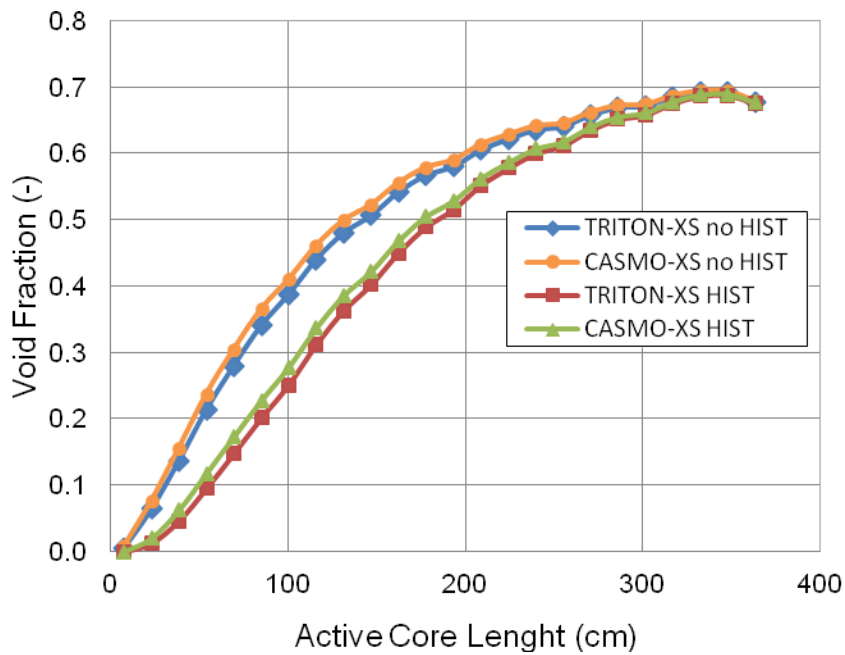


Figure 5-24: Computed void fraction as a function of the core height of a BWR core at 6.6 FLD for TRACE/PARCS simulations based on different cross-section sets with and without incorporating history (HIST) effects..

Figure 5-25 and Figure 5-26 illustrate the deviations of the radial power predicted by PARCS using TRITON and respectively CASMO-4 cross-section sets considering the history effect (HIST) and not considering the history effect (no HIST). The deviations for the TRITON and the CASMO-4 simulations are similar and vary from -7.7 % to 9.5 % for TRITON and from -7.7 % to 9.9 % for PARCS.

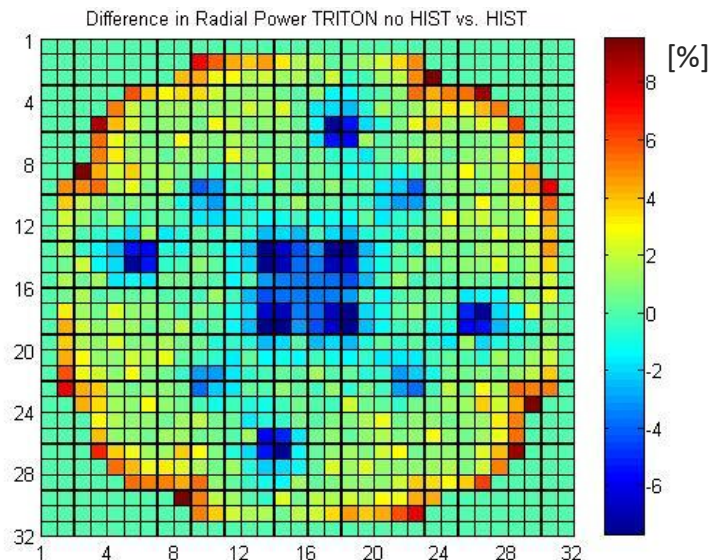


Figure 5-25: Computed deviation of the average radial power distribution at 6.6 FLD for TRACE/PARCS simulations based on a TRITON cross-section set considering and not considering history (HIST) effects.

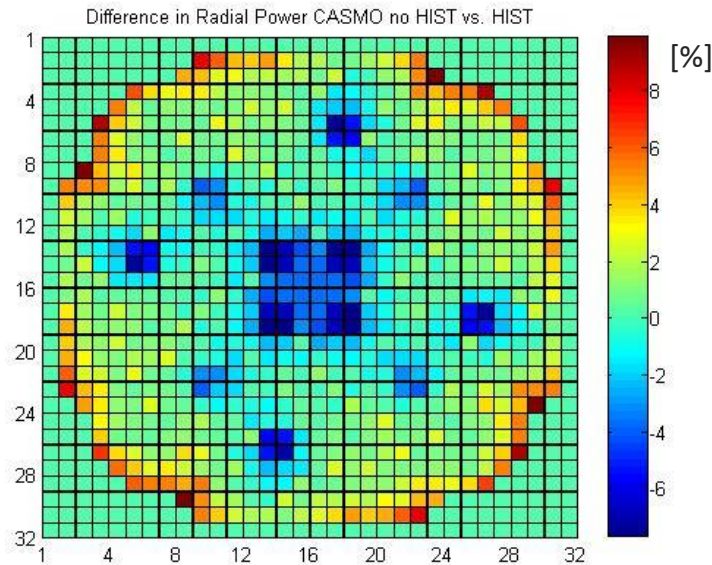


Figure 5-26: Computed deviation of the average radial power distribution at 6.6 FLD for TRACE/PARCS simulations based on a CASMO-4 cross-section set considering (HIST) and not considering (no HIST) history effects.

In both cases PARCS tends to overpredict the radial power at the core boundary to the reflector region. Further the fuel assembly positions with drawn-in control rods (rodded FA) show large deviations. The more the control rods are withdrawn, the bigger is the deviation. This indicates the importance of considering the history effects, particular in regions with strong flux gradients as the control rod and the reflector region.

The deviation of radial power profile predicted by PARCS using the different cross-section sets of TRITON and CASMO-4 considering and not considering the history effect is illustrated in Figure 5-27 and Figure 5-28. For the “no HIST” case the deviation varies from -5.1 % to 3.5 % and for the “HIST” case it varies between -4.7 % and 3.5 %. This is the same behavior as shown in section 5.2.2. The simulations using the TRITON cross-section set underpredict the fuel assembly power at the core boundary to the reflector region.

Summarizing it can be stated that, the coupled TRACE/PARCS simulations confirm the single fuel assembly depletion and stand-alone PARCS results presented in section 5.1 and section 5.2 respectively. The simulations show the importance of considering history effects as well as adequate modeling of the reflector region and the control rods. Though there are deviations of more than 10 % between the use of the different cross-section sets, the used computational route of SCALE6/NEWT/TRITON and TRACE/PARXS is seen as appropriate approach for transient analysis and for further calculations.

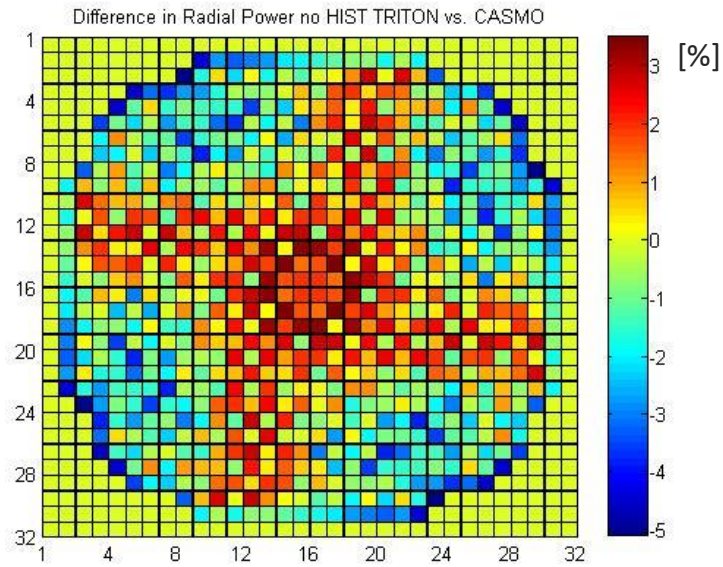


Figure 5-27: Computed deviation of the average radial power distribution at 6.6 FLD for TRACE/PARCS simulations using either TRITON or CASMO-4 cross-section sets considering no history effects (no HIST).

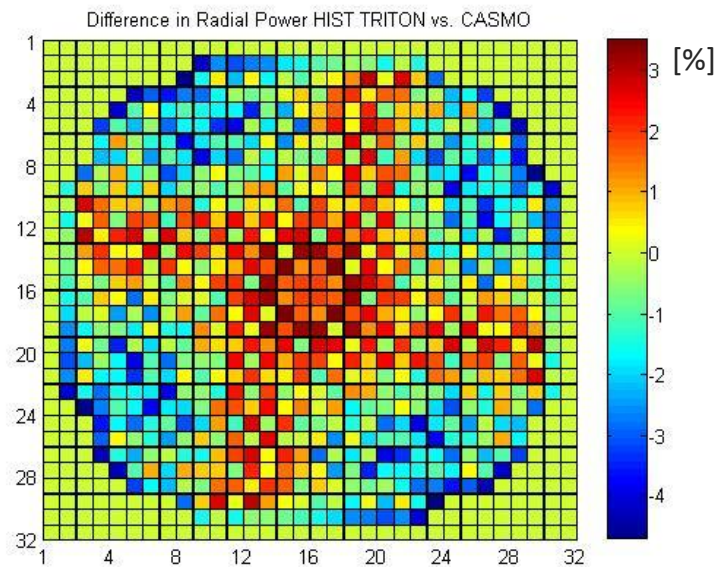


Figure 5-28: Computed deviation of the average radial power distribution at 6.6 FLD for TRACE/PARCS simulations using either TRITON or CASMO-4 cross-section sets considering the history effects (HIST).

6 Validation of a Turbine Trip Event with TRACE/PARCS using BWR Plant Data

The validation of the whole computational framework described in the former sections is performed using plant data measured in the reference plant during an unplanned Turbine Trip event (TT) that took place in 1998 when the plant was operated at nominal power.

For this purpose, an integral plant model comprising all relevant systems and components with a three-dimensional core model for TRACE/PARCS is elaborated. The integral model of the reference plant is constructed by the merging of the 3D TH and NK core model presented in Chapter 5 and the plant model developed in [99]. This model includes the entire reactor pressure vessel consisting of the internal recirculation pumps, steam separators, dryers, downcomer and the lower and upper plenum. The details of the models are outlined below.

6.1 Description of the Turbine Trip Event

The Turbine Trip (TT) event occurred the 26th July 1998 at 14.57 pm when the reference plant was operated at nominal power of 3840 MW_{th}. The TT-event was initiated by a sudden closure of the Turbine Stop Valve (TSV) due to the false alert of the condenser pressure controller (the condenser pressure limit of 0.145 bar was never exceeded). The pressure control system of the plant started the opening of the Turbine Bypass Valve (TBV) approximately 0.05 seconds after the closure of the TSV to ameliorate the pressure spike. The change of the position of the TSV and TBV after the TT-start is indicated in Figure 6-1. Since the diameter of the piping system of the TBV is about 60 % of the one of the TSV and due to the time shift for the opening and closure of these valves, a pressure wave propagated from the steam line to the reactor core leading to a void collapse and as a consequence to a sudden power increase. It must be noted that the operators also manually opened some safety relief valves for short time to control the pressure increase in the steam lines and to avoid SCRAM.

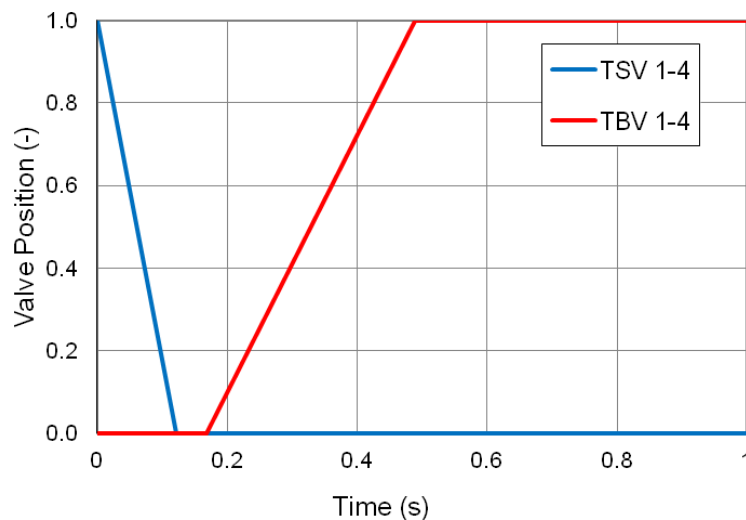


Figure 6-1: Detected positions of the turbine stop and turbine bypass valves (1 open, 0 closed).

Additionally the rotation speed of all eight main recirculating pumps (MRP) were reduced within few seconds to the lower limit (611 rpm). During this procedure the MRP number 7 failed and was completely shut down, see Figure 6-2. A partial insertion of the control rods was also carried out to control this event. Consequently, the reactor power stabilized after few minutes at around 35 % of the nominal power. At the begin of the transient the rise of the fuel temperature stopped the rapid power jump due to the increased neutron capture in uranium 238 – the so called Doppler broadening effect. Later, the reduced mass flow rate led to a higher void generation and thereby to reduced neutron moderation.

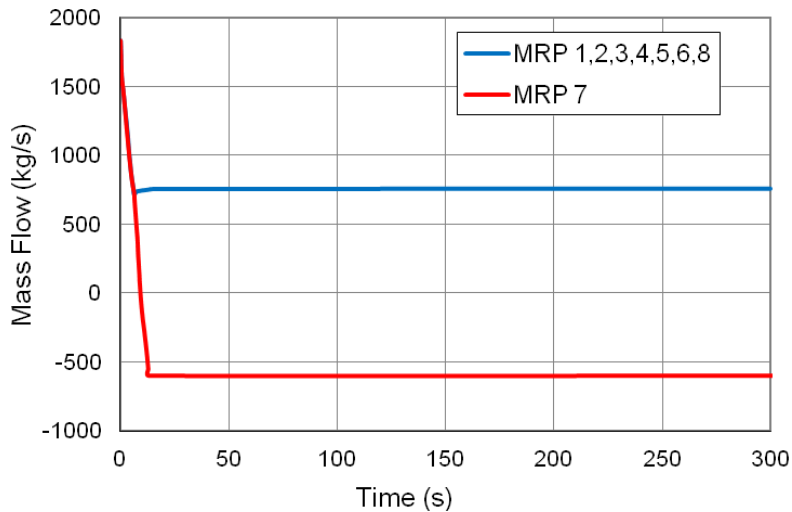


Figure 6-2: Measured mass flow of the 8 main recirculation pumps MRP 1-8.

Due to the reduced speed of the MRPs the total amount of feed water decreased and also the temperature of the feed water were reduced at the end of the transient as indicated in the Figure 6-3 and Figure 6-4.

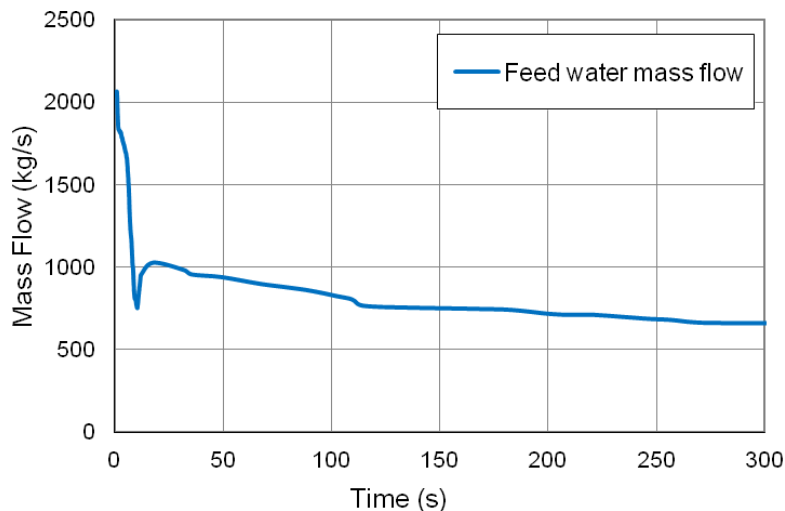


Figure 6-3: Measured total feed water mass flow.

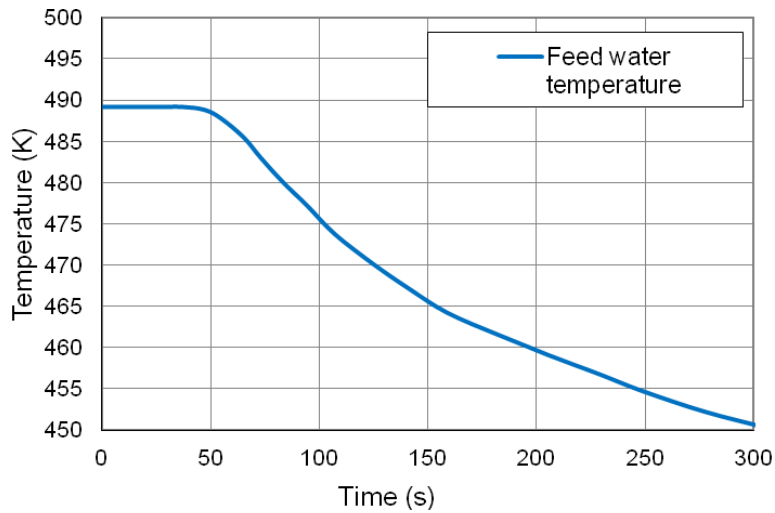


Figure 6-4: Measured feed water temperature.

The movement of the control rods just after the TT-start is exhibited in Figure 6-5. In total, 8 absorber cross banks were inserted into the core.

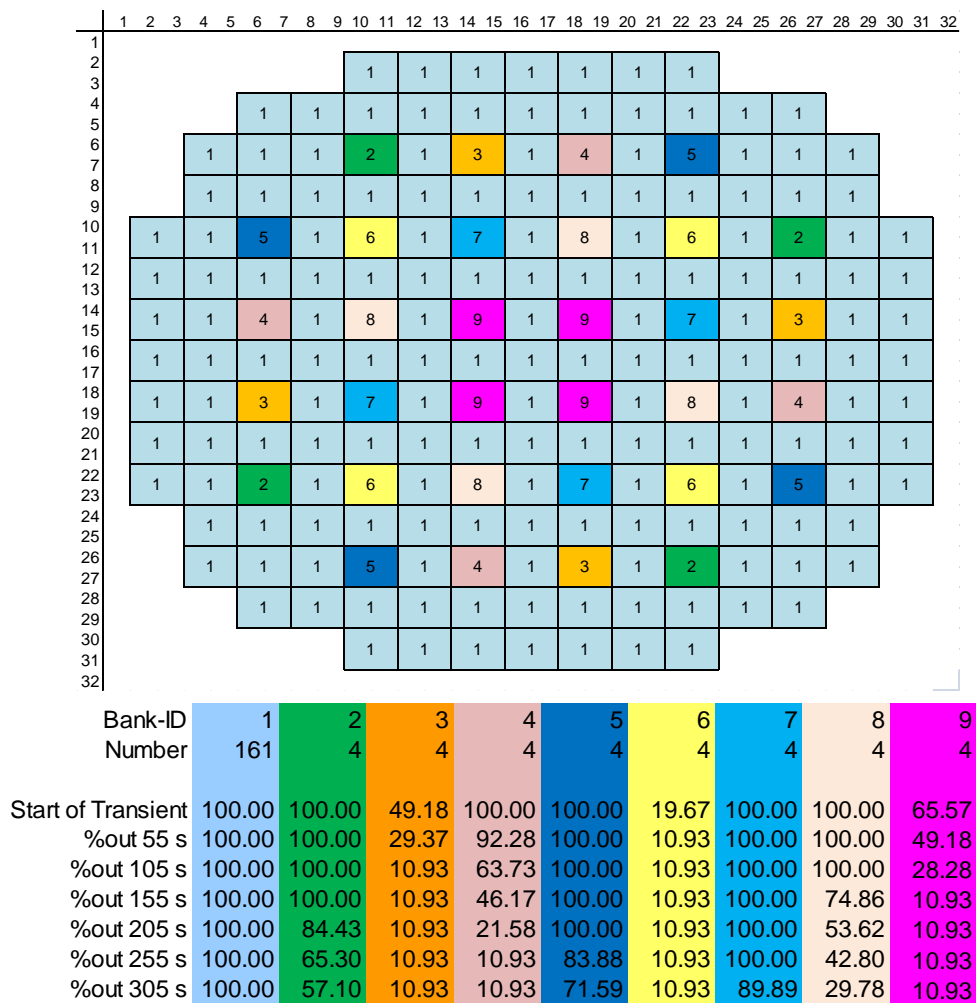


Figure 6-5: Sketch of the positions of the control rods and their temporal positions during the TT event.

6.2 TRACE integral plant model

The integral TRACE model of the reference plant is shown in Figure 6-6. The most challenging part is the development of the reactor pressure vessel with the key components in all geometrical details of the fuel assemblies' foot and head parts, the lower and upper grid plate, the separators and dryers, etc. As described in [99], the RPV is represented with the three-dimensional VESSEL component of TRACE. The RPV is subdivided in 22 axial nodes to taking into account constructive peculiarities of the internals. In radial direction, the RPV is divided into two rings, one for the core region and the other for the downcomer region. Two different nodalizations of the core are considered in azimuthal direction: The first one consists of one azimuthal sector (1 az) resulting in a 2D thermal-hydraulic model. The second one consists of eight equal segmented sectors (8 az) describing a coarse 3D thermal-hydraulic model. For the "one-sector model (2D)" the main internal components of the core e.g. the eight recirculation pumps, the separators, the dryers are represented by only one component (PUMP, SEPARATOR) while for the "eight-sector model (3D)" eight components, one per azimuthal sector, are considered.

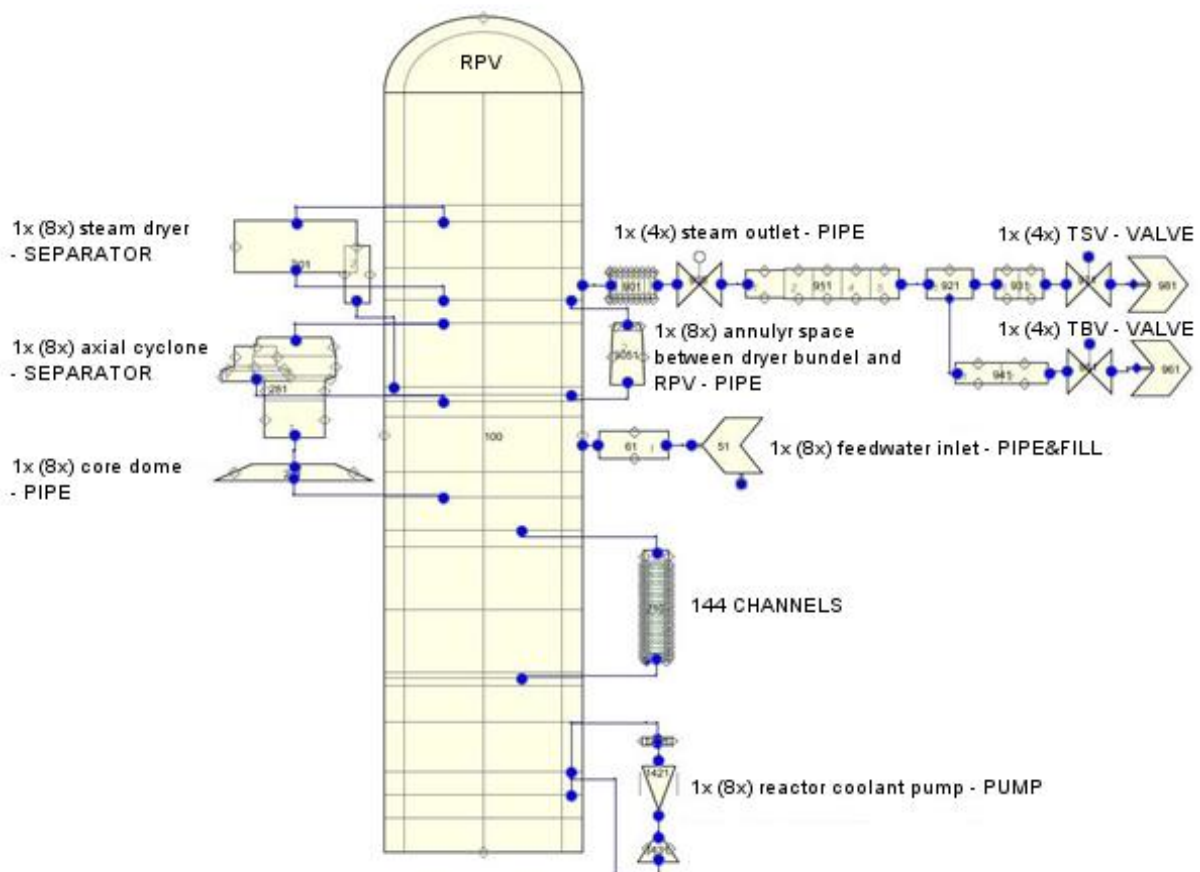


Figure 6-6: Integral BWR plant model realized in TRACE (in brackets the number of components for 8 azimuthal sectors).

The different fuel assembly types, radially distributed within the core, loaded at the time of the TT-event are grouped in 144 CHAN TRACE components. Hence, in each azimuthal core sector contains 18 CHANs. The CHAN component allows a representation of each BWR-fuel assembly in terms of water rods, different types of fuel rods e.g. full and part length fuel rods, canister etc. The CHAN component is axially subdivided in 27 nodes from which only 24 nodes correspond to the fuel part, one to the inactive foot (bottom) and the two other nodes to the fuel assembly head (top). The fuel assembly foot is connected with the bypass by a leak path. The bypass is represented by the inner ring of the VESSEL component.

The calculation of thermal-hydraulic parameters such as form loss coefficients, flow areas, hydraulic diameters for geometrically complex structures is very challenging and their quality will determine the quality of the predictions (here FA values provided in [93] are used). This is valid for all coarse mesh 2D/3D and even 1D thermal-hydraulic codes. Hence, assumptions and simplifications are often introduced by the model developers to describe the underlying physical phenomena correctly. For example, the flow path through the control rod guide tube head is not modelled but is taken into account by a pressure loss coefficient at the fuel assembly foot.

The core dome and the free volume between the reactor pressure vessel wall and the steam dryer bundles are modelled by PIPE components. The numerous axial cyclones and steam dryers are modelled in contrast to other studies [21], [100] by two SEPARATOR components at different axial elevations of the RPV. The reactor pressure vessel is connected with four (or eight) steam line. They are modelled with PIPE components while the safety valves, the TSV and the TBV are represented by the VALVE component. The feed water lines are represented in a simplified manner by a PIPE and a FILL component while the turbine is modelled as a mass sink by the BREAK component. There, the pressure boundary condition is defined in TRACE. Additionally signal variables, TRIP and CONTROL components are implemented in the TRACE thermal-hydraulic model for the description of some actions such as opening or closure of valves, shutdown of a PUMP component, or for the control rod movement.

6.3 Neutron-kinetic PARCS 3D Model

The 3D core model for PARCS corresponds to that in Section 5.2.1. Since the thermal-hydraulic core model consists of 144 CHANs, the mapping between the TH nodes and the NK homogenized nodes is different to that of the previous chapters. As mentioned, the core is subdivided in eight sectors with 18 CHANs in each sector. These 144 CHANS are representing six fuel assembly types and one reflector.

The radial position of the TH computational domains which corresponds to one NK homogenized is defined in the TRACE/PARCS mapping as illustrated in Figure 6-7.

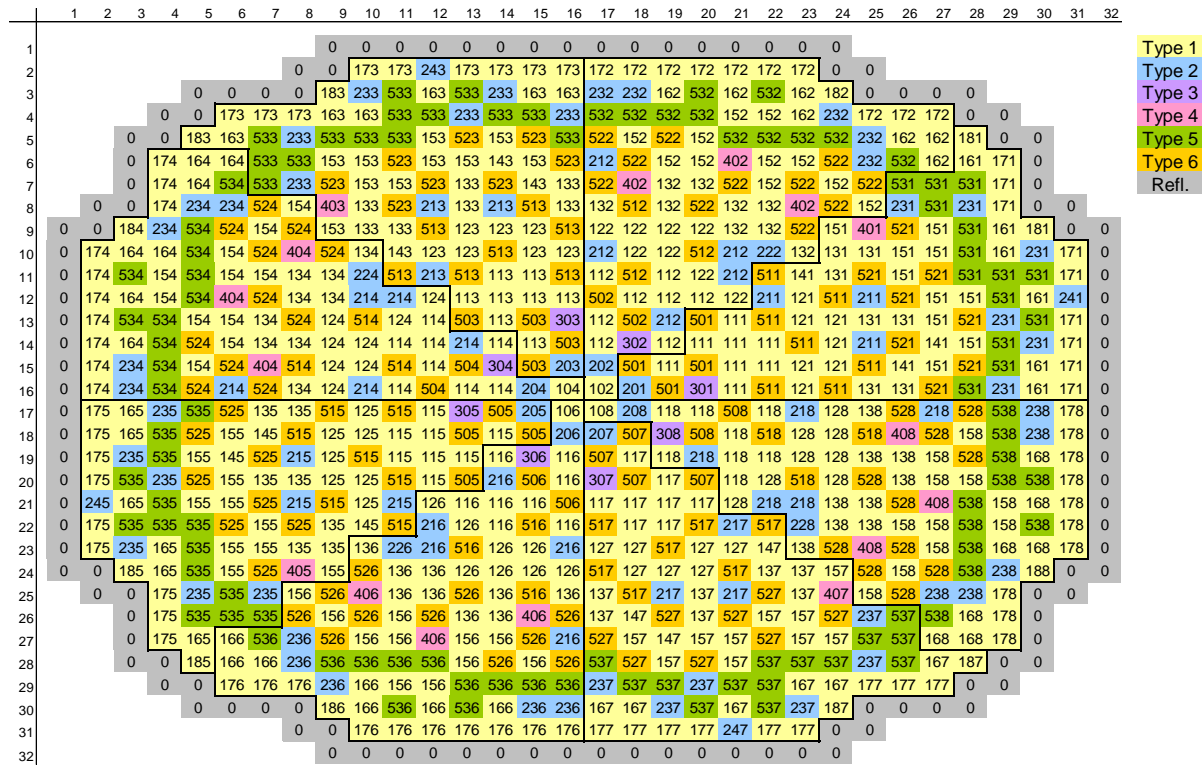


Figure 6-7: TRACE/PARCS mapping for 144 CHANs (0: Reflector; 102-538: CHAN)

6.4 Analysis of the Turbine Trip Event with TRACE/PARCS

The TT-event is analysed with the coupled TRACE/PARCS code system with the TRACE Version V5P2 and the PARCS Version 3.0. First of all, a steady state simulation of the plant conditions just before the TT-event is performed with both the TRACE stand-alone and the TRACE/PARCS coupled code. This step is necessary to ensure that both models are able to describe the initial plant conditions adequately. Based on these simulations, the appropriateness of the thermal-hydraulic and neutron physical TRACE and PARCS models is analysed.

The transient phase of the TT-event has been analysed by TRACE/PARCS using two different cross-section libraries generated with CASMO-4 and SCALE6.0/TRITON/NEWT, respectively. The following four simulations were performed:

- Simulation 1: TRACE/PARCS with TRITON XS and a 2D RPV model (TRITON-XS 1 az)
- Simulation 2: TRACE/PARCS with TRITON XS and a 3D RPV model (TRITON- XS 8 az)
- Simulation 3: TRACE/PARCS with CASMO XS and a 2D RPV model (CASMO- XS 1 az)
- Simulation 4: TRACE/PARCS with CASMO XS and a 3D RPV model (CASMO- XS 8 az)

6.5 Comparison of the TRACE/PARCS Predictions with the plant data

During the TT-event few integral parameters of the plant were recorded with time intervals of roughly 50 seconds. Hence, only few integral data with limited resolution in time are available for comparison with the code predictions. The pressure evolution in the RPV dome predicted by the simulations 1, 2, 3, and 4 is compared to the measured data in Figure 6-8. All predictions are close to each other and differ about 3 % to the measured data. This means that for areas, where is no physical cut-off, the pressure is not a sensitive measurement and 2D RPV models are sufficient enough to predict global pressures.

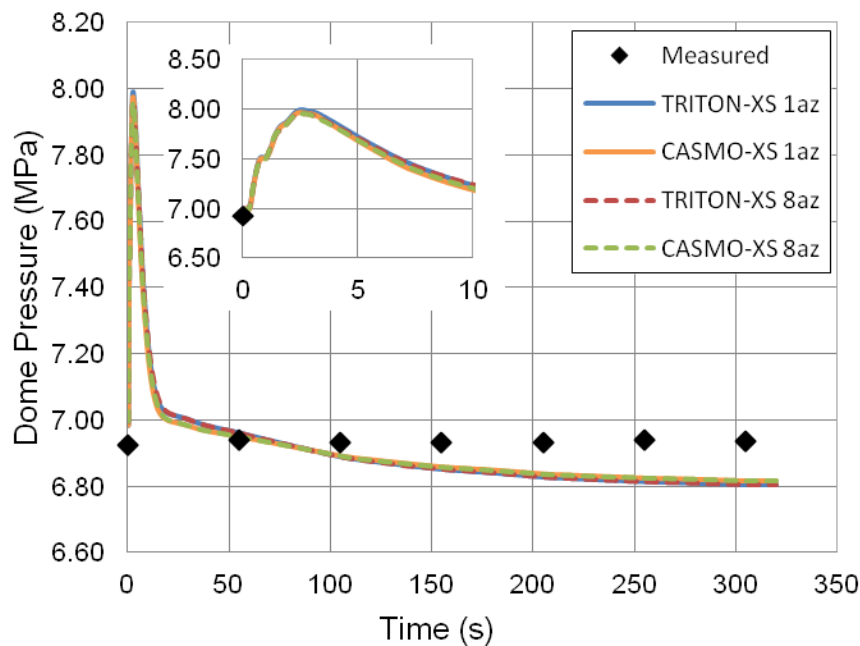


Figure 6-8: Comparison of the steam dome pressure calculated with TRACE/PARCS for different azimuthal TRACE models and cross-section sets to measured plant data.

Figure 6-9 shows a comparison of the predicted void fraction with a “derived core averaged void fraction” which was obtained based on the information of the “process computer” (Überwachungsrechner). There the initial values are quite well predicted by all simulations (1 to 4). The subsequent trend of the simulations shows an underprediction of about -10 % for the CASMO simulations and about -15 % for the TRITON calculations. Thereby, the predicted void fractions by CASMO and TRITON show the same behaviour as shown in Section 5.3.3. As the core averaged void fraction wasn't be directly measured and possibly local effects affected the estimation of the core average void fraction by the process computer data, this deviation is seen as acceptable. This also becomes more clear as the range of underprediction is not reflected in the power and the steam dome pressure. The simulations 1 and 2 show a maximal deviation of the pressure dome prediction of -1.903 %. The simulation 3 and simulation 4 show a deviation of -1.745 % and -1.759 %. It should be noted that the design pressure of 8.63 MPa of the RPV has been never exceeded by one simulation.

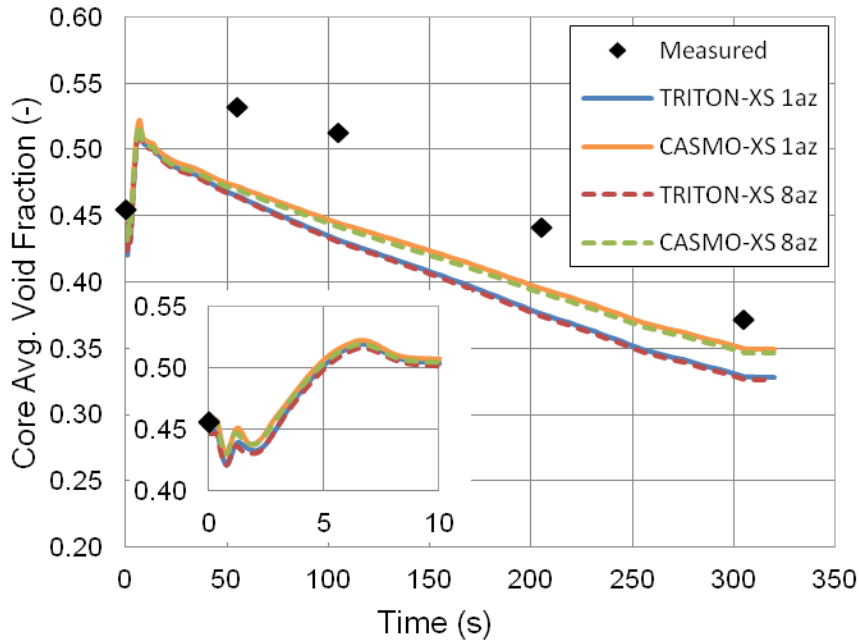


Figure 6-9: Comparison of the core average void fraction calculated with TRACE/PARCS for different azimuthal TRACE models and cross-section sets to process computer data.

In Figure 6-10 the predicted total power is compared to the measured data. It can be observed that the large power spike calculated by TRACE/PARCS was not recorded in the plant. However the global temporal evaluation of the predicted power is similar to the one of the measurement. The underprediction after the power peak is becoming smaller with increasing time. It must be noted that all simulations (1 to 4) predict similar power rises independent of the cross-section data as well as the 2D or 3D RPV modelling. The partial insertion of control rod banks and the reduced recirculation and feedwater mass flow reduces later in the transient the power to about 31 % (simulation 1 and 2) or respectively about 32 % (simulation 3 and 4). The total power evolution is a result of the interplay of competing reactivity feedback coefficients such as Doppler, void and control rod. The power trend is correlated to the core averaged fuel temperature, shown in Figure 6-11. Due to the so called “Doppler Effect” the power rise is stopped few seconds after event initiation preventing a fuel rod damage. The analysis of the simulations show:

- The simulation 1 predicts a lower maximum power (5407 MW) than the simulation 2 (5522 MW). The time of maximum power occurs at 0.729 s and 0.699 s for the simulation 1 and simulation 2.
- The simulation 3 predicts a higher power (5464 MW) than the simulation 4 (5234 MW). The time of maximal power is 0.715 s and 0.688 s for simulation 3 and 4.
- The maximal fuel temperatures predicted by simulation 1 and 2 is 818.48 K and 816.95 K while the ones calculated by simulation 3 and 4 are 819.56 K and 817.98 K.

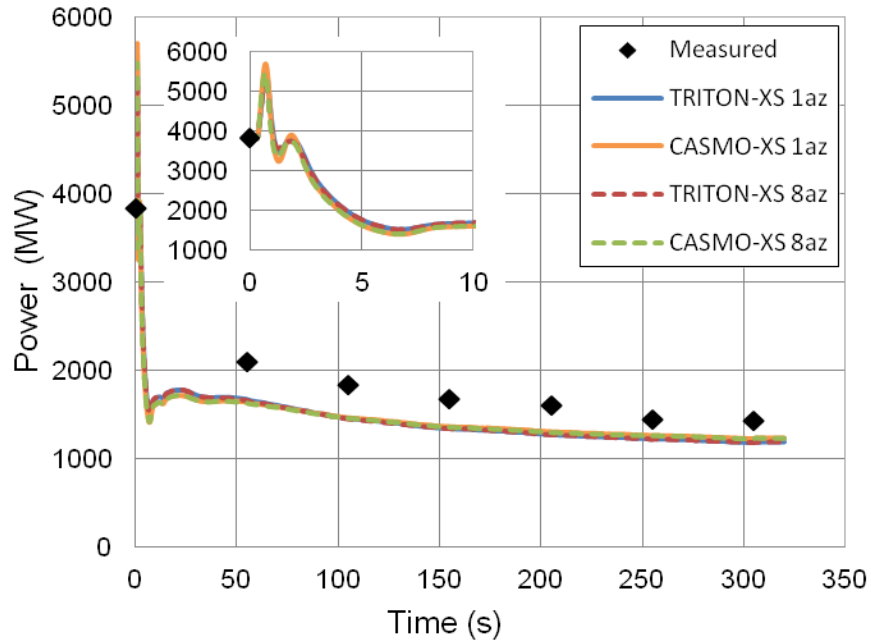


Figure 6-10: Comparison of the predicted total core power calculated with TRACE/PARCS for different azimuthal TRACE models and cross-section sets to process computer data.

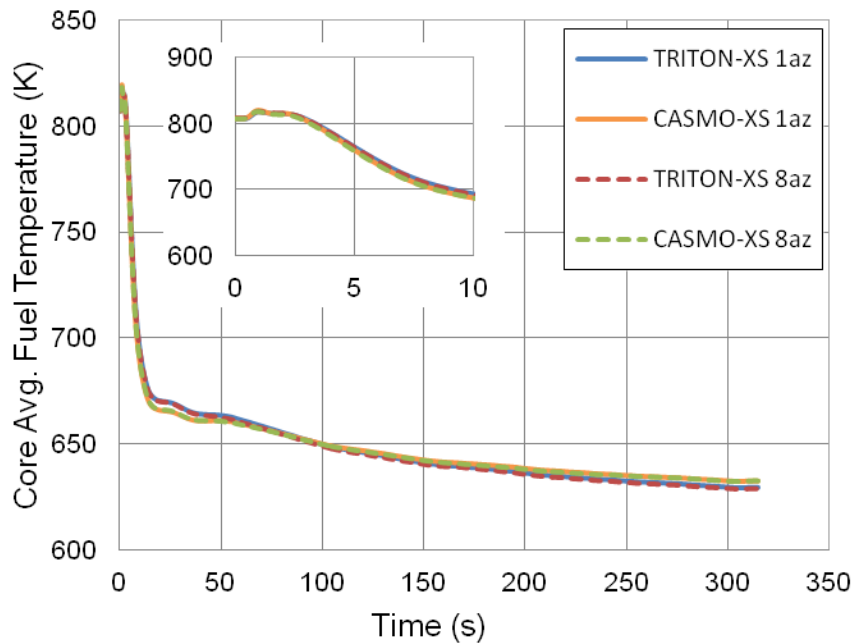


Figure 6-11: Comparison of the core averaged fuel temperature calculated with TRACE/PARCS for different azimuthal TRACE models and cross-section sets.

In Figure 6-12 and Figure 6-13, the evolution of the predicted reactivity contributors due to fuel temperature (TF), coolant density (DC) and control rod (CR) as well as the total reactivity (SUM) as calculated by the simulations 1 to 4 are exhibited. The reactivity coefficients predicted with 2D (1az) and 3D (8az) thermal-hydraulic RPV models as well as for the different cross-section sets are in a good agreement.

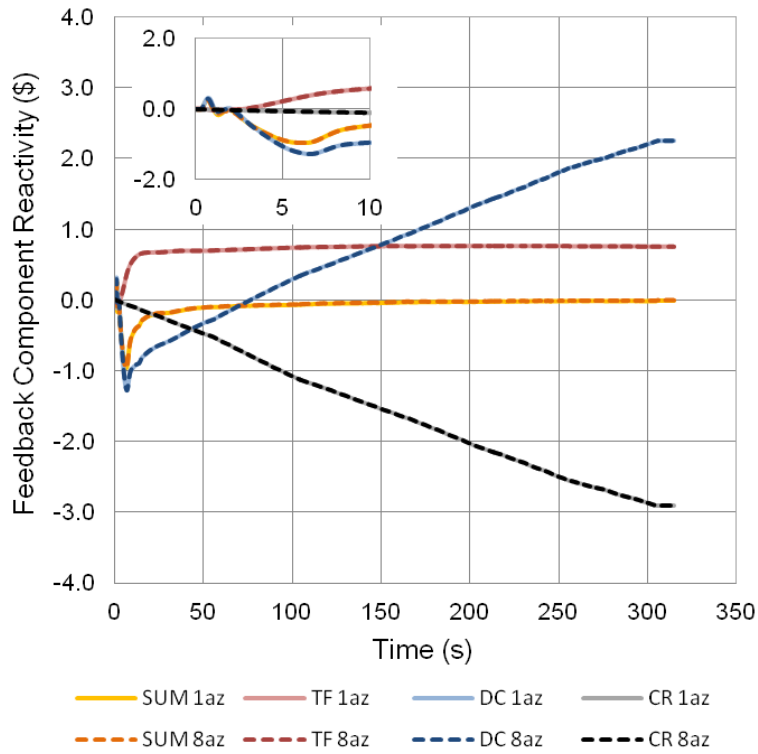


Figure 6-12: Comparison of the reactivity feedbacks calculated with TRACE/PARCS for different azimuthal TRACE models using TRITON cross-section sets.

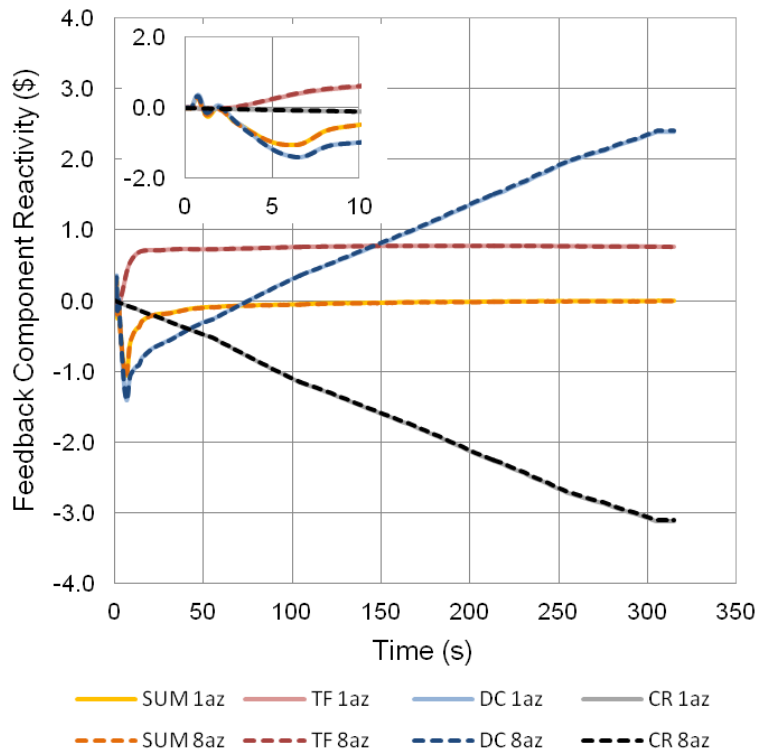


Figure 6-13: Comparison of the reactivity feedbacks calculated with TRACE/PARCS for different azimuthal TRACE models using CASMO cross-section sets.

The Figure 6-14 and Figure 6-15 illustrate the deviation of the core averaged radial power distribution predicted with TRACE/PARCS using the TRITON XS and CASMO XS. Since this event is no symmetrical, a difference in the radial power profile predicted with a core model consisting of one azimuthal sector (1az) or eight sectors naturally appears. Especially in the sector 7, where the failed main recirculation pump is located, deviations are visible. Thereby the deviations for both cross-section sets are the same range. This indicates the importance of multidimensional models for local events.

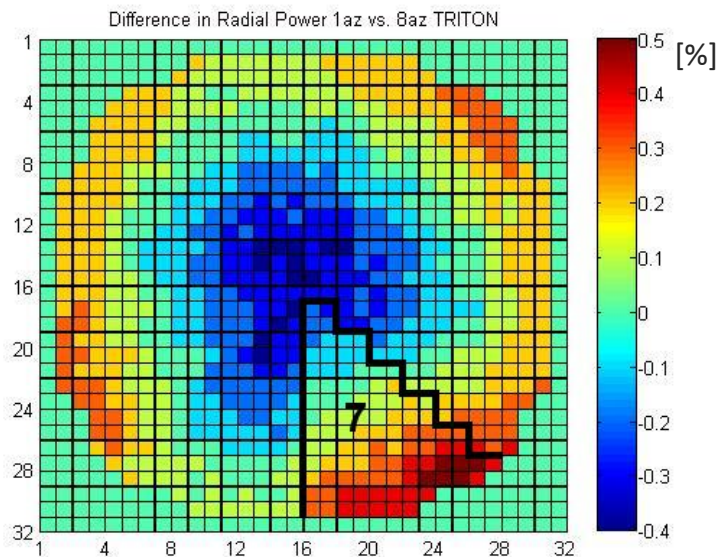


Figure 6-14: Computed deviation of the average radial power distribution at the time of the maximum power peak for TRACE/PARCS simulations based on TRITON cross-section sets considering different azimuthal TRACE models.

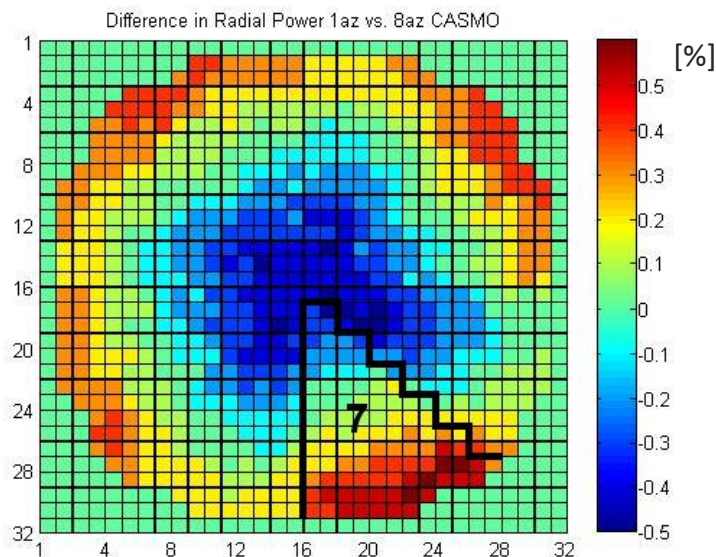


Figure 6-15: Computed deviation of the average radial power distribution at the time of the maximum power peak for TRACE/PARCS simulations based on CASMO cross-section sets considering different azimuthal TRACE models.

In addition, the deviations of the radial power profile predicted with different cross-section sets (TRITON and CASMO) are illustrated in Figure 6-16 for the eight sectors RPV model. The simulations show the same range of deviations as already presented in Section 5.3.3.

Summarized, the coupled TRACE/PARCS simulations of a turbine trip using different cross-section sets are in a good agreement with plant data. Thereby the deviation of the results for 8 azimuthal sectors using TRITON cross-section sets to the ones predicted with CASMO cross-section sets are in the same range as shown in Section 5.3.3 for the simplified TRACE core model with 1 azimuthal sector.

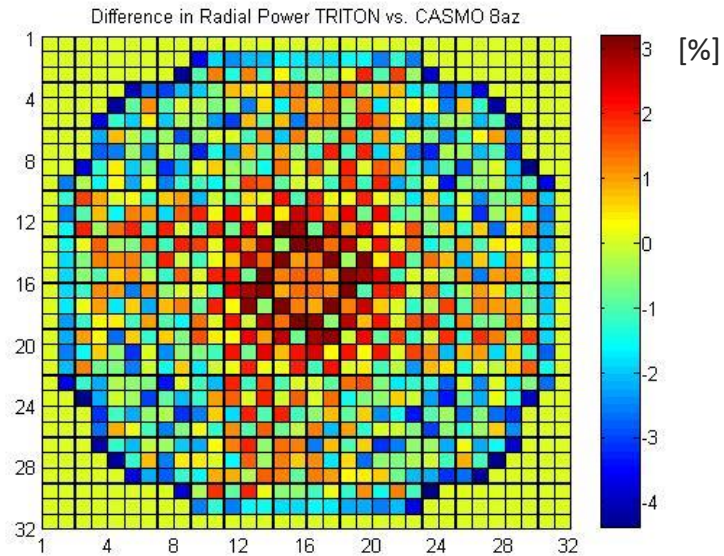


Figure 6-16: Computed deviation of the average radial power distribution at the time of the maximum power peak for TRACE/PARCS simulations using either TRITON or CASMO-4 cross-section sets considering the TRACE model with 8 azimuthal sector.

7 Uncertainty and Sensitivity Analysis

To analyse the influence of the cross-section uncertainties on transient analysis, the methodology to quantify the code's uncertainty described in Section 3.5 will be applied for the analysis of a postulated pressure perturbation transient with TRACE/PARCS. The simplified transient has been chosen because of the large calculation time one run of the turbine trip event requires.

One of the most important safety relevant parameter is the peak cladding temperature (PCT), which indicates the point beyond a fuel rod failure can be assumed. According to the United States Nuclear Regulatory Commission (U.S.NRC) the calculated maximum fuel rod cladding temperature shall not exceed 2200° F (1200 °C) [103]. Thereby a significant change or error is one which results in a calculated peak fuel cladding temperature different by more than 50 °F (10 °C) from the temperature calculated for the limiting transient using the last acceptable model, or is a cumulation of changes and errors such that the sum of the absolute magnitudes of the respective temperature changes is greater than 50 °F (10 °C).

The used methodology is working with the PARCS output, which contains no PCT. Thus, the core average fuel temperature and the following parameters will be analysed to show the influence of neutronic parameters:

- Reactivity
- Core Power Level
- Core Average Fuel Temperature
- Core Average Coolant Density

A two sided tolerance limit, with a 95 % fractile and a confidence level of 95 % is used for the uncertainty analysis. According to Wilk's formula (Eq. 3.17) 100 runs of TRACE/PARCS with a simplified TH core model of section 6.3 at Hot Full Power (HFP) conditions are performed for each case, using the uncertainty values generated by SUSA. Thereby type 4 of the cross-section modification in PARCS is used.

7.1 Uncertainties in neutronic data

As describe in Section 2.4, a key step performing uncertainty and sensitivity (U&S) studies is the selection of a determined number of parameters which could affect the result. To perturb, for each uncertain parameter the nominal value, the maximum and the minimum values as well as the type of the probabilistic distribution given by the probability density function (PDF) must be defined. In this case, the neutron-kinetic parameters of PARCS will be perturbed just after they are read in from the cross-section tables (PMAXS) during the PARCS simulation (XS update).

A selection of neutronics parameters, based on the work of Gajev [101], is presented in Table 7-1. The cross-section parameters uncertainties are approximated using the results of the target accuracy study for cross-sections of a PWR reactor [102]. It should be noted that these uncertainties are rather illustrative than precise. Due to this engineering judgment and since the type of PDF is not known a uniform distribution was chosen.

Table 7-1: Selection of perturbed neutronic parameters and their uncertainties [101].

Parameter		1- σ Uncertainty	Type of Distribution
<i>Cross-section Parameter</i>			
Macroscopic transport cross-section:	Σ_t	2.5 %	Uniform
Macroscopic absorption cross-section:	Σ_a	2.5 %	Uniform
Macroscopic fission cross-section:	Σ_f	2.5 %	Uniform
Macroscopic v-fission cross-section:	$v\Sigma_f$	2.5 %	Uniform
Macroscopic scattering cross-section:	Σ_s	7.5 %	Uniform
Macroscopic κ -fission cross-section:	$\kappa\Sigma_f$	2.5 %	Uniform
Assembly discontinuity factor:	ADF	2.5 %	Uniform
<i>Kinetic Parameter</i>			
Prompt neutron generation time:	λ	0.6 %	Uniform
Delayed neutron fraction:	β	0.7 %	Uniform
Inverse neutron group velocity:	$\ln v$	0.7 %	Uniform
Fission yield:	yield	0.7 %	Uniform
<i>Poison Related Parameters</i>			
Microscopic Xenon cross-section:	σ_{Xe}	5.0 %	Uniform
Microscopic Samarium cross-section:	σ_{Sm}	5.0 %	Uniform

7.2 Uncertainty Quantification for the Pressure Perturbation Case

7.2.1 Quantification of uncertainties

One of the most important transients of a BWR is the turbine trip, where a pressure wave cause void collapsing. In this case to simulate a turbine trip event a sudden pressure jump within 0.01 s from 7.09 MPa to 7.30 MPa is assumed, as shown in Figure 7-1.

Figure 7-2 to Figure 7-5 show the curves of reactivity, power level, coolant density and fuel temperature predicted by TRACE/PARCS considering the uncertainties, as listed in Table 7-1, within the TRITON cross-sections. Thereby the reference case is the TRACE/PARCS transient calculation without any perturbation of kinetic parameters. The maxima and minima curves indicate the upper and lower boundary of the uncertainty band. At any point of time, at least 95% of the combined influence of all considered uncertainties on

the calculated parameters is in the range of the presented uncertainty limit (two-sided tolerance limit), at a confidence level of at least 95 %. Mean corresponds to the 50 %-fractile and is lying as the median and the reference case in the middle of of the uncertainty band. This indicates that the analysed parameters are symmetrical regarding to the uncertain parameters.

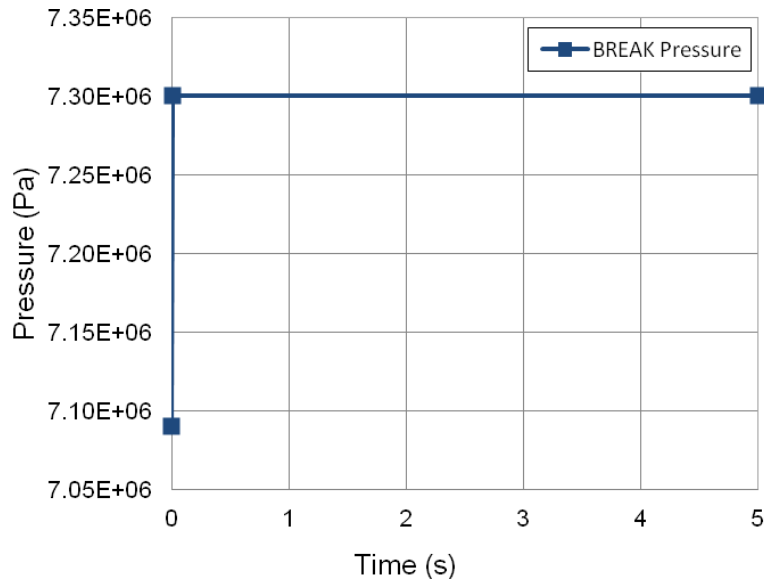


Figure 7-1: Gradient of the postulated pressure jump within 0.01 s.

As in the case of a turbine trip, void collapsing is leading to a higher coolant density (Figure 7-4). Neutrons are better moderated, the reactivity increases (Figure 7-2) and thus also the power (Figure 7-3). As the result of power increase the fuel temperature increases (Figure 7-5) and stops the power increase due to the doppler effect. This leads after a second power peak caused by delayed neutrons to a higher power level.

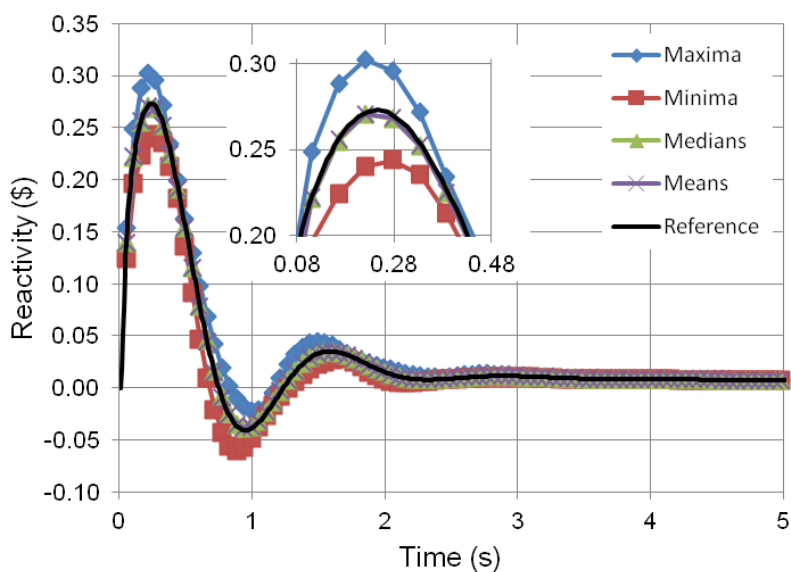


Figure 7-2: Computed reactivity for TRACE/PARCS simulations considering uncertainties within TRITON cross-section sets.

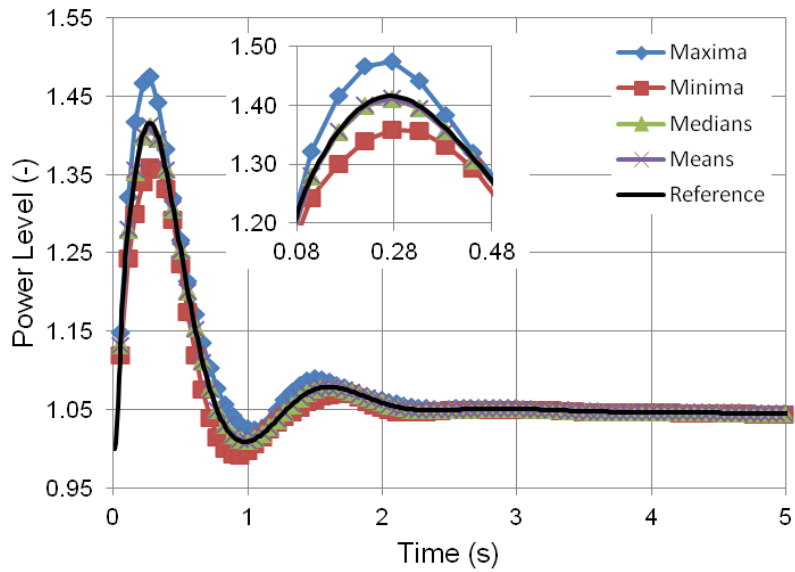


Figure 7-3: Computed core power level for TRACE/PARCS simulations considering uncertainties within TRITON cross-section sets.

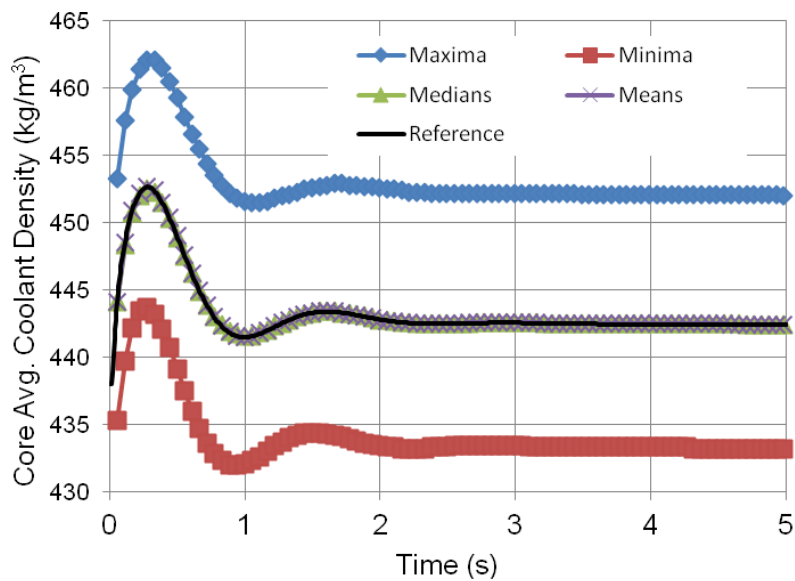


Figure 7-4: Computed core average coolant density for TRACE/PARCS simulations considering uncertainties within TRITON cross-section sets.

Whereas the results of the reactivity, power level and coolant density vary between the minima and maxima of about 20 %, 10 % and 4 % by considering cross-section uncertainties, the influence on the core average fuel temperature is small. The fuel temperature varies only about 0.1 % or 1 K. This is within the limit of 10 °C given by the U.S.NRC for PCT.

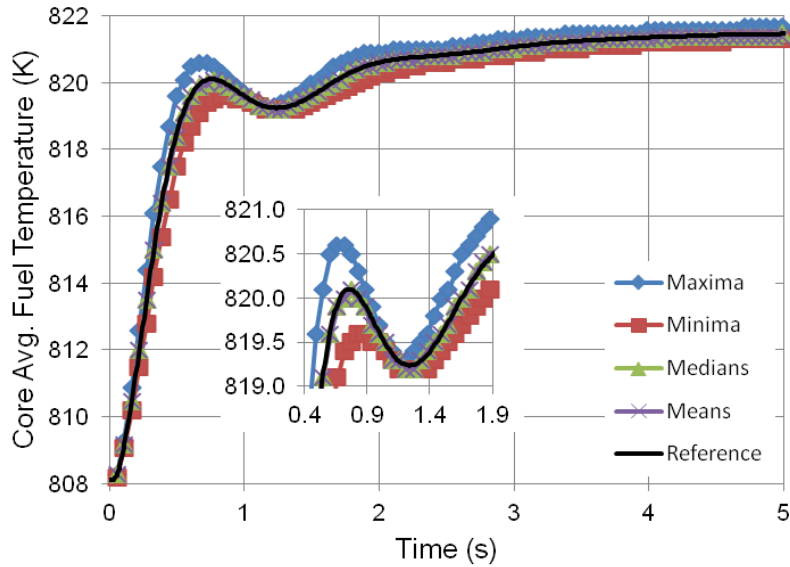


Figure 7-5: Computed core average fuel temperature for TRACE/PARCS simulations considering uncertainties within TRITON cross-section sets.

7.2.2 Sensitivity analysis for the pressure perturbation case

The Figure 7-6 to Figure 7-9 show the ordinary Pearson correlation coefficients predicted by SUSA for four target parameters in dependence on the uncertain parameters, which are listed in Table 7-2.

The reactivity, the power and the coolant density have their maximum peak around 0.25 seconds, the maximum fuel temperature is at the end of transient, since the power stabilizes after 2 seconds at around 105 % of nominal value. The uncertain parameters with the biggest influence are the macroscopic cross-sections of transport (Σ_t), ν -fission ($\nu\Sigma_f$) and absorption (Σ_a), that is the sum of capture (Σ_c) and fission (Σ_f). The subscript 1 corresponds to the fast and subscript 2 to the thermal spectrum. As can be seen an increase of the thermal $\nu\Sigma_f$ is leading to a higher maximum power peak. Contrary a larger fast cross-section of ν -fission corresponds with a less maximum power peak. An explanation of these effects will be given later for the time dependent sensitivity analysis in section 7.2.3.

Table 7-2: Index of Parameter

Index	1	2	3	4	5	6	7	8	9	10	11
Parameter	$\Sigma_{t,1}$	$\Sigma_{t,2}$	$\Sigma_{a,1}$	$\Sigma_{a,2}$	$\nu\Sigma_{f,1}$	$\nu\Sigma_{f,2}$	$\kappa\Sigma_{f,1}$	$\kappa\Sigma_{f,2}$	$\sigma_{Xe,1}$	$\sigma_{Xe,2}$	$\sigma_{Sm,1}$
Index	12	13	14	15	16	17	18	19	20	21	22
Parameter	$\sigma_{Sm,2}$	$\Sigma_{f,1}$	$\Sigma_{f,2}$	Σ_{s12}	ADF ₁	ADF ₂	lnV ₁	lnV ₂	yield	β	λ

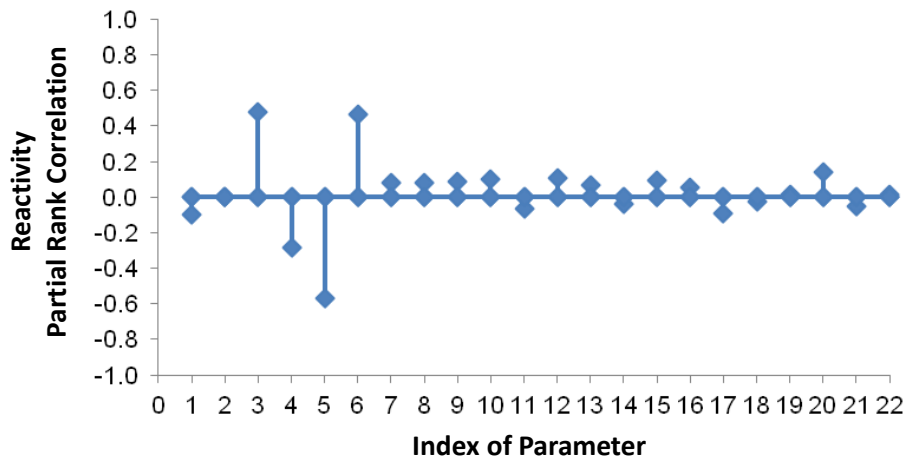


Figure 7-6: Ordinary product-moment correlation coefficients determined by SUSA for the maximum reactivity.

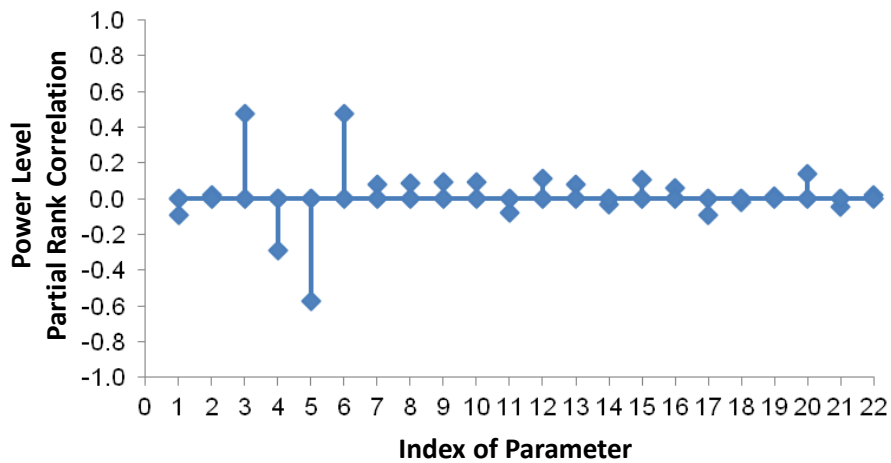


Figure 7-7: Ordinary product-moment correlation coefficients determined by SUSA for the maximum power level.

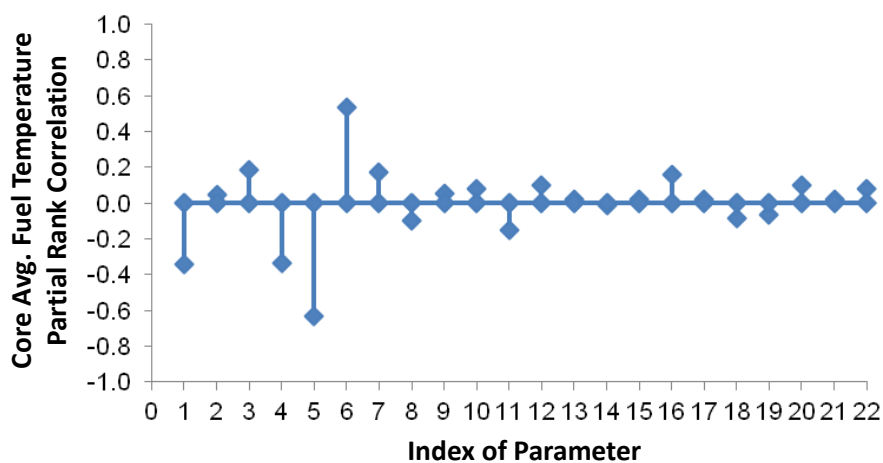


Figure 7-8: Ordinary product-moment correlation coefficients determined by SUSA for the maximum core average fuel temperature.

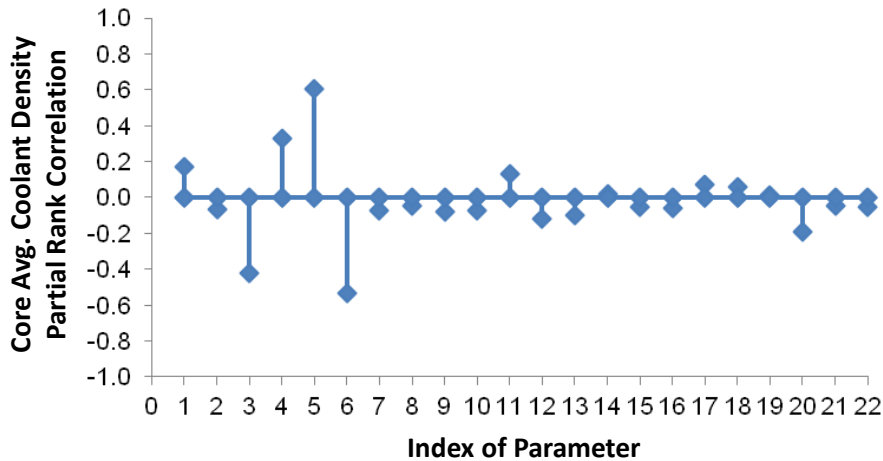


Figure 7-9: Ordinary product-moment correlation coefficients determined by SUSA for the maximum core average coolant density.

Because in these calculations 22 parameters are taken into account, combined influences of two or more uncertainty parameters are observed. However to figure out the behaviour of cross-section perturbations on the four output parameters, uncertainty calculations with perturbations of only one parameter are done for the most affecting Σ_a and $\nu\Sigma_f$. 20 runs are performed to investigate this.

In Figure 7-10 to Figure 7-13 the output parameters as a function of the XS multiplication factor are shown for Σ_a . The XS multiplication factor is the random value generated by SUSA and multiplied with the macroscopic cross-section according to type 4 in the PARCS cross-section modification (section 3.3). For the reactivity (Figure 7-10) and the power level (Figure 7-11) a quasi linear behavior is detected. The larger the fast absorption cross-section, a trend to greater reactivity and power can be observed. The contrary behaviour is given for the thermal absorption cross-section.

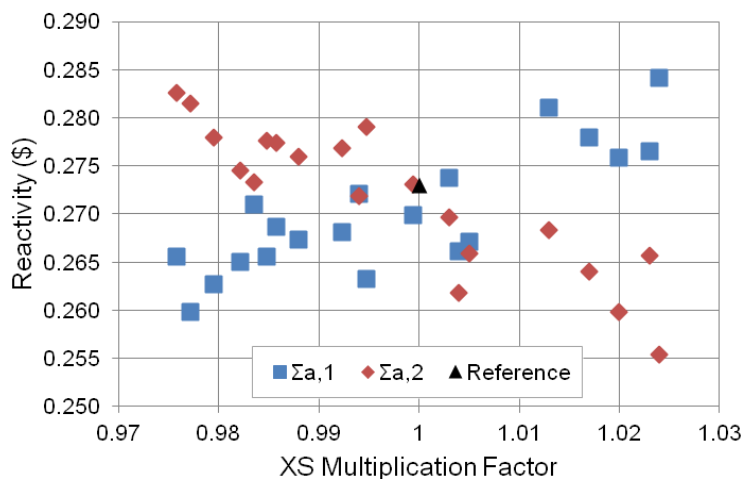


Figure 7-10: Computed maximum reactivity for TRACE/PARCS simulations vary the both Σ_a cross-sections by a random multiplication factor predicted by SUSA.

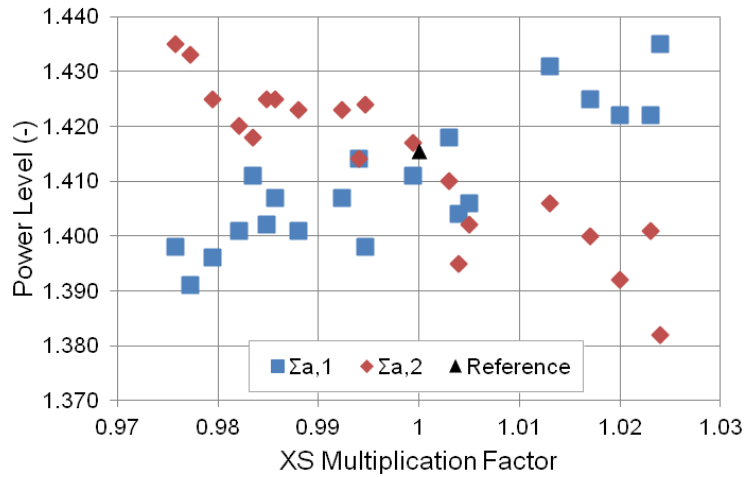


Figure 7-11: Computed maximum power level for TRACE/PARCS simulations vary both Σ_a cross-sections by a random multiplication factor predicted by SUSAs.

As the values for the core average fuel temperature presented in Figure 7-12 are rounded to the first number after the decimal point and the differences in the temperature cases are so small, no qualitative conclusion can be made and the fuel temperature can be assumed as constant. The perturbation of the absorption cross-section Σ_a has no or insignificant influence on the fuel temperature.

For the coolant density a linear behaviour can be observed (Figure 7-13). The coolant density trends to smaller values for the fast absorption cross-section and vice versa for the thermal one.

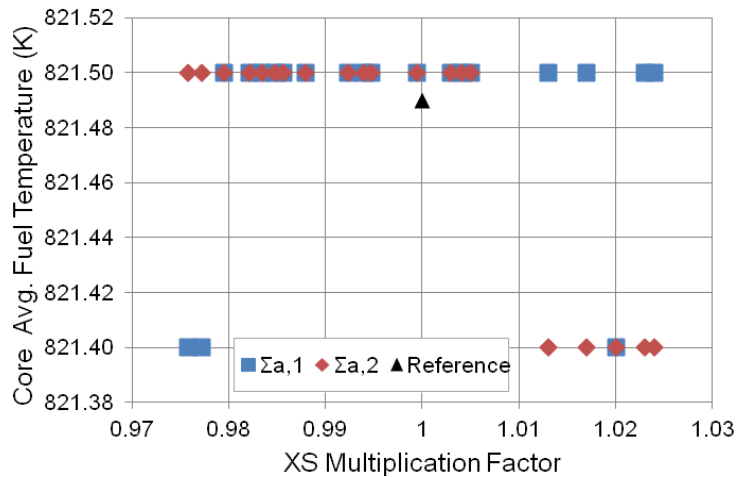


Figure 7-12: Computed maximum fuel temperature for TRACE/PARCS simulations vary both Σ_a cross-sections by a random multiplication factor predicted by SUSAs.

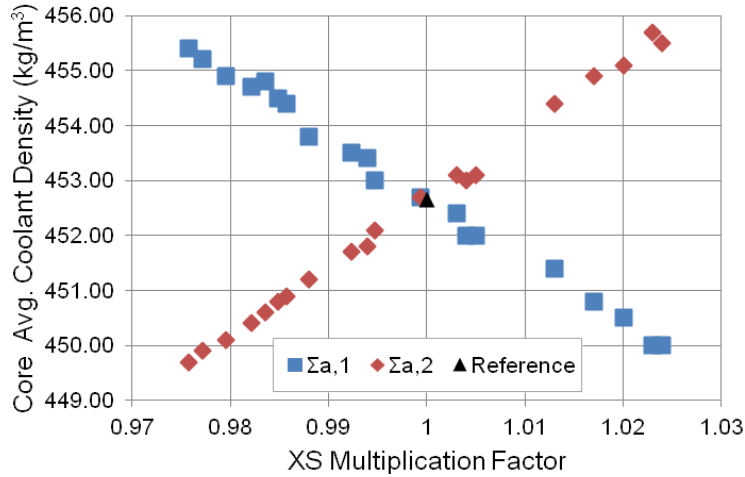


Figure 7-13: Computed maximum coolant density for TRACE/PARCS simulations vary both Σ_a cross-sections by a random multiplication factor predicted by SUSA.

A similar behaviour can be noticed for the cases with the $\nu\Sigma_f$ cross-sections. However, the greater the random value, the smaller is the maximum reactivity (Figure 7-14) and power peak (Figure 7-15) for the fast spectra and vice versa for the thermal one. The same contradiction applied for the absorption cross-section case as well as to the temperature (Figure 7-16) and the coolant density (Figure 7-17).

The results of the single cross-section perturbations correspond to the ordinary correlation coefficients. All relations of Σ_a and $\nu\Sigma_f$ to their variation can be found in the sensitivity analysis presented in Figure 7-6 to Figure 7-9. However, to investigate the behaviour of the uncertain parameters and their influence on target parameters during a pressure perturbation transient a time dependent sensitivity analysis is necessary.

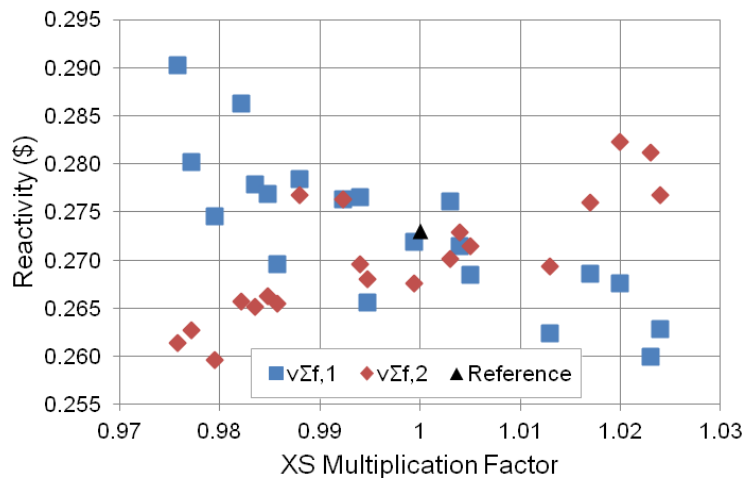


Figure 7-14: Computed maximum reactivity for TRACE/PARCS simulations vary both $\nu\Sigma_f$ cross-sections by a random multiplication factor predicted by SUSA.

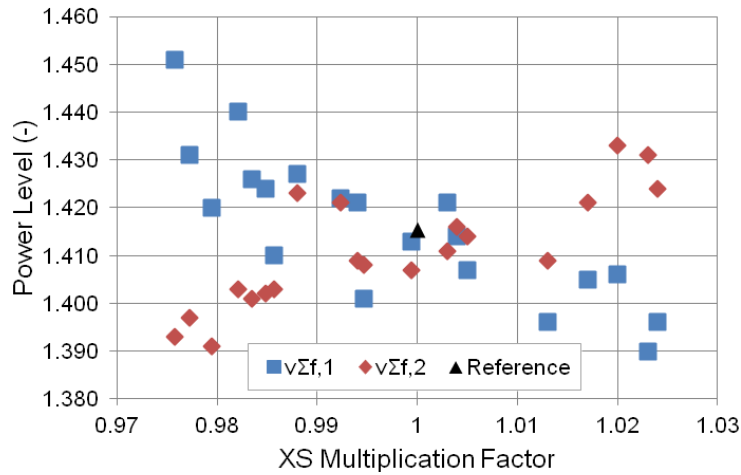


Figure 7-15: Computed maximum power level for TRACE/PARCS simulations vary both $v\Sigma_f$ cross-sections by a random multiplication factor predicted by SUSAs.

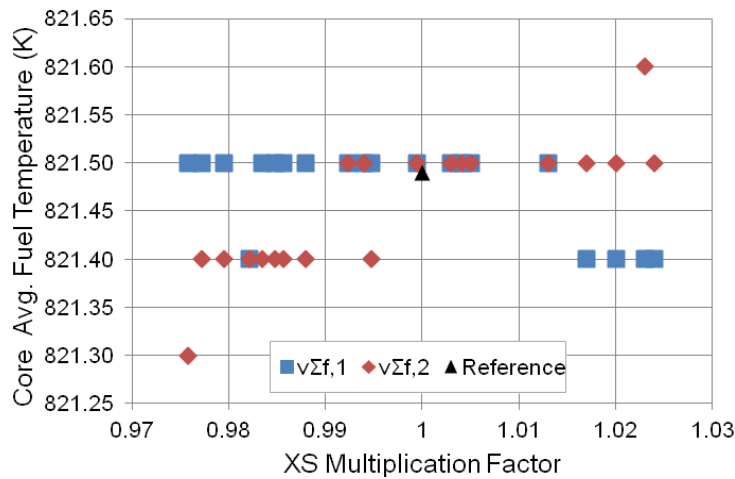


Figure 7-16: Computed maximum fuel temperature for TRACE/PARCS simulations vary both $v\Sigma_f$ cross-sections by a random multiplication factor predicted by SUSAs.

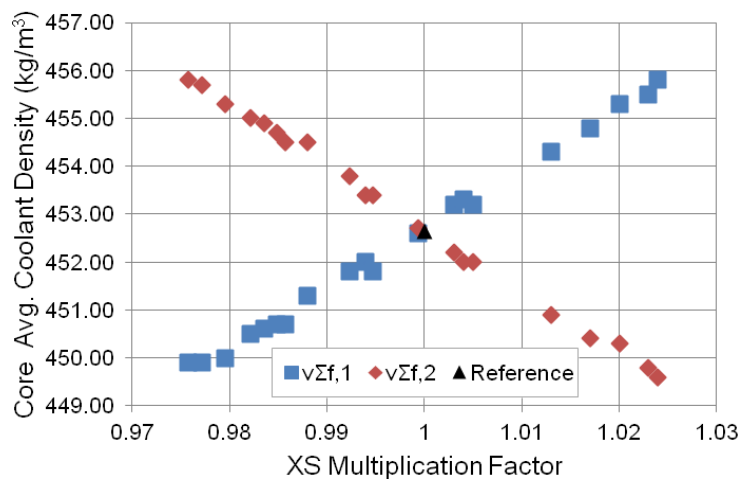


Figure 7-17: Computed maximum coolant density for TRACE/PARCS simulations vary $v\Sigma_f$ cross-sections by a random multiplication factor predicted by SUSAs.

7.2.3 Time dependent sensitivity analysis

Selected results of a time dependent sensitivity analysis of Σ_a and $v\Sigma_f$ are shown in the following diagrams (Figure 7-18 to Figure 7-25). Thereby the red lines indicate the upper and lower power peaks (1 = first power peak, 2 = minimum peak, 3 = second power peak). As can be seen the correlation coefficients for the reactivity (Figure 7-18 and Figure 7-19) and power level (Figure 7-20 and Figure 7-21) are changing sign a couple of times during the transient, whereas for the core average fuel temperature (Figure 7-22 and Figure 7-23) the gradient of absolute values is not so strong. The coolant density (Figure 7-24 and Figure 7-25) doesn't change with time.

Figure 7-18 shows the correlation coefficients for the absorption cross-sections. At the begin the fast absorption cross-section $\Sigma_{a,1}$ has a positive sign, then it becomes negative before it turns positive. This is repeating several times till it correlates to zero. The thermal absorption cross-section $\Sigma_{a,2}$ is showing an opposite trend. At the positions with maximum reactivity a larger $\Sigma_{a,1}$ tends to a higher reactivity while for $\Sigma_{a,2}$ the opposite is the case. With increasing reactivity, power and consequently the fuel temperature are increasing. The Doppler Effect causes more absorption and because the absorption cross-section including both capture and fission the fast absorption in U-238 is leading to a positive correlation factor due to the fast fission resonances. The opposite occurs to the thermal absorption, because in this case neutron capture is predominated.

The correlation coefficients of v-fission cross-section ($v\Sigma_f$) exhibit a similar behaviour as the one of Σ_a on the reactivity (Figure 7-19). Also a change of sign of the correlation coefficients $v\Sigma_{f,1}$ and $v\Sigma_{f,2}$ at the positions with maximum or minimum peaks can be observed. However, a larger thermal cross-section leads to a higher reactivity at maximum peak and a larger $v\Sigma_{f,1}$ causes a lower reactivity. The flux shifts to a faster spectrum, if $v\Sigma_{f,2}$ is larger and the thermal flux decreases when $v\Sigma_{f,1}$ increases. The Doppler Effect in a faster spectrum induces more fission in U-238 and leads to a higher reactivity. On the contrary a reduction of the thermal flux leads to a reduction of the reactivity.

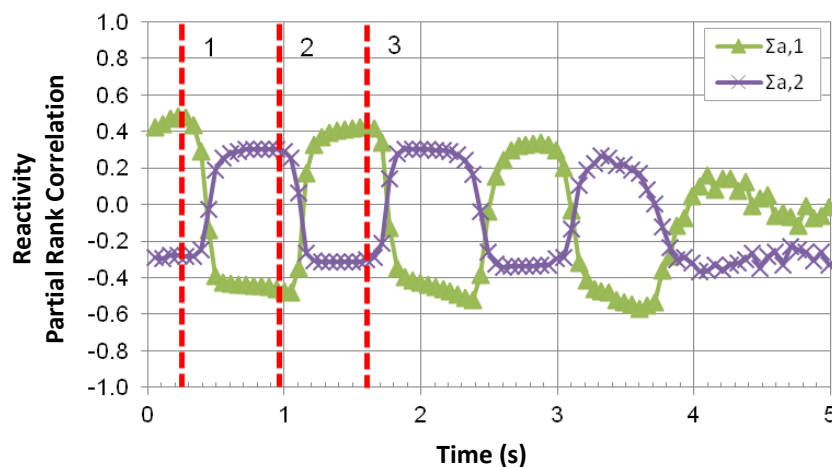


Figure 7-18: Time dependent ordinary product-moment correlation coefficients of Σ_a determined by SUSA for the reactivity.

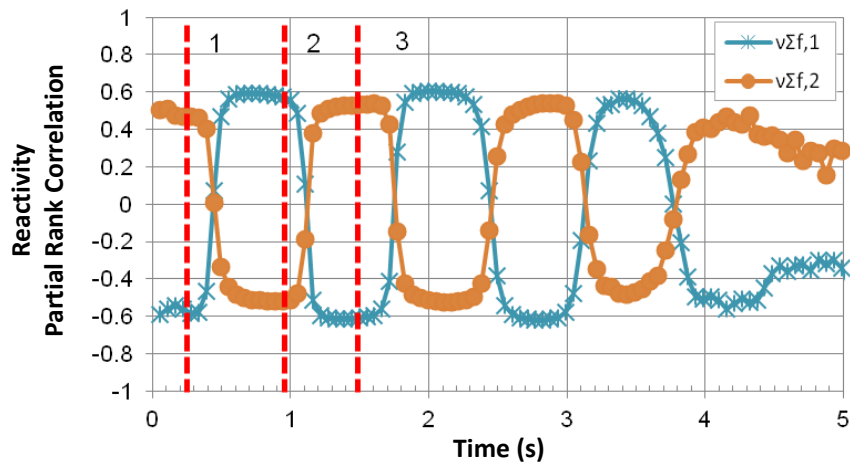


Figure 7-19: Time dependent ordinary product-moment correlation coefficients of $v\Sigma_f$ determined by SUSA for the reactivity.

The same explanation as for the reactivity correlation coefficients can be applied for the power level, because reactivity and power correspond to each other.

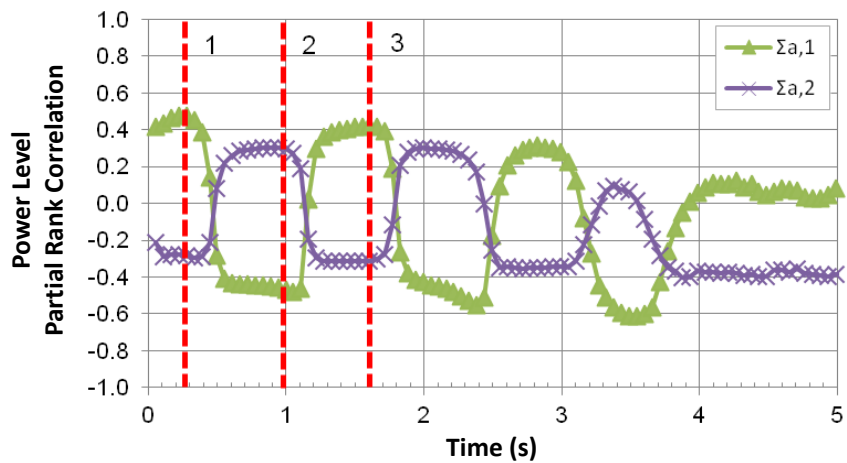


Figure 7-20: Time dependent ordinary product-moment correlation coefficients of Σ_a determined by SUSA for the core power level.

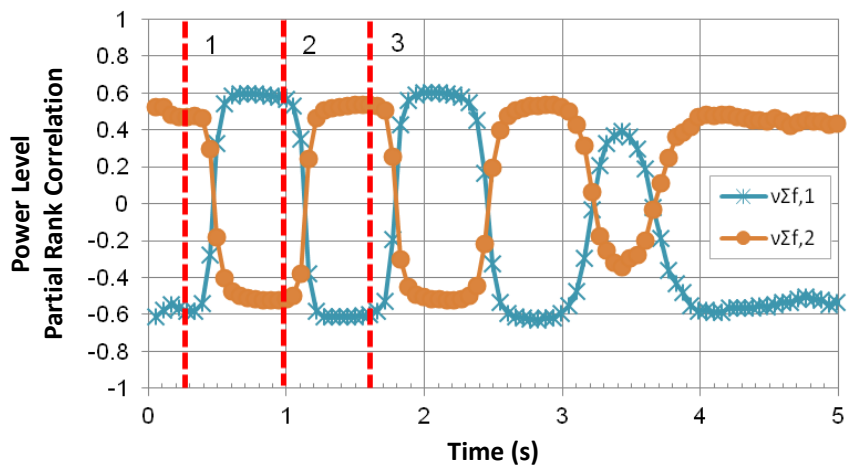


Figure 7-21: Time dependent ordinary product-moment correlation coefficients of $v\Sigma_f$ determined by SUSA for the core power level.

As the time scale of thermal effects is very large compared to neutronic effects no impact to the correlation coefficient over time for the coolant density can be observed. This is confirmed by the results in Figure 7-24 and Figure 7-25. Also the uncertainties in Σ_a and $\nu\Sigma_f$ almost have no big temporal impact on the correlation coefficient of the fuel temperature, Figure 7-22 and Figure 7-23. Only between point 2 and 3 bigger changes can be detected with time for the case of the fast absorption cross-section is less important.

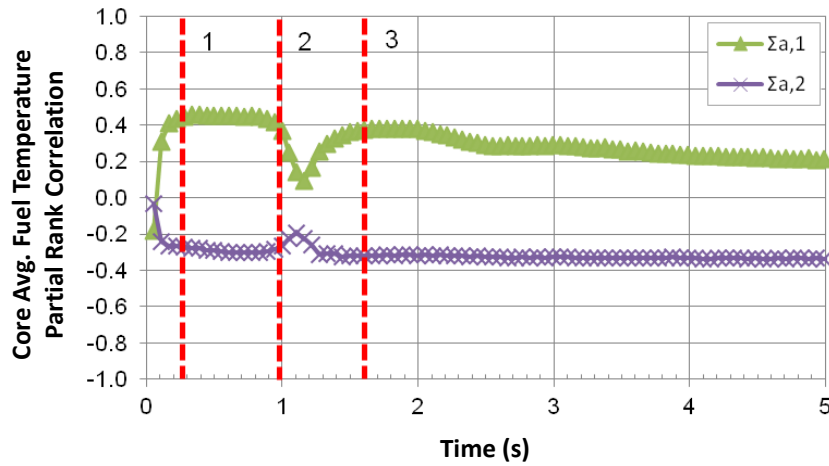


Figure 7-22: Time dependent ordinary product-moment correlation coefficients of Σ_a determined by SUSA for the core average fuel temperature.

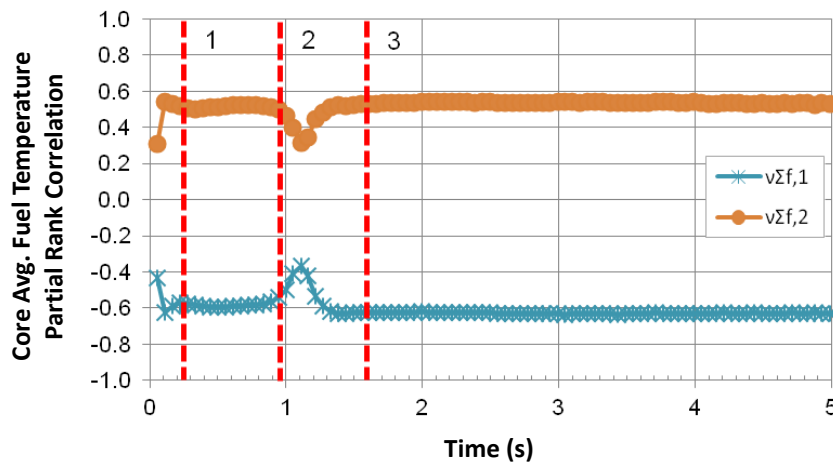


Figure 7-23: Time dependent ordinary product-moment correlation coefficients of $\nu\Sigma_f$ determined by SUSA for the core average fuel temperature.

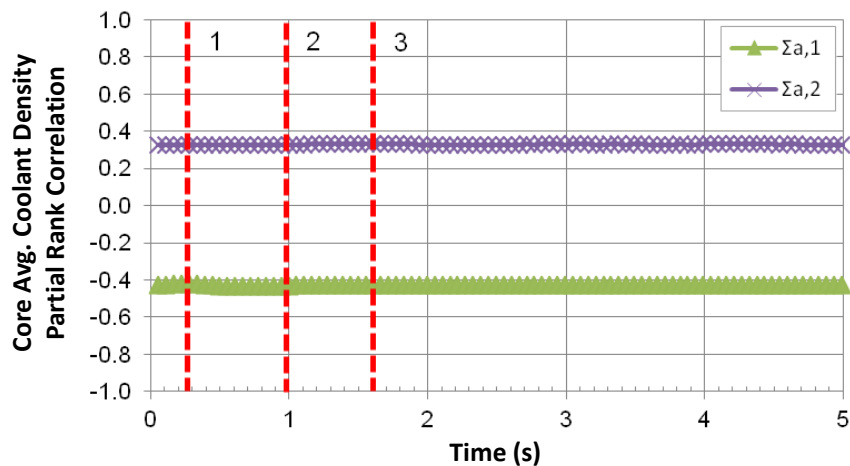


Figure 7-24: Time dependent ordinary product-moment correlation coefficients of Σ_a determined by SUSA for the core average coolant density.

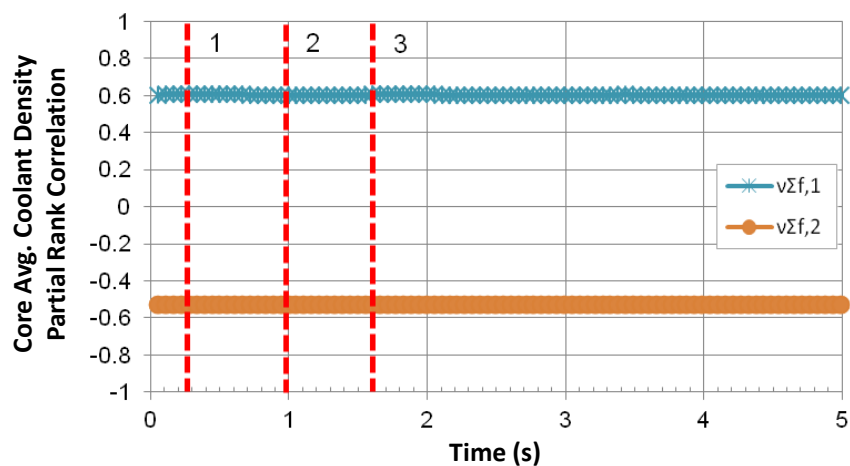


Figure 7-25: Time dependent ordinary product-moment correlation coefficients of $v\Sigma_f$ determined by SUSA for the core average coolant density.

7.3 Conclusions

The uncertainty study has shown that the TRACE/PARCS calculation using the reference cross-sections from TRITON are lying within the uncertainty band calculated by SUSA. Though the core average fuel temperature has been observed in this study instead of the PCT, the behaviour of the core average fuel temperature also gives a good indication of the PCT behaviour considering cross-section uncertainties. Further studies also have to include thermal-hydraulic uncertainties.

Furthermore a sensitivity analysis indicates that the absorption and v-fission cross-sections have the largest impact on safety relevant target parameters during the transient progression. A disadvantage of this uncertainty method is, that it is very computation intensive. Especially, when a very detailed thermal-hydraulic model with a fine mapping between thermal-hydraulic and neutron-kinetic is used. Reducing the number of changed parameters doesn't help because the statistical approach of SUSA is independent of the

number of parameters. In general the TRACE/PARCS and SUSA codes are working fine and the interface between them allows the quantification of the code's parameters uncertainties. All uncertainties of XS in the PMAXS format can be covered by the implemented PARCS module.

8 Summary

The main goal of this thesis was to establish and validate a comprehensive BE computational route for BWR transient analysis using coupled neutron-kinetic/thermal-hydraulic codes.

In chapter 3 a computational route from cross-section generation to transient analysis with subsequent uncertainty and sensitivity study of a BWR was presented and the used codes were described in detail. The cross-section sets are generated with SCALE6/TRITON and transformed via PYTHON script and GenPMAXS into the PMAXS format. Thereby the missing yields and the bugs in the SCALE output are compensated. For uncertainty and sensitivity analysis the PARCS code has been extended by an uncertainty module, that allows a communication between PARCS and SUSA.

The computational route has been tested stepwise. The cross-sections of the FA of a BWR-72 reference plant, as described in chapter 4, were generated and then validated in chapter 5 by a code-to-code comparison.

The single fuel assembly depletion calculations of SCALE/TRITON and PARCS showed that the yield of Promethium predicted by SCALE/TRITON is far below the one used in PARCS. The reason of this underestimation is the wrong prediction of capture reaction in Pm-148 and Pm-148m in the SCALE output file. Thus the PYTHON script has been modified. Further the influence of different evaluated nuclear data libraries and of the history effect on the FA depletion calculation is analysed. Considering that the influence of different nuclear data libraries is below 1.1 %, the prediction of the history effects may lead to deviations in k_{eff} of about 8 % for high burnup fuels. The code-to-code comparison between SCALE/TRITON and CASMO-4 for a representative FA showed that SCALE/TRITON predicts a higher k_{eff} . This is also reflected in the evaluation of the void and fuel temperature reactivity coefficient. In general the reactivity coefficients predicted by CASMO-4 for fresh and burnt fuel conditions are always larger than the ones predicted with SCALE/TRITON.

In a next step a full BWR core depletion analysis with PARCS has been using SCALE/TRITON cross-sections as well as CASMO-4 cross-sections. Therefore a PARCS 3D model of BWR core has been developed and different PARCS stand-alone calculations for HFP conditions have been performed. As the single FA depletions showed, all four cases with ARI and ARO at BOL and 6.6 FLD overpredicts the multiplication factor k_{eff} using SCALE/TRITON XS compared to the PARCS calculations using CASMO-4 XS. The highest deviation has observed with 1.5 % for ARI at BOL. The comparison of the axial power profiles indicated that the control rod as well as the reflector modeling plays an important role. The importance of cross-section modeling is also reflected by comparing the radial power distribution of the PARCS calculations with SCALE/TRITON XS and CASMO-4 XS. In core regions with strong flux gradients such as in the interface between MOX and UO₂ FA, in the neighbourhood of control elements and in the interface core/reflector ADFs must be taken into account in the simulations to improve the prediction accuracy of the diffusion approximation.

In a last step the PARCS 3D model has been coupled to TRACE. As observed also before, the multiplication factor k_{eff} using SCALE/TRITON cross-sections is higher than using CASMO-4 cross-sections. The coupled calculations indicated the importance of considering the history effect on the axial power level and thus on the axial void fraction and axial fuel and coolant temperature predictions.

A real turbine trip event with TRACE/PARCS using the two different cross-section libraries generated with SCALE/TRITON and CASMO-4 has been performed. Thereby the influence of different azimuthal nodalization has been analysed. Whereas the initial values are quite good predicted by all simulations, the subsequent trend is underpredicted, compared to the measured data, by the simulations. It has to be noted that because of the rough time resolution of 50 seconds of the measured data, no conclusion about the power peak could be done. However the tendency is caught by the predictions. The more interesting results of this comparison is the fact that the simulations using the different XS libraries predicted very similar values for the steam dome pressure, core average fuel temperature and total core power. Only the void fractions differed larger for longer times. The deviations between the 2D RPV model and 3D RPV model are small for the steam dome pressure, core average void fraction, core average fuel temperature, total core power and the reactivity feedbacks. Hence, the comparison of local parameters e.g. including azimuthal and radial nodes makes more sense than the one of global integral parameters to show the capability of 3D models compared to 2D models.

An uncertainty and sensitivity analysis, based on the SUSA method as described in section 3.5, has been performed for a pressure perturbation. Because the uncertainty analysis consuming large computation capacity, only a simplified model, which reflect the physical phenomena of the turbine trip has been used. The variation of the XS generated with SCALE/TRITON resulted in an uncertainty band calculated by SUSA, which shows the upper and lower boundaries. During the sensitivity study the parameters with the most impact were identified to the absorption and ν -fission cross-section. In total the proposed method is an effective tool to cover and analyse the uncertainties of neutronic parameters in the PMAXS format.

The performed investigations have shown that the selected computational route is also applicable for the analysis of real BWR core loadings and real plant events. Important bugs of the involved codes were identified and ways to overcome it were developed and proposed. Based on these investigations it can be stated that 3D models of both thermal-hydraulics and neutronics are mandatory for an adequate description of the physics of non-symmetrical transients.

9 Outlook

The investigations presented have demonstrated the prediction capability of a modern computational route including cross-section generation, 3D neutronic/thermal-hydraulic simulations and uncertainty quantifications based on best-estimate codes under development. It was the first time that a real core loading of a BWR under operation was simulated with SCALE/TRITON and TRACE/PARCS. Despite of it, many code's deficiencies and both neutronics and thermal-hydraulics were identified for future work. The main areas for further investigations are listed hereafter based on the gained experience during this doctoral work:

- Improvement of the nodal cross-section generations with SCALE/TRITON to consider the ADFs for reflector (outer FA row and reflector) as well as for fuel assemblies located close to the absorber blades.
- Application of the Pin Power Reconstruction capability of SCALE/TRITON and PARCS for the prediction of the pin power of the hot fuel assembly or of a cluster of fuel assemblies surrounded the hottest one in order to calculate the power of fuel rods. These values as well as the thermal-hydraulic boundary conditions of single fuel rods within a fuel assembly can be extracted and passed to a sub-channel code for the prediction of local safety parameters. This approach can be validated using either deterministic transport codes or Monte Carlo codes coupled with thermal-hydraulic models or if available with experimental data.
- Extension of the uncertainty and sensitivity tools based on SUSA that permits the propagation of the code's uncertainty from both the thermal-hydraulic and neutron-kinetics modules into a coupled thermal-hydraulic/neutron-kinetic simulation.
- Further validation of the developed integral model of the BWR reference plant using additional plant data
- Selection of non-symmetrical BWR transients that are challenging for N/TH coupled codes to test their capabilities.

10 Literature

- [1] "Auswertungstabellen zur Energiebilanz für die Bundesrepublik Deutschland 1990 bis 2010", Arbeitsgemeinschaft Energiebilanzen e.V., Juli 2011
- [2] Deutsches Atomgesetz in der Fassung vom 8.12.2010
- [3] "Leitfäden zur Durchführung von Periodischen Sicherheitsüberprüfungen (PSÜ) für Kernkraftwerke in der Bundesrepublik Deutschland", Bekanntmachung des BMU vom 18. August 1997 (BAnz. 1997, Nr. 232a)
- [4] "ILK-Empfehlungen zur Weiterentwicklung der Periodischen Sicherheitsüberprüfungen in Deutschland", Internationale Länderkommission Kerntechnik, ILK-27 D, November 2006
- [5] "Neutronics/Thermal-hydraulics Coupling in LWR Technology, Vol. 1", CRISSUE-S - WP1, NEA No. 4452, 2004
- [6] "Neutronics/Thermal-hydraulics Coupling in LWR Technology, Vol. 2", CRISSUE-S – WP2, NEA No. 5436, 2004
- [7] Borkowski, J. et al., "TRAC-BF1: An Advanced Best-Estimate Computer Program for BWR accident analysis", NUREG/CR-4356, 1992
- [8] The Thermal Hydraulics Group, "RELAP5/MOD3.3 Code Manuel", NUREG/CR-5535/Rev P3-Vol I-VII. 2001-6
- [9] E. Krepper, F. Schäfer, "Verifikation des ATHLET-Rechenprogrammes anhand der Nachanalyse zweier Experimente an der CCTF-Versuchsanlage", Forschungszentrum Rossendorf, Wissenschaftlich-Technische Berichte, FZR-315, März 2001
- [10] H. S. Cheng and U. S. Rohatgi: "RAMONA-4B Code for BWR Systems Analysis", BNL-NUREG-63265, Winter meeting of the American Nuclear Society (ANS) and the European Nuclear Society (ENS), Washington, DC (United States), 10-14 Nov 1996.
- [11] "TRACE V5.0 User's Manuel", Division of System Analysis, Office of Nuclear Regulatory Research, U. S. Nuclear Regulatory Commission, Washington, DC 20555-0001
- [12] "RELAP5-3D Code Manual Revision 2.4", INEEL-EXT-98-00834, Idaho National Laboratory, June 2005
- [13] U. Graf, "Implicit coupling of fluid-dynamic systems: application to multidimensional counter-current two-phase flow of water and steam", Nuclear Science and Engineering, vol. 129, no. 3, p. 305-310, 1998

- [14] T. Downar, Y. Xu, V. Seker, "PARCS 3.0: U.S. NRC Core Neutronics Simulator", User Manual (Draft), Department of Nuclear Engineering and Radiological Sciences, University of Michigan, Ann Arbor, MI, Dezember 2009
- [15] U. Grundmann, U. Rohde, S. Mittag: DYN3D – Three Dimensional Core Model for Steady-State and Transient Analysis of Thermal Reactors. Proc. PHYSOR2000, Pittsburgh, CD-ROM
- [16] D. Pevec, D. Grgic, S. Langenbuch, K. Velkov, "Calculation of NEA_NSC 3D PWR Control rods withdrawl benchmark using QUABOX/CUBBOX-HYCA code", Nuclear Society of Slovenia 2nd Regional Meeting: Nuclear Energy in Central Europe Portoroz, SLOVENIA, 11.-14. September 1995
- [17] Gerardo M. Grandi und Kord S. Smith, "BWR Stability Analysis with SIMULATE-3K", PHYSOR 2002, Seoul, Korea, October 7-10, 2002
- [18] J. Judd, G. Grandi, "A Best-estimate Coupled Code for Reactor Safety Analyses using SIMULATE-3K and RELAP5-3D", ANFM-IV, 2009, Hilton Head Island, South Carolina, USA
- [19] U. Grundmann und S. Kliem, "Validierung des gekoppelten neutronenkinetischen-thermohydraulischen Codes ATHLET/DYN3D mit Hilfe von Messdaten des OECD Turbine Trip Benchmarks", Wissenschaftlich-Technische Berichte, FZR-384, Dezember 2003
- [20] S. Langenbuch, K. Velkov, D. Pevec und D. Grgić, "Capability of the QUABOX/CUBBOX-ATHLET Coupled Code System", Proceedings of International Conference: Nuclear Option in Countries with Small and Medium Electricity Grid, Opatija, Croatia, 07-09 October 1996
- [21] Y. Xu et al., "Application of TRACE/PARCS to BWR stability analysis", Annals of Nuclear Energy 36 (2009) 317-323, April 2009
- [22] D. Panayotov, "OECD/NRC BWR TURBINE TRIP BENCHMARK: SIMULATION BY POLCA-T CODE", PHYSOR 2002; Seoul, Korea, October 7-10, 2002
- [23] D.J. Diamond, "Multi-dimensional Reactor Kinetics Modelling", Proceedings of the OECD/CSNI Workshop on Transient Thermal-hydraulic and Neutronics Codes Requirements, NEA/CSNI/R(97)4, 5-8 November 1996
- [24] K. Tada, "Applicability of the Diffusion and Simplified P3 Theories for Pin-by-Pin Geometry of BWR", NUCLEAR SCIENCE and TECHNOLOGY, Vol. 45, No. 10, p. 997–1008, 2008
- [25] A. M. Gómez Torres, "Further Developments of Multiphysics and Multiscale Methodologies for Coupled Nuclear Reactor Simulations ", PhD Thesis, 11th November

2011

- [26] G.Th. Analytis and P. Coddington: “Analysis and sensitivity studies of postulated SB-LOCAs in the Mühleberg (KKM) BWR/4 by TRAC-BF1”, *Annals of Nuclear Energy*, Vol. 29, p. 1525–1549, September 2002
- [27] J. Solís-Rodarte et al., “Developing and modeling of the ‘Laguna Verde’ BWR CRDA benchmark”, *Annals of Nuclear Energy*, Vol 29, p. 585–593, March 2002
- [28] H. Fu, J. Solis-Rodarte and K. Ivanov, “TRAC-BF1/NEM Modeling and results of OECD/NEA BWR core transient benchmarks”, *Annals of Nuclear Energy*, Volume 27, p. 1051–1058, August 2000
- [29] U. Grundmann, S. Kliem and U. Rohde, “Analysis of the Boiling Water Reactor Turbine Trip Benchmark with the codes DYN3D and ATHLETH/DYN3D”, *Nuclear Science and Engineering*, Vol. 148, No. 2, p. 226-234, October 2004
- [30] M. Kajimoto and N. Tanaka, “Analysis of Severe Accident Mitigation of ATWS Sequence for a typical BWR with MARK-II Containment”, *International Conference on Nuclear Engineering*, Tokyo, April 19-23 1999
- [31] L. Neymotin, C. J . Hsu and P. Saha, “Assesment of TRAC-BD1 and RAMONA-3B Codes for BWR ATWS Application”, *BNL-NUREG-35582*, January 1984
- [32] T. Levert, “BWR STABILITY BENCHMARK - Final Specifications”, *NEA/NSC/DOC(94)15*, March 1994
- [33] J. Solis, K. Ivanov, and B. Sarikaya, “Boiling Water Reactor Turbine Trip (TT) Benchmark - Volume I: Final Specifications”, *NEA/NSC/DOC(2001)1*, February 2001
- [34] T. Kozlowski et al., “TRACE/PARCS VALIDATION FOR BWR STABILITY BASED ON OECD/NEA OSKARSHAMN-2 BENCHMARK”, *NURETH-14*, Toronto, Ontario, Canada, September 25-30, 2011
- [35] C.A. Wemplea et al., “Recent Advances in the HELIOS-2 Lattice Physics Code”, *International Conference on the Physics of Reactors “Nuclear Power: A Sustainable Resource”*, Interlaken, Switzerland, September 2008
- [36] Rhodes, J., Edenius, M., “CASMO-4. A Fuel Assembly Burnup Program. User’s Manual”, *Studsвик Scandpower SSP-01/400 Rev 1*, 2001
- [37] S. M. Bowman, “SCALE6: Comprehensive Nuclear Safety Analysis Code System”, *Nuclear Technology*, Vol. 174, p. 126-148, May 2011.
- [38] R. Sanchez et al, “APOLLO2 year 2010”, *Nucl. Eng. and Technology*, 42, 474 (2010)

- [39] G. Marleau, R. Roy and A. Hébert, "DRAGON: A Collision Probability Transport Code for Cell and Supercell Calculations", Report IGE-157, Institut de génie nucléaire, École Polytechnique de Montréal, Montréal, Québec (1994)
- [40] R.J.J. Stamm'ler and M.J. Abbate, "Methods of Steady-State Reactor Physics in Nuclear Design", ACADEMIC PRESS INC. (LONDON) LTD, 1983
- [41] A. Trkov, „From Basic Nuclear Data to Applications“, Workshop on Nuclear Data and Nuclear reactors: Physics, Design and Safety, Trieste, 13. March – 14. April, 2000
- [42] C. Beckert, "Entwicklung des Neutronentransportcodes TransRay und Untersuchungen zur zwei- und dreidimensionalen Berechnung effektiver Gruppenwirkungsquerschnitte", Dissertation, TU Dresden, 2007
- [43] "ENDF-102, ENDF-6 Formats Manual" BNL-90365-2009, Brookhaven National Laboratory, June 2009
- [44] (Eds.) A. Santamarina, D. Bernard, Y. Rugama: "The JEFF-3.1.1 Nuclear Data Library", JEFF Report 22 (2009)
- [45] K. Shibata et al., "JENDL-4.0: A New Library for Nuclear Science and Engineering", Journal of NUCLEAR SCIENCE and TECHNOLOGY, Vol. 48, No. 1, pp. 1-30 (2011)
- [46] Nuclear Data Viewer, Los Alamos, <http://t2.lanl.gov/data/ndviewer.html>
- [47] R. E. MacFarlane und D.W. Muir, "The NJOY nuclear data processing system: Version 91" The NJOY nuclear data processing system, version 91", LA-12740-M, 1994
- [48] M. E. Dunn and N. M. Greene, "AMPX-2000: A Cross-Section Processing System for Generating Nuclear Data for Criticality Safety Applications," Trans. Am. Nucl. Soc. 86, 118–119 (2002)
- [49] R. Goldstein, E.R. Cohen, "Theory of Resonance Absorption of Neutrons", Nucl.Sci.Eng. 13, pp. 132-140, 1962
- [50] J. K. Watson and K. Ivanov, "Improved cross-section modeling methodology for coupled three-dimensional transient simulations", Annals of Nuclear Energy, Vol. 29, pp. 937–966, May 2002
- [51] T. Downar, Y. Xu, "GenPMAXS Code for Generating the PARCS Cross-section Interface File PMAXS", Purdue University, School of Nuclear Engineering, West Lafayette, IN, USA. , December 2005
- [52] M. Stálek, C. Demazière, "Development and validation of a cross-section interface for PARCS", Annals of Nuclear Energy 35 (2008) 2397-2409

-
- [53] B. Ivanov, "Methodology for Embedded Transport Core Calculations", Thesis, Pennsylvania State University, 2007
- [54] K. Yamaji et al., "Development of the New Pin-by-Pin Core Calculation Method with Embedded Heterogeneous Assembly Calculation", PHYSOR-2006, Canada, September 10-14, 2006
- [55] M. Tohjoha, M. Watanabe and A. Yamamoto, "Application of continuous-energy Monte Carlo code as a cross-section generator of BWR core calculations", *Annals of Nuclear Energy*, Vol. 32, pp. 857–875, May 2005
- [56] K. Yoshioka et al. "Multi-Group Constants Generation System for 3D-Core Simulation Using a Continuous Energy Monte Carlo Technique", *Progress in Nuclear Science and Technology*, Vol. 2, pp.334-340, 2011
- [57] E. Fridman, J. Leppänen, "On the use of the Serpent Monte Carlo code for few-group cross-section generation", *Annals of Nuclear Energy*, Vol. 38, pp. 1399–1405, June 2011
- [58] K. Ivanov, M. Avramova, "Challenges in coupled thermal-hydraulics and neutronics simulations for LWR safety analysis", *Annals of Nuclear Energy* Vol. 34, pp. 501-513, 2007
- [59] B. Chanaron et al., "The European Project NURISP for Nuclear Reactor Simulation", *Transactions of the American Nuclear Society*, Vol. 103, pp. 671-672, 2010
- [60] J. Peltonen and T. Kozlowski, "Development of Effective Algorithm for Coupled thermal-Hydraulic-Neutron-Kinetics Analysis of Reactivity Transient", *Nuclear Technology*, Vol. 176, (2), pp. 195-210 (2011)
- [61] J. K. Watson, "Implicit Time-Integration Method for Simultaneous Solution of a Coupled Non-Linear system", PhD Thesis, Pennsylvania State University, May 2010
- [62] International Atomic Energy Agency, "Best Estimate Safety Analysis for Nuclear Power Plants: Uncertainty Evaluation", IAEA Safety Reports Series No. 52 , IAEA, Vienna 2008
- [63] Reaktor-Sicherheitskommission (RSK), "RSK-Empfehlung: Anforderungen an die Nachweisführung bei Kühlmittelverluststörfall-Analysen", 385. Meeting, 20./21. July 2005
- [64] 10 CFR 50.46, "Acceptance criteria for emergency core cooling systems for light water nuclear power reactors," Appendix K, "ECCS Evaluation Models", to 10 CFR Part 50, Code of Federal Regulations, 1996

- [65] H. Glaeser, "GRS Method for Uncertainty and Sensitivity Evaluation of Code Results and Applications", Science and Technology of Nuclear Installations, Volume 2008
- [66] A. Petrucci und F. D'Auria, "Approaches, Relevant Topics, and Internal Method for Uncertainty Evaluation in Predictions of Thermal-Hydraulic System Codes", Science and Technology of Nuclear Installations, Volume 2008
- [67] B.E. Boyack, "Quantifying reactor safety margins part 1: An overview of the code scaling, applicability, and uncertainty evaluation methodology", Nuclear Engineering and Design 119 (1990) 1-15
- [68] D. G. Cacuci, "Sensitivity and Uncertainty Analysis, Theory, Volume I", Chapman & Hall/CRC, Boca Raton, Fla, USA, 2003
- [69] OECD Nuclear Energy Agency, "Benchmark for Uncertainty Analysis in Best-estimate Modelling (UAM) for Design, Operation and Safety Analysis of LWRs - Volume I: Specification and Support Data for the Neutronics Cases (Phase I)", NEA/NSC/DOC(2007)23, December 2007
- [70] M. Klein et al., "GRS results for Phase I", OECD UAM-6 workshop, KIT, Karlsruhe, Germany, May 9-11, 2012
- [71] A. Yankov, "Comparison of Stochastic XSUSA and "Two-Step" GPT Approaches for Full-Core Uncertainty Quantification", OECD UAM-6 workshop, KIT, Karlsruhe, Germany, May 9-11, 2012
- [72] M. Pourgol-Mohammad, "Thermal-hydraulics system codes uncertainty assessment: A review of the methodologies", Annals of Nuclear Energy Vol. 36, pp. 1774-1786, 2009
- [73] C. Frepoli and A. Pertuzzi, "Scaling, Uncertainty, and 3D Coupled Code Calculations in Nuclear Technology", Science and Technology of Nuclear Installations, 2008
- [74] J. Juanas et al., "Uncertainty and Sensitivity Analysis in the Neutronic Parameters Generation over the Coupled Thermalhydraulic-Neutronic Nuclear Power Plant Simulations", M&C, New York, May 2009
- [75] B. Salah et al., "Uncertainty and sensitivity analyses of the Kozloduy pump trip test using coupled thermal-hydraulic 3D kinetics code", Nuclear Engineering and Design Vol. 236, pp. 1240-1255, 2006
- [76] D. J. Diamond, "Experience Using Phenomena Identification and Ranking Technique (PIRT) for Nuclear Analysis", PHYSOR-2006, Vancouver, September 10-14, 2006

-
- [77] A. Petruzzi et al., "Methodology of internal assessment of uncertainty for safety analysis code", Nuclear Mathematical and Computational Sciences: A Century in Review, Gatlinburg, Tennessee, April 6-11, 2003
- [78] D. M. Hamby, "A Review of Techniques for Parameter Sensitivity Analysis of Environmental Models", Environmental Monitoring and Assessment 32, p. 135-154, 1994
- [79] M. D. DeHart, "TRITON: A Two-Dimensional Transport and Depletion Module for Characterization of Spent Nuclear Fuel", ORNL/TM-2005/39, Version 6, Vol. I, Sect. T1, January 2009
- [80] S. Goluoglu et al., "Monte Carlo Criticality Methods and Analysis Capabilities in SCALE", Nuclear Technology, Vol. 174, p. 214-235-148, May 2011
- [81] M. D. DeHart, "NEWT: A New Transport Algorithm for Two-Dimensional Discrete Ordinates Analysis in Non-Orthogonal Geometries", ORNL/TM-2005/39, Version 6, Vol. II, Sect. F21, January 2009
- [82] M. D. DeHart and S. M. Bowman, "Reactor Physics Methods and Analysis Capabilities in SCALE", Nuclear Technology, Vol. 174, p. 196-213, May 2011
- [83] N. M. Greene, "BONAMI: Resonance Self-Shielding by the Bondarenko Method", ORNL/TM-2005/39, Version 6, Vol. II, Sect. F1, January 2009
- [84] M. L. Williams, M. Asgari, and D. F. Hollenbach, "CENTRM: A ONE-DIMENSIONAL NEUTRON TRANSPORT CODE FOR COMPUTING POINTWISE ENERGY SPECTRA", ORNL/TM-2005/39, Version 6, Vol. II, Sect. F18, January 2009
- [85] M. L. Williams and D. F. Hollenbach, "PMC: A PROGRAM TO PRODUCE MULTIGROUP CROSS-SECTIONS USING POINTWISE ENERGY SPECTRA FROM CENTRM", ORNL/TM-2005/39, Version 6, Vol. II, Sect. F19, January 2009
- [86] M. D. DeHart, "A Discrete Ordinates Approximation to the Neutron Transport Equation Applied to Generalized Geometries," Ph.D. Dissertation, Texas A&M University (1992)
- [87] I. C. Gauld and O. W. Hermann, "COUPLE: SCALE SYSTEM MODULE TO PROCESS PROBLEM-DEPENDENT CROSS-SECTIONS AND NEUTRON SPECTRAL DATA FOR ORIGEN-S ANALYSES", ORNL/TM-2005/39, Version 6, Vol. II, Sect. F6, January 2009
- [88] I. C. Gauld et al., "Isotopic Depletion and Decay Methods and Analysis Capabilities in SCALE", Nuclear Technology, Vol. 174, p. 169-195, May 2011

- [89] I. C. Gauld and J. E. Horwedel, "OPUS/PLOTOPUS: AN ORIGEN-S POST-PROCESSING UTILITY AND PLOTTING PROGRAM FOR SCALE", ORNL/TM-2005/39, Version 6, Vol. II, Sect. F15, January 2009
- [90] G. van Rossum and F. L. Drake, "The Python Language Reference", Release 2.7.2, October 2011
- [91] T. Downar, Y. Xu, V. Seker, "PARCS 3.0: Theory Manual", Department of Nuclear Engineering and Radiological Sciences, University of Michigan, Ann Arbor, MI, December 2009.
- [92] R. Macian, "Personal information", TU München
- [93] R. Holzer, "Personal information", NIS Ingenieurgesellschaft
- [94] F. Jatuff et al., "Void reactivity coefficient benchmark results for a 10x10 BWR assembly in the full 100% void fraction range", Annals of Nuclear Energy, Vol. 36, pp. 835-858, 2009
- [95] Hesse et al., "Comparison of Burn-Up Calculations for a UO₂ PWR Fuel Assembly", Jahrestagung Kerntechnik, Karlsruhe (2007)
- [96] F. Jatuff et al., "Effects of void uncertainties on the void reactivity coefficient and pin power distributions for a 10x10 BWR assembly", Annals of Nuclear Energy, Vol. 33, pp. 119-125, 2006
- [97] M. Avramova, K. Ivanov, "Verification, validation and uncertainty quantification in multi-physics modeling for nuclear reactor design and safety analysis", Progress in Nuclear Energy 52 (2010) 601-614
- [98] Anlagenbeschreibung KRB II Gundremmingen PSÜ, PSÜ-Nr.: 7.0/01-A, Akten-Nr.: A-50/249-216, Stand 17.12.1997
- [99] M. Thieme, internal Report
- [100] K. Nikitin et al., "Peach Bottom 2 Turbine Trip 2 Simulation by TRACE/S3K Coupled Code", Physor 2010, Pittsburgh, May 2010
- [101] Ivan Gajev et al. "Ranking of input parameters importance for BWR stability based on Ringhals-1", M&C, Rio de Janeiro, May 2011
- [102] G. Aliberti et al., "Nuclear data sensitivity, uncertainty and target accuracy assessment for future nuclear systems", Annals of Nuclear Energy 33 (2006) 700-733

- [103] United States Nuclear Regulatory Commission (U.S.NRC), “§ 50.46 Acceptance criteria for emergency core cooling systems for light-water nuclear power reactors”
NRC Regulations 10 CFR

Annex A PMAXS format

The PMAXS library has a structure as indicated in Figure A-1. The position 5 (history case identification) contains the following data: inverse neutron velocity, the yields of Xenon, Iodine and Promethium and delayed neutrons.

1	XS Control Information
2	Branches Information
3	Burnup Information
XS Set/(History case) wise data	
4	XS Set identification
5	History case identification
6	T/H invariant variable block (repeat for burnup)
6.1	Inverse neutron velocity
6.2	Yields
6.3	Beta of delayed neutron
6.4	Lambda of delayed neutron
Reference state data	
7	State identification
8	XS Data Block (repeated for burnup points)
8.1	$\Sigma_{tr}, \Sigma_a, \nu\Sigma_f, \kappa\Sigma_f, \sigma_{Xe}, \sigma_{Sm}, \Sigma_f$
8.2	Σ_s
8.3	ADF
lth type branches (same structure with Ref. State case)	

Figure A-1: PMAXS data block structure for transient calculations with PARCS.

At position 8 (XS Data Block) the following data is stored: macroscopic cross-sections of transport (Σ_{tr}), absorption (Σ_a), nu*fission ($\nu\Sigma_f$), kappa fission ($\kappa\Sigma_f$), fission (Σ_f), the microscopic capture cross-sections of Xenon (σ_{Xe}) and Samarium (σ_{Sm}), the scattering cross-sections (Σ_s), the ADFs for the fast and thermal energy group and for each branch and burnup point.

The structure of the reflector cross-section PMAXS does not include data on depletion and branches. It scopes data such as the inverse neutron velocities, history variables and Σ_{tr} , Σ_a and Σ_s for the reference branch only.

Annex B Branch structure

Table B-1: Branch structure of material composition A&B

BRANCH	CR	DC	TF	TC
RE	no	0.45854	760.40	559.00
CR	yes	0.45854	760.40	559.00
DC	no	0.17720	760.40	559.00
DC	no	0.31787	760.40	559.00
DC	no	0.59921	760.40	559.00
DC	no	0.73989	760.40	559.00
DC	yes	0.17720	760.40	559.00
DC	yes	0.31787	760.40	559.00
DC	yes	0.59921	760.40	559.00
DC	yes	0.73989	760.40	559.00
TF	no	0.17720	559.00	559.00
TF	no	0.17720	1200.00	559.00
TF	no	0.17720	1600.00	559.00
TF	no	0.17720	2000.00	559.00
TF	no	0.31787	559.00	559.00
TF	no	0.31787	1200.00	559.00
TF	no	0.31787	1600.00	559.00
TF	no	0.31787	2000.00	559.00
TF	no	0.45854	559.00	559.00
TF	no	0.45854	1200.00	559.00
TF	no	0.45854	1600.00	559.00
TF	no	0.45854	2000.00	559.00
TF	no	0.59921	559.00	559.00
TF	no	0.59921	1200.00	559.00
TF	no	0.59921	1600.00	559.00
TF	no	0.59921	2000.00	559.00
TF	no	0.73989	559.00	559.00
TF	no	0.73989	1200.00	559.00
TF	no	0.73989	1600.00	559.00
TF	no	0.73989	2000.00	559.00

Table B-2: Branch structure of material composition C

BRANCH	CR	DC	TF	TC
RE	no	0.45854	739.70	559.00
CR	yes	0.45854	739.70	559.00
DC	no	0.17720	739.70	559.00
DC	no	0.31787	739.70	559.00
DC	no	0.59921	739.70	559.00
DC	no	0.73989	739.70	559.00
DC	yes	0.17720	739.70	559.00
DC	yes	0.31787	739.70	559.00
DC	yes	0.59921	739.70	559.00
DC	yes	0.73989	739.70	559.00
TF	no	0.17720	559.00	559.00
TF	no	0.17720	1200.00	559.00
TF	no	0.17720	1600.00	559.00
TF	no	0.17720	2000.00	559.00
TF	no	0.31787	559.00	559.00
TF	no	0.31787	1200.00	559.00
TF	no	0.31787	1600.00	559.00
TF	no	0.31787	2000.00	559.00
TF	no	0.45854	559.00	559.00
TF	no	0.45854	1200.00	559.00
TF	no	0.45854	1600.00	559.00
TF	no	0.45854	2000.00	559.00
TF	no	0.59921	559.00	559.00
TF	no	0.59921	1200.00	559.00
TF	no	0.59921	1600.00	559.00
TF	no	0.59921	2000.00	559.00
TF	no	0.73989	559.00	559.00
TF	no	0.73989	1200.00	559.00
TF	no	0.73989	1600.00	559.00
TF	no	0.73989	2000.00	559.00

Table B-3: Branch structure of material composition D

BRANCH	CR	DC	TF	TC
RE	no	0.45854	761.90	559.00
CR	yes	0.45854	761.90	559.00
DC	no	0.17720	761.90	559.00
DC	no	0.31787	761.90	559.00
DC	no	0.59921	761.90	559.00
DC	no	0.73989	761.90	559.00
DC	yes	0.17720	761.90	559.00
DC	yes	0.31787	761.90	559.00
DC	yes	0.59921	761.90	559.00
DC	yes	0.73989	761.90	559.00
TF	no	0.17720	559.00	559.00
TF	no	0.17720	1200.00	559.00
TF	no	0.17720	1600.00	559.00
TF	no	0.17720	2000.00	559.00
TF	no	0.31787	559.00	559.00
TF	no	0.31787	1200.00	559.00
TF	no	0.31787	1600.00	559.00
TF	no	0.31787	2000.00	559.00
TF	no	0.45854	559.00	559.00
TF	no	0.45854	1200.00	559.00
TF	no	0.45854	1600.00	559.00
TF	no	0.45854	2000.00	559.00
TF	no	0.59921	559.00	559.00
TF	no	0.59921	1200.00	559.00
TF	no	0.59921	1600.00	559.00
TF	no	0.59921	2000.00	559.00
TF	no	0.73989	559.00	559.00
TF	no	0.73989	1200.00	559.00
TF	no	0.73989	1600.00	559.00
TF	no	0.73989	2000.00	559.00

Table B-4: Branch structure of material composition E&F

BRANCH	CR	DC	TF	TC
RE	no	0.45854	739.50	559.00
CR	yes	0.45854	739.50	559.00
DC	no	0.17720	739.50	559.00
DC	no	0.31787	739.50	559.00
DC	no	0.59921	739.50	559.00
DC	no	0.73989	739.50	559.00
DC	yes	0.17720	739.50	559.00
DC	yes	0.31787	739.50	559.00
DC	yes	0.59921	739.50	559.00
DC	yes	0.73989	739.50	559.00
TF	no	0.17720	559.00	559.00
TF	no	0.17720	1200.00	559.00
TF	no	0.17720	1600.00	559.00
TF	no	0.17720	2000.00	559.00
TF	no	0.31787	559.00	559.00
TF	no	0.31787	1200.00	559.00
TF	no	0.31787	1600.00	559.00
TF	no	0.31787	2000.00	559.00
TF	no	0.45854	559.00	559.00
TF	no	0.45854	1200.00	559.00
TF	no	0.45854	1600.00	559.00
TF	no	0.45854	2000.00	559.00
TF	no	0.59921	559.00	559.00
TF	no	0.59921	1200.00	559.00
TF	no	0.59921	1600.00	559.00
TF	no	0.59921	2000.00	559.00
TF	no	0.73989	559.00	559.00
TF	no	0.73989	1200.00	559.00
TF	no	0.73989	1600.00	559.00
TF	no	0.73989	2000.00	559.00

Table B-5: Branch structure of material composition G&H&I

BRANCH	CR	DC	TF	TC
RE	no	0.45854	739.60	559.00
CR	yes	0.45854	739.60	559.00
DC	no	0.17720	739.60	559.00
DC	no	0.31787	739.60	559.00
DC	no	0.59921	739.60	559.00
DC	no	0.73989	739.60	559.00
DC	yes	0.17720	739.60	559.00
DC	yes	0.31787	739.60	559.00
DC	yes	0.59921	739.60	559.00
DC	yes	0.73989	739.60	559.00
TF	no	0.17720	559.00	559.00
TF	no	0.17720	1200.00	559.00
TF	no	0.17720	1600.00	559.00
TF	no	0.17720	2000.00	559.00
TF	no	0.31787	559.00	559.00
TF	no	0.31787	1200.00	559.00
TF	no	0.31787	1600.00	559.00
TF	no	0.31787	2000.00	559.00
TF	no	0.45854	559.00	559.00
TF	no	0.45854	1200.00	559.00
TF	no	0.45854	1600.00	559.00
TF	no	0.45854	2000.00	559.00
TF	no	0.59921	559.00	559.00
TF	no	0.59921	1200.00	559.00
TF	no	0.59921	1600.00	559.00
TF	no	0.59921	2000.00	559.00
TF	no	0.73989	559.00	559.00
TF	no	0.73989	1200.00	559.00
TF	no	0.73989	1600.00	559.00
TF	no	0.73989	2000.00	559.00